Superhydrophobic Polymeric Surfaces: Fabrication, Wettability, and Antibbacterial activity

by

Salma Falah Toosi

M.Sc., McMaster University, Hamilton, Ontario 2010
B.Sc., Sharif University of Technology, Iran, 2007

A THESIS SUBMITTED IN PARTIAL FULFILLMENT OF
THE REQUIREMENTS FOR THE DEGREE OF

DOCTOR OF PHILOSOPHY

in

THE FACULTY OF GRADUATE AND POSTDOCTORAL STUDIES
(Chemical and Biological Engineering)

THE UNIVERSITY OF BRITISH COLUMBIA
(Vancouver)

July 2017

Abstract:

This PhD thesis studies fabrication of superhydrophobic polymeric surfaces, their wetting properties, and their antibacterial activities as potential application to medical sciences. A femtosecond laser technique was used to fabricate mico/nano- structures on the surface of PTFE and PU. The effect of laser parameters (fluence, scanning speed, and overlap) on the wettability of the resulted micro/nano-patterns was studied. Two techniques were used to laser-scan the surface, namely uniaxial and biaxial scan. Uniaxial scan creates channeled morphology with direction-dependent wettability. To produce uniform wettability independent of direction, biaxial scanning was examined, which creates well-defined pillars with very high contact angle (CA) and very low contact angle hysteresis (CAH).

To facilitate and speed up the surface micro/nano-structuring, laser-ablation was coupled with thermal imprinting. The metallic femtosecond laser-ablated templates were employed to imprint micron/submicron periodic structures onto the surface of several polymers. The CA of imprinted polymers increased to above 160°, while their CAH varied significantly depending on the surface thermophysical and chemical properties.

A unique technique was developed to create superomniphobic patterns on HDPE through hot embossing. The filefish skin dual scale superoleophobic patterns were used as a biological model to develop angled microfiber arrays on HDPE. The obtained bioinspired surface is highly capable of repelling both water and liquids with low surface tensions that meets the superomniphobic criteria.

The effect of superhydrophobicity on protein adsorption and bacterial adhesion of laser-ablated PTFE substrates were investigated. Samples were incubated in Gram negative (*E.coli*) and Gram positive (*S.aureus*) bacteria cultures, BSA solution, IgG solution, and blood plasma for 4 hours. All superhydrophobic surfaces were found to be more resistant to protein /bacteria adhesion compared to the corresponding smooth samples. However, some of the most superhydrophobic PTFE surfaces were found to exhibit the highest adherence with protein/bacteria; while some other did not allow any adsorption/adherence of protein/bacteria respectively towards the end of the incubation. Besides the CA, CAH, average height of pillars, and spacing distance between

the pillars, this study showed that there are other roughness factors, which play crucial role in the durability of the superhydrophobic surfaces such as the distribution of pillar heights.

Lay Summary

Anti-bacterial biomedical substrates were fabricated through manufacturing of micro/nano-structured surfaces with excellent liquid-repellency and self-cleaning properties. These types of surfaces are called superhydrophobic showing contact angle greater than 150° and contact angle hysteresis less than 10°. When the liquid droplet comes into contact with these surfaces, air pockets are trapped between the dual-scale patterns and the droplet, which leads to a low contact area and superhydrophobicity.

Two methods used for fabricating superhydrophobic polymeric surfaces in this PhD work are femtosecond laser ablation of PTFE substrates and replicating the micro/nano-patterns of laser-ablated Stainless Steel templates onto polymeric substrates through hot- embossing.

Superhydrophobic PTFE samples were characterized for protein adsorption and Gram-positive and Gram-negative bacteria adhesion. It was found that in addition to water contact angle and water contact angle hysteresis of the samples, size and topography of the patterns also significantly impact the efficiency of superhydrophobic surfaces in repelling biological species.

Preface

This thesis entitled "Superhydrophobic Polymeric Surfaces: Fabrication, Wettability, and Antibacterial activity" presents the research the author performed during her PhD study under the supervision of Professor Savvas G. Hatzikiriakos. This thesis is original, independent work by the author, Salma Falah Toosi.

The following journal papers have been published from the research work presented in this dissertation.

Journal Papers

- Salma Falah Toosi, Sona Moradi, Savvas G. Hatzikiriakos "Fabrication of Micro/Nano Patterns on Polymeric Substrates: A Critical Review", 2017, submitted. (This paper is based on the data presented in Chapter 2 of this thesis.)
- Salma Falah Toosi, Sona Moradi, Saeid Kamal, Savvas G. Hatzikiriakos "Superhydrophobic laser ablated substrates", 2015, Journal of Applied Surface Science. (This paper is based on the data presented in Chapter 5 of this thesis.)
- Salma Falah Toosi, Sona Moradi, Savvas G. Hatzikiriakos "Microfabrication of polymers with extreme wettability using hot embossing", 2016, Journal of Applied Surface Science . (This paper is based on the data presented in Chapter 7 of this thesis.)
- Salma Falah Toosi, Narges Hadji-esfandiari, Kai Yu, Jayachandran Kizhakkedathu, Savvas Hatzikiriakos, "Hierarchical Surface Structures for Reducing Bacteria Adhesion" fully written and ready to be submitted, 2017. (This paper is based on the data presented in Chapter 3 of this thesis)

Conference Presentations

- Salma Falah Toosi, S. Moradi, K.Yu, J. Kizhakkedathu, S. G. Hatzikiriakos "The Effect of Superhydrophobicity on the Bacterial Adhesion on Polymeric Surfaces", Contact angle, wettability and adhesion symposium, Hoboken, New Jersey, July 2016
- Salma Falah Toosi, S. Moradi, K.Yu, J. Kizhakkedathu, S. G. Hatzikiriakos "Nano/micro patterned polymers: Fabrication and biocompatibility", Conference of the Polymer Processing Society, Graz, Austria, September 2015.
- Salma Falah Toosi, S. Moradi, Kai Yu, J. Kizhakkedathu, S. G. Hatzikiriakos, "Superhydrophobic Polymeric Surfaces: Protein Adsorption and Platelet Adhesion", International Conference on Multifunctional, Hybrid and Nanomaterials , Barcelona, Spain, March 2015.

Table of Contents

List of Tables

List of Figures

List of Symbols

μ	Micron
E_P	Laser beam pulse energy
P_{emboss}	Embossing pressure
R_a	Arithmetic average of surface roughness
R_t	Maximum height of the profile
R_z	Average of five maximum heights of the profile
T_{emboss}	Embossing Temperature
T_g	Glass transition temperature
T_m	Melting point temperature
V	Scan speed
Z_R	Half of the Rayleigh range
α	Slope angle of the surface
γ	Interfacial tension
θ_{Adv}	Advancing contact angle
θc	Critical intrinsic contact angle
θ_{CB}	Cassie-Baxter contact angle
θ_{Rec}	Receding contact angle
θ_W	Wenzel apparent contact
θ_Y	Young apparent contact
λ	Wavelength
Φ (r)	Laser fluence profile
Φ_0	Beam peak fluence
Φ_0	Beam peak fluence
Φ_{th}	Ablation threshold
ω_0	Gaussian beam radius at the focal point

List of Abbreviations

ATR	Attenuated Total Reflectance
CFU	Colony Forming Unites
BSA	Bovine serum albumin
CA	Contact angle
CAH	Contact abgle hysteresis
E. coli	*Escherichia coli*
FITC	Fluorescein isothiocyanate
fs	femtosecond
FTIR	Fourier Transform Infrared
HDPE	High-density polyethylene
IgG	Immunoglobulin G
ND	Neutral density
PBS	Phosphate Buffered Saline
PLA	Poly Lactic Acid
PTFE	Polytetrafluoroethylene
PVC	Polyvinyl chloride
S. aurus	*Staphylococcus aureus*
SEM	Scanning Electron Microscope
SH	Superhydrophobic
SS	Stainless Steel
Tg	Glass transition temperature
Tm	Melting point
XPS	X-ray Photoelectron Spectroscopy

Acknowledgements

I would like to acknowledge my supervisor, Prof. Savvas G.Hatzikiriakos for the aid, guidance, and his never-ending supports during this course of work. His continuous encouragement and support has been a source of continuous motivation.

My sincere thanks goes to the member of my supervisory committee, Prof. Jay Kizhakkedathu, whose knowledge and assistance helped me to accomplish this project. He and his team were very welcoming and they generously allowed me to use their state-of-the-art lab facilities.

I would also like to acknowledge Dr. Saeid Kamal also member of supervisory committee, the manager of Laboratory for Advanced Spectroscopy and Imaging Research (LASIR) of Chemistry Department of UBC for the all guidance, and help during the course of this research project.

I would also like to thank my friends and research colleagues Marzieh Ebrahimi, Narges Hadjesfandiari, and Sona Moradi as well as all members of the rheology lab in the department of Chemical and Biological Engineering at the University of British Columbia.

Finally, I am grateful to my dear husband, Morteza, for his encouragement and support. I am also grateful to my beloved son, Aiden, for his sweet smile and understanding. My love and appreciation go to my parents, Hossein and Farzaneh, and to my brother, Soroush, for their never-ending love and support during all stages of my study.

Chapter 1: Introduction

Urinary catheter is the most common indwelling device, with 17.5% of patients in 66 European hospitals having a catheter and 23.6% in 183 US hospitals[1]. Unfortunately, indwelling urinary catheters considerably increase the risk of infection, in particular, in an already weak and sensitive patient population. For example, a survey of medical intensive care units in the United States showed that 95% of urinary tract infections (UTIs) are catheter associated [1]. Strategies to prevent catheter-associated infections can considerably decrease the rate of morbidity, mortality, and health care costs. The keystone to any preventive strategy of catheter infections is strict attention to design and development of anti-bacterial or anti-biofouling catheters which could resist bacteria adhesion and biofilm formation[2]. Anti-biofouling surfaces are of high importance due to their essential roles in biosensors, biomedical devices, food processing, the marine industry, and others. Anti-biofouling surfaces can prevent and resist bacterial adhesion due to the presence of an unfavorable chemistry and/or topography on the surface with respect to the microorganisms[3][4][5]. Presence of nano/micro roughness is closely related to surface wettability which has huge effect on bacterial adhesion to the surface.

Other types of catheters which cause high risk of infection are intravascular catheters and blood central lines. A survey done by one of medical intensive care units in north America revealed that 87% of primary bloodstream infections were associated with central lines[2]. Unfortunately, the patients who receive blood central lines are plagued with the risk of surface induced thrombosis as well. When blood contacts with a foreign object, a series of responses occur at the blood-biomaterial interface. The plasma proteins adsorb to the surface of the biomaterial. The adsorption of blood plasma proteins to biomaterial surfaces is usually a rapid process that within seconds creates a biologically active layer which is capable of interacting with other blood borne mechanisms. The protein coating can serve as a substrate for cell and platelet adhesion [6]. Therefore, for blood contacting biomaterials, the protein response can ultimately lead to the implant failure [7]. The ability of a blood contacting biomaterial surface to minimize protein adsorption to the surface is believed to be part of the implant biocompatibility. In addition to chemistry, it has been also demonstrated that the presence of surface structure (nano/micro roughness) which is closely related to surface wettability, has important influence on dictating

protein adsorption to the surface [8]. A substantial amount of research show that manipulating the surface morphology and topography changes the surface wettability (hydrophobicity/hydrophilicity). Changes in surface wettability change the amount protein/bacteria adhesion onto the surface.

A superhydrophobic surface is a surface with water contact angle greater than 150° and water contact angle hysteresis of less than 10°-15° (the droplet stickiness onto the surface is known to be proportional to the contact angle hysteresis which is defined as the difference between the advancing and the receding contact angles) [10][11]. The poor wettability of such surfaces is caused by low surface energy of the material in combination with the cooperative effect of nanostructure within the micrometer scale patterns (the so-called hierarchical structure)[12].

The wetting behavior of a liquid droplet on a rough surface can be explained by the Wenzel [13] and/or the Cassie–Baxter [14] models. In the Wenzel state, the liquid droplet completely collapses on the surface filling up the spaces between the micro bumps. Droplets in this state have the tendency to adhere to the rough surface more than in a similar flat surface. On the other hand, in the Cassie–Baxter state, the liquid droplet sits on top of the micro/nano-asperities with air bubbles trapped underneath. In the Cassie-Baxter state, the droplets roll off the surface easily. Superhydrophobic surfaces offering self-cleaning properties are stable in Cassie-Baxter state.

Inspired by examples in nature, excessive attention has been devoted to design and fabrication of such surfaces with extreme water repellency properties so called superhydrophobicity. Nature presents various examples of surfaces which offer superhydrophoic properties such as lotus leaf [9]. Due to contamination resistance and self-cleaning property, these plants and animals have been remaining extraordinarily clean of fouling in highly bacteria-rich aquatic systems. Micro/ nanostructured surfaces artificially created to mimic these effects have also been shown to exhibit similar non-adhesive /self-cleaning properties. They also show resistance to protein adsorption, cell adhesion and biofilm formation [15][16][17][18][19]. These observations suggest that surfaces with extremely poor wettability and low adhesion can be a potential solution to increase the protein/bacteria resistance of temporary polymeric and metallic medical tools. In these surfaces, the hierarchical structure is responsible for trapping air pockets between micro/nano features and prevent direct connection between protein/bacteria and the surface. The air layer is also responsible for the low contact angle hysteresis and self-cleaning properties.

The main objective of this work is to design and fabricate superhydrophobic polymeric surfaces that reduce protein adsorption and bacterial adherence to be used in several applications in the biomedical sciences such as for the manufacturing of catheters and blood contacting devices.In this PhD work, the bioinspired examples will be used as models to fabricate similar hierarchical patterns on polymeric surfaces to mimic their superhydrophobic behaviour.

In order to obtain superhydrophobic polymeric substrates, dual scale nano/micro structures are fabricated on various polymeric surfaces through two different methods; femtosecond laser ablation and thermal imprinting.

Chapter 2: Literature Review

2.1 Wettability, Surface Tension and Contact Angle—Young's Equation

Controlling the wetting of a solid surface is important in many technological and industrial areas. The wettability of flat solid surface range from complete wetting to partial wetting (Figure 2-1). The contact angle (CA) is a quantitative measurement for surface wettability. The contact angle (see Figure 2-1) first described by Thomas Young [15] in 1805, was formed at the intersection of solid-liquid interface and liquid- vapor interface[20] :

$$\frac{\gamma_{SV} - \gamma_{SL}}{\gamma_{LV}} = \cos\theta_Y \qquad (1)$$

where θ_Y, is the Young contact angle of flat surface, γ is the interfacial tension and the uperscripts " *S*", "*L* ", and " *V*" stand for solid , liquid, and vapor phases, respectively.

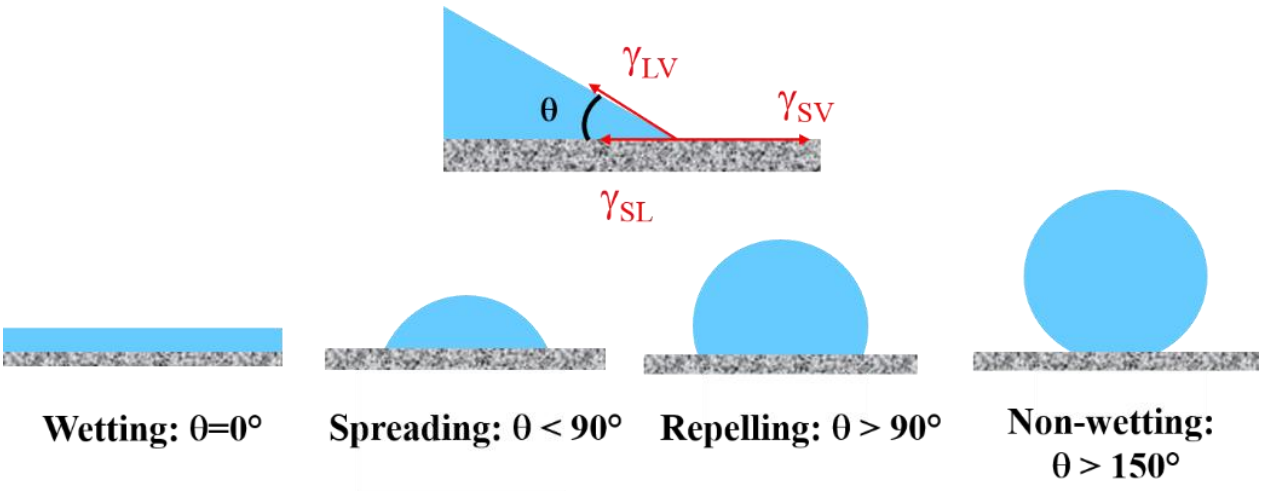

Figure 2-1. Young's equation and different wetting states from complete wetting to non-wetting

Complete wetting results from the high affinity of the liquid molecules to the solid surface, while, partial wetting results from high affinity of the water molecules to themselves compared to their affinity with the solid surface. The wetting state with water CA less than 90° is referred to as hydrophilic, and the wetting state with water CA greater than 90° is referred to as

hydrophobic (Figure 2-1). For surface wetting by oil and organic liquids, the term of "oleophilic/phobic" and "omniphilic/phobic) are used.

The affinity of liquid to wet a solid surface results from the interaction between cohesive and adhesive forces. The liquid-air interfacial tension is called surface tension of the liquid. The shape of a liquid droplet is ideally determined by the surface tension of the liquid. Each molecule in the bulk of a liquid is pulled equally in every direction by its neighboring molecules, which results into a net force of zero. However, the molecules at the surface do not have neighboring molecules and they are pulled inward by the neighboring molecules, creating an internal pressure. As a result, the liquid droplet contracts its surface area to maintain the lowest surface free energy. This intermolecular force to contract the surface is called surface tension, and it is responsible for cohesive forces between liquid molecules [21].

The contact angle of a liquid drop on an ideal solid surface is defined when all three interfacial tensions are in thermodynamic equilibrium (air-liquid-solid are in balance) (see Figure 2-1).

2.2 Wetting States, Regimes, and Roughness

In Young's equation, surface hypothetical is a smooth, rigid, chemically homogeneous, unreactive, and insoluble solid. However, in the real world, solid surfaces are usually rough and chemically heterogeneous[22]. By adding roughness to the surface, the CA changes locally from one point to another. The contact angle of each point is called the "intrinsic contact angle" or "actual contact angle", θ_{Act}. Instead of Actual contact angle which varies from one point to another point, "apparent contact angle", θ_{App} is usually reported for rough surfaces. θApp is defined as the angle between the tangent lines of the nominal solid-liquid interface and liquid-vapour interface [20].

The wetting behaviour of a liquid droplet on a rough surface can be explained by two theories. These theories namely are Wenzel [13] and/or the Cassie-Baxter [14] models. First in the Wenzel state (Figure 2-2), the liquid droplet totally collapses on the surface, filling up the spaces between the micro-features (homogeneous wetting). Due to the higher surface area, droplets in this state have more tendency to adhere to the rough surface compared to a similar flat surface. Equation (2) is referred to as the Wenzel equation which is relating the Young contact angle θ_Y to the apparent contact angle in Wenzel state, θ_W :

$$\cos\theta_W = r_f \cos\theta_Y \quad (2)$$

where r_f (roughness factor) is the ratio of actual solid surface area to the projected area, and is always greater than 1. In the Wenzel wettability model, the presence of roughness makes an inherently hydrophobic surface ($\theta_Y > 90^\circ$) more hydrophobic and an inherently hydrophilic surface ($\theta_Y < 90^\circ$) more hydrophilic. However, the Wenzel equation may fall into non-physical states for surfaces with a high roughness when $\left|r_f . \cos\theta_Y\right|$ is greater than 1. Additionally, the Wenzel model predicts only one apparent CA for a droplet on a rough surface, while a range of apparent CAs exist on a rough surface[23] .

In cases where the liquid does not penetrate into the grooves, the Wenzel equation does not apply. Depending on the surface topography and surface chemistry, the liquid might not fully penetrate into the micro grooves to completely wet the surface (Figure 2-a). Instead it might be sitting on top of asperities with air pockets trapped underneath (Figure 2-b). This "heterogeneous wetting" or "composite" state is called Cassie-Baxter model. The Cassie equation was first developed to describe heterogeneous surfaces, with two different components. The equation describing this state was developed by Cassie-Baxter (CB) in 1944 [14]:

$$cos\theta_{CB} = f_1 .cos\theta_1 + f_2 .cos\theta_2 \quad (3)$$

In the equation (3), f_1 and f_2 are the area fractions of material 1 and 2 ($f_1+f_2=1$), and θ_1 and θ_2 contact angles of pure material 1 and 2 respectively. If the second area is air like shown in Figure 2-2, then equation (3) can be written as

$$cos\theta_{CB} = f_{air} .cos\theta_{air} + f_{solid} .cos\theta_{solid} \quad (4)$$

Since contact angle against liquid and air can be considered to be 180 ° ($cos\theta_{air}$ is -1) and the area fraction $f2 = 1 - f1$. Equation (5) was developed by Cassie and Baxter and is thus often called the Cassie-Baxter equation. Please note that the simplification can only be done exactly for cases that the tops of the surface texture are flat. In all other cases there will be some degree

of error involved.

$$Cos\theta_{CB}=r.\,f\,.\,cos\theta_{solid}+f-1 \tag{5}$$

Where r the ratio of wetted area to the projected area, f is the fraction of solid surface which is in contact with the liquid, and θ_{CB} is the Cassie-Baxter CA. When f=1, Cassie- Baxter equation (3) reduces to Wenzel equation with $r=r_f$ (1) [24].

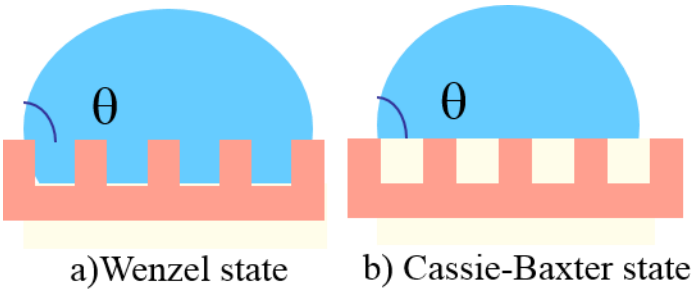

Figure 2-2: A droplet on a surface depicting the two distinct wetting states (a) The Wenzel and (b) Cassie-Baxter state

According to the Cassie-Baxter model creating a hydrophobic and/or superhydrophobic surface using an intrinsically hydrophilic surface is possible through adding roughness. Depending on the roughness factor and the amount of partial penetration of liquid into troughs, a range of CAs can be predicted [25].

From a thermodynamic point of view, the wetting state of a droplet on a solid surface is the minima of Gibbs free energy. While the local minima correspond to metastable states, the global minimum corresponds to a stable state [20]. The geometrical details of the roughened surface or the existence of external forces such as pressure, vibrational and gravitational can cause thermodynamic transitions between Cassie-Baxter and Wenzel [26][27][28]. By comparing the total Gibbs free energy of the system in the two states, the most stable state is determined. It is shown that the Cassie-Baxter state is the most stable state if the CA satisfies the following condition [28]:

$$\theta_Y > \theta_C \ , \qquad \text{with} \qquad \cos\theta_C = \frac{f-1}{r_f - f} \tag{6}$$

Where θ_c is the critical intrinsic CA of the flat surface above which a stable composite state is possible. If $\theta_Y > \theta_c$, Cassie–Baxter mode (unpenetrated) wetting is favorable. If $\theta_Y < \theta_c$, Wenzel (penetrated) wetting model is instead favorable[29].

The relationship between $\cos\theta_{rough}$ and $\cos\theta_Y$ for Cassie- Baxter and Wenzel states is plotted in Figure 2-3 according to eqs 2 and 5, as demonstrated by Cao et al. The two lines shown in figure 2-3 corresponding to the two states intersect at one critical angle (equation 6). Because $f < 1$ and $r > 1$, θ_{crit} (θ_c) is greater than 90°.

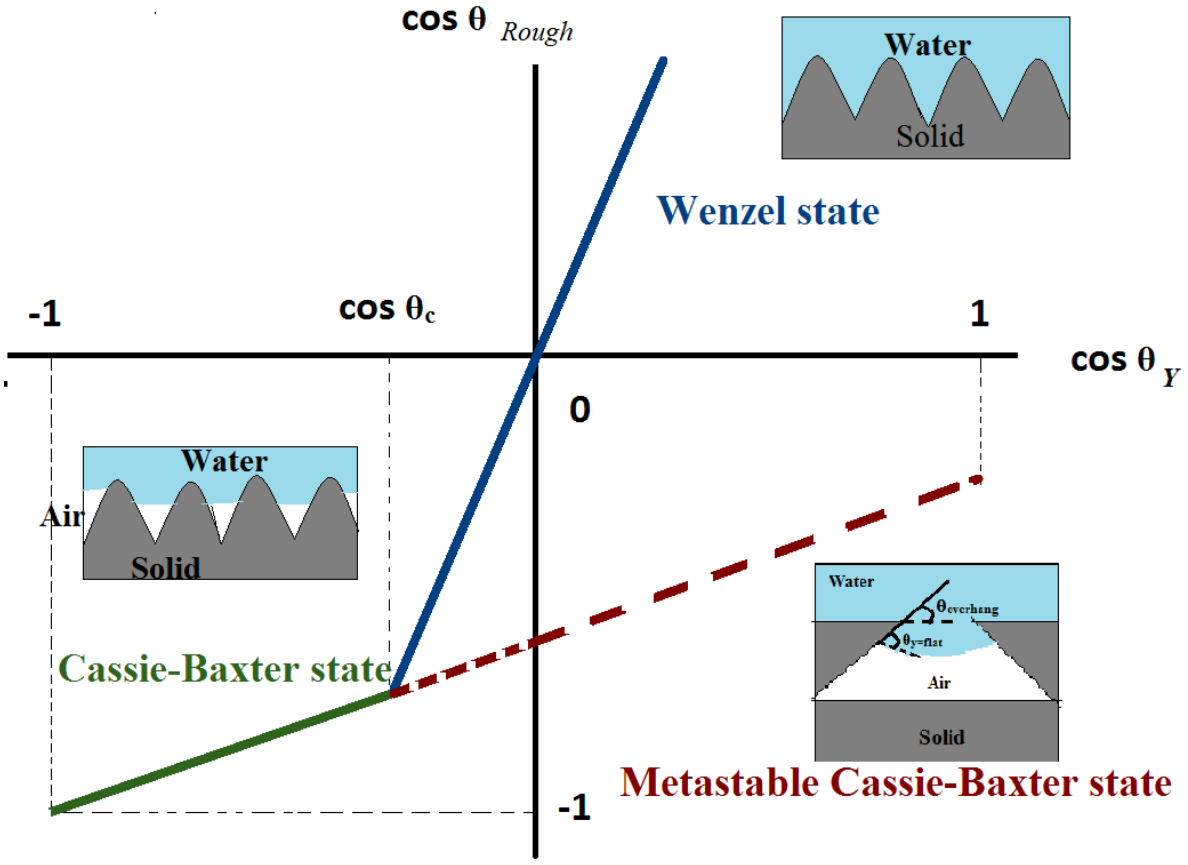

Figure 2-3. Relationship of $\cos\theta_{Rough}$ with $\cos\theta_Y$. The black solid, blue solid, red dotted, and red dashed lines correspond to the Wenzel state, the Cassie state, the metastable Cassie state when $\theta_Y > 90^\circ$, and the metastable Cassie state when $\theta_Y < 90^\circ$, respectively

It has also been proven that by decreasing the CA of the rough surface (Cassie-Baxter to Wenzel), the surface total energy monotonically decreases, so that the state with less rough CA is more stable as shown in Figure 2-3 [30]. As it can be concluded from this figure, for materials inherently hydrophilic ($\theta_{flat} < 90°$), the Wenzel state is always the most stable state.

The metastable Cassie state also exists when $\theta_{flat} < 90°$ (i.e., $\cos \theta_{flat} > 0$). This state is represented by the dashed line as an extension of the Cassie state into the fourth quadrant in Figure 2-3. In the case of $\theta_{flat} < 90°$, overhanging structures (shown in the lower-right quarter of Figure 2-3) are needed to provide positions for the water-solid contact line to suspend water above the bottom surface. A critical parameter in the overhang structure is the overhang angle ($\theta_{overhang}$) formed between the sidewalls of the indent and the horizontal line. When $\theta_{overhang}$ is greater than θ_{flat} of the sidewall surface, water is forced to enter into the indent and have complete contact with the solid. When $\theta_{overhang}$ is equal to θ_{flat}, the water-air interface is flat and stays at a circular intersection of the indent, assuming that the gravity is ignored. When $\theta_{overhang}$ is smaller than θ_{flat} (shown in the lower-right quarter of Figure 2-3), the water-air interface inside the indent is convex, and water is prevented from entering into the indent. Therefore, the Cassie state is only possible if $\theta_{overhang}$ is smaller than θ_{flat}.

For inherently hydrophobic surfaces ($\theta_{flat} > 90°$), depending on the roughness geometry and surface roughness, and the CA of the flat surface, the Cassie-Baxter can be the most stable state (if $\theta_{flat} > \theta_{critic}$).

2.3 Contact Angle Hysteresis

The presence of chemical heterogeneity and roughness on the surface make the droplet contact line to pin into these imperfections of the surface, resulting in a range of apparent CAs instead of a single value[31]. The difference between the maximum and minimum values of this range is referred to as contact angle hysteresis (CAH) and usually is measured by two methods[32][33]. The first method is a variation of the sessile-drop growth/shrinkage approach (Figure 2-4a). By gradually increasing the volume of the droplet the contact line between the liquid and solid advances (advancing CA). By reducing the volume of the droplet, the contact line recedes (receding CA)[34]. The difference between the maximum advancing CA and the minimum receding CA is referred to as CAH [35][36].

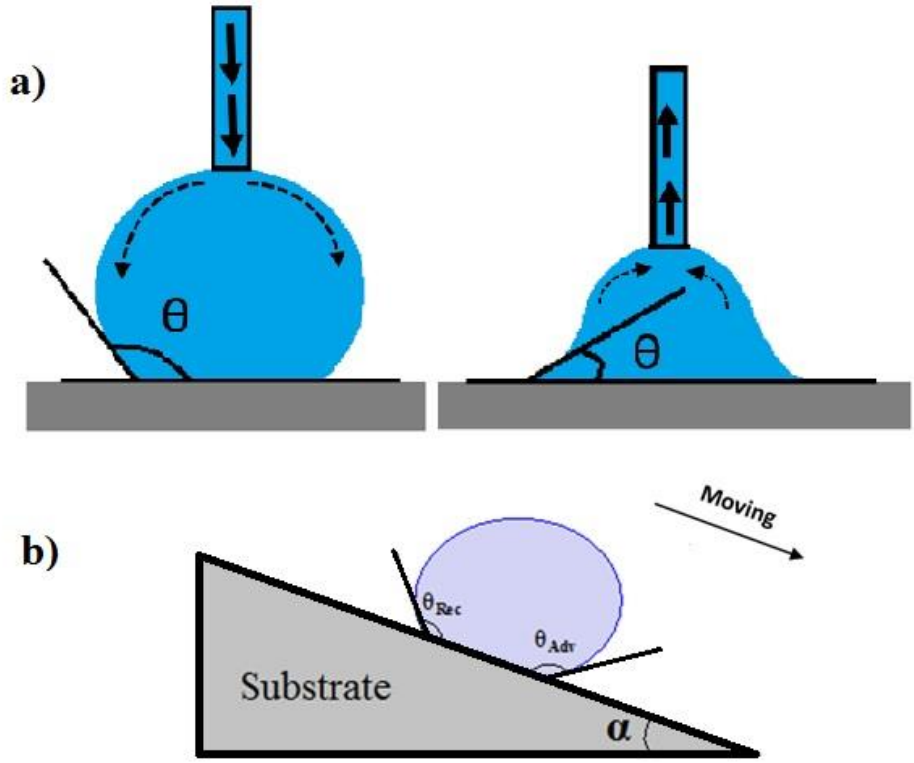

Figure 2-4. (a) Schematic of the sessile-drop method to measure contact angle hysteresis by pumping into and out of a water droplet (CAH), (b) Schematic of advancing and receding contact angles on the tilting plate [37]

The second method is the tilting plate method also referred to as the "inclined plate" method, was introduced to modify the sessile drop method. In this method, the surface is set at a certain inclination angle in order to cause rolling of the droplet. The CA of droplet in the moving direction at the front of droplet is referred to as the advancing CA and the value at the back of the droplet as the receding CA. Both measurements (sessile-drop variation and tilting plate) are equivalent in spite of some debate in the literature [38]. The tilting angle of the surface at which the droplet starts rolling is called the sliding angle or roll-off angle.

The value of the static CA always lies between those of the advancing and receding CAs. It must be mentioned that reported CA and the CAH values in the literature are sensitive to the experimental techniques used for their measurement[39], [40]. The droplet stickiness onto the surface is known to be proportional to the CAH [41].

2.4 Non-wetting Surface, Superhydrophobicity

The material surface energy and surface morphology both have a significant influence on the wetting behaviour of solid surfaces. Patterned polymeric substrates, which possess dual-scale roughness (micro/nano- structure) in combination with low surface energy, are known as superhydrophobic surfaces. These surfaces have lately found numerous applications in various industrial sectors such as biomedical, anti-corrosive, packaging, aerospace, fuel cell, and microfluidics [42][43][44][45][46]. Several creatures and plants in nature use superhydrophobicity for survival on a daily basis, so research in this area has been mainly inspired by nature[47][48][49][50].

Superhydrophobic surfaces are defined as those having a water contact angle (CA) above 150° and contact angle hysteresis (CAH) of less than 10°. The low contact angle hysteresis of superhydrophobic samples develop a property known as self-cleaning. This property was inspired by nature where several hundreds of species benefit from the proper combination of surface chemistry, morphology, and topography to stay dry and clean. This phenomenon was initially discovered by Neinhaus and Barthlott on the surface of lotus leaf and was subsequently patented and named as the "Lotus-effect" [51]. The superhydrophobic surfaces have a low contact angle hysteresis which allows water droplets to roll-off the surface at very low tilt angles. These rolling droplets easily pick up dust particles and contaminations from the surface and remove them[52].

2.5 Superhydrophobic Bioinspired Surfaces

Nature offers an enormous number of examples of surfaces with peculiar properties in terms of structures and functions. Exploring plants and animals leads to finding a great diversity of complex surfaces with different functions. A brief review of few different repellent surfaces found in nature is explained below.

The most famous natural superhydrophobic surface is the surface of the lotus leaf. The extreme water- repellent properties of the lotus leaf results from the dual micro/nano roughness with micro pillars in the size between 5 to 10μm covered with nano grains waxes with size of approximately 150nm[9]. The dual scale structure of lotus leaf minimizes the contact between

the water droplet and the surface, rising the CA to more than 150° and lowering the CAH to less than 5°. As a result, the droplet easily rolls off the leaf carrying contaminations (self-cleaning).

Nature has also developed anisotropic superhydrophobic surfaces in which the droplets can roll off following a preferential direction dictated by the direction of the structural features. Remarkable example of self-cleaning superhydrophobic surface with anisotropic properties is rice leaves [47].

An opposite function is shown by the rose petals, which have relatively high contact angle with high adhesion properties. The rose petals have the ability to retain water droplets without letting them roll off when the surface is inclined or even tilted down[53]. By comparing the size of the micro pillars with lotus leaves, rose petals have larger distances between the micro pillars. This makes the droplet fully or partially to penetrate into the microgrooves to assume a Wenzel state; thus resulting into a strong adhesion between the droplet and the surface.

The feet of some animal and insects are superhydrophobic as well. It was found that the gecko feet in addition to the superhydrophobicity, possesses a high adhesive forces towards both water and solid. The origin of the high adhesive forces to water is attributed to the high density of nanopillars that contact the water and take the droplet to Wenzel state. The ability of gecko feet to adhere to solid surfaces enables this animal to walk on vertical and inverted surfaces. This behaviour is due to very high solid-solid adhesion which can be explained by the presence of microscopic hairs with the length of 20-70μm and the diameter of 3-7μm on gecko's feet. In addition, each of the micro-hairs is split into hundreds of nanometric spatula with the size between 100 to 200 nm. These micro/nano scale hairs are mainly composed of α- and β-keratins proteins, which have great influence on the adhesion. The high adhesion is also due to capillary forces and van der Waals interactions, which are amplified by the larger surface area of the rough foot [54].

The skin of some sea creatures are also exhibit extreme water and oil repellency. The filefish has sandpapery bony skin instead of common flaky scales seen on other fish. In oil-spilled sea areas, filefish is observed to be free of oil contamination. Additionally, it was found that oil droplets tend to roll off along a head-to-tail (HT) direction. This anisotropic oil repellence (superoleophobic) may endow the filefish with directional easy-cleaning in oil spilled seawater, meanwhile avoiding accumulation of oil at its head[50].

2.5.1 Lotus effect

When a raindrop falls onto a lotus leaf, it carries away all contaminant particles from the leaf by rolling on the surface. This self-cleaning property is termed as the "lotus effect" [55]. The surface of lotus leaf, shown in Figure 2-5(a), was first investigated in 1997 by Barthlott[56][57]. Studies on the structural morphology of the lotus leaf revealed that the poor wettability of the surface is attributed to the combined effects of surface chemistry (low surface energy) and surface micro/nano asperities (Figure 2-5 (b)). The surface of a lotus leaf is made up of a hierarchical roughness structure where randomly distributed micro-pillars are covered with a dense coating of agglomerated nano-scale wax tubules (Figure 2-5 (c) and (d)). This dual roughness in combination with the low surface energy waxy layer leads to superhydrophobic surface[9][58]. The average diameter of the micro-pillars on the lotus leaf surface is around 20μm and the nano-scale waxy chains have an average diameter of about 200 nm[59].

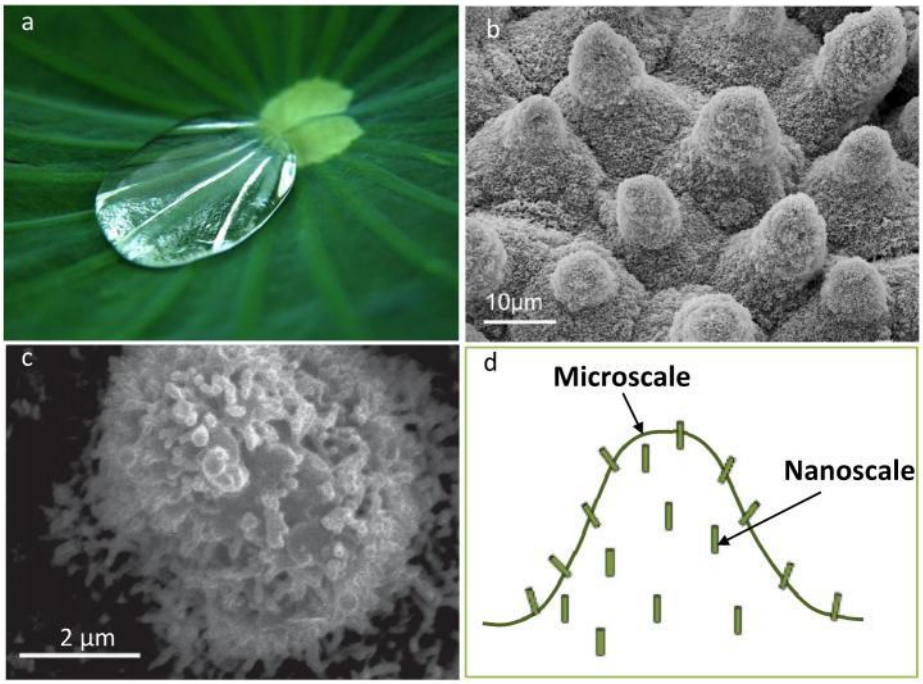

Figure 2.5. (a). Lotus leaf, (b). SEM image of Lotus leaf [59], (c). Higher magnification image of part (b) [60], (d). Schematic illustration of micro/nano structure of a single papilla constituting the surface of lotus leaf [37]

The reported contact angle on the lotus leaf surface is about 161° with a contact angle hysteresis of 2° [61]. When water droplets come into contact with the lotus leaf, air bubbles are trapped beneath the droplet between the mico/nano features (Cassie-Baxter state). The air bubbles prevent the water to fully penetrate into the valleys of the patterns and consequently, the droplet is not pinned to the surface and easily rolls off the surface carrying away dust contaminants.
The surface roughness and chemistry are two crucial parameters that significantly affect surface wettability. The methylated and fluorinated carbons have the lowest surface energy among all of the chemicals, in the following order[62]:

$$-CH2- > -CH3 > -CF2- > CF2H > -CF3$$

Flat surfaces coated by trifluoromethyl (−CF3) groups with the CA of 119° which is the highest CA that can be obtained on a flat surface [63].

2.6 Methods to Create Roughness

Superhydrophobicity is the result of combined low surface energy and roughness. Several methods have been used to create superhydrophobic rough surfaces[64] included but not limited to: micro/nano imprinting[65][66][67], photo- and E-beam lithography[68], plasma treatment[69][70][71], electroplating[72][73], and laser ablation[74][75][76][77][78][79].

2.6.1 Ultra-short laser ablation

Superhydrophobic surfaces are made from a great variety of materials such as metals, inorganic, and organic compounds[80]. Polymers are versatile and cost-effective materials easy to manufacture and typically possess low surface energies suitable to develop superhydrophobic surfaces for manufacturing smart materials and biomaterials [80]**.** PTFE $(–CF2–)_{n,}$ is technologically perhaps the most important polymer with numerous applications such as in electronics, food processing, packaging, and biomedical products. PTFE is a fully fluorinated polymer, which possesses excellent properties including thermal, chemical, mechanical, biological stability, low surface adhesion, low friction and resistance to degradation. By virtue of its great versatile properties, its potential use appears to be limitless [81].

Micromachining of PTFE can be accomplished with techniques such as oxygen plasma treatment [69], anodic aluminum oxide (AAO) templates [82], electrospining [83], and laser

ablation [78]. With these methods, surface properties can be selectively modified without altering the PTFE bulk composition.

Ultra-short pulsed laser ablation is an accurate and effective method to produce controlled roughness on the surface of metallic and polymeric materials [78]. The morphology, and the scale of the roughness are influenced by a variety of parameters originating from laser irradiation environment, and laser parameters such as laser pulse energy, scan speed, and number of pulses [84]. However, most importantly, the material properties dictate the laser performance. The properties which most matter have to do with energy and light adsorption in the material. Once the target material is understood, laser parameters can be selected.

The main advantages of using laser-based techniques for micromachining of polymers is attributed to advantages such as high resolution, mask-less patterning, fast and precise ablation under typical environmental conditions. The main reasons behind using ultra-short pulse lasers (e.g. femtosecond laser) for polymeric surface modification over using long pulse laser is the negligible heat conduction produced during laser irradiation and the minimized energy loss into the sample. Hence, high quality micromachining of the polymeric materials without thermal damage of the surrounding area is possible.

The morphology and topography (the scale of the roughness) of the ablated sample are influenced by a variety of parameters such as material properties, processing environment, and most importantly, laser parameters such as laser pulse energy, scan speed, laser beam overlap, and number of pulses [84]. In order to obtain truly superhydrophobic structures, the height and width of the patterns have to be adjusted by tuning the laser parameters[85].

Recently, nano/micro-patterning of PTFE substrates using femtosecond laser irradiation has been investigated by several authors[80][86][87][88][89][90]. Küper and Stuke studied the nano/micro patterning of PTFE with femptosecond pulses that leads to high quality structures and neat edges[91]. Kumagai et al. and Niino et al. [92][93] have reported that laser irradiation leaves a clean etching without debris on the surfaces of PTFE. Wang et al. [94]also investigated PTFE ablation using a femtosecond laser in ambient air and presented that the number of laser pulses has a significant influence on the quality and depth of the formed patterns. The laser ablated PTFE surface exhibited strong adhesion properties to water. In another work by Hashida et al.,

expanded PTFE (with porous foam structure) material was ablated using femtosecond laser without changing the fine structure of the bulk material [95]. Huber et al. have investigated the effect of wavelength (λ) and pulse duration on the ablation rate of PTFE[96]. In a recent publication by Liang et al. a PTFE surface scanned with femtosecond laser, exhibited a forest like fiber entangled structure with superhydrophobic properties, which can be used in biomedical applications [78].

2.6.2 Hot embossing imprinting

Another method to create hierarchical roughness on polymeric surfaces is thermal imprinting through hot embossing techniques. This method is a common technique in creating rough structures on a thermoplastic polymer substrate, as thermoplastics have the capability to be moldable above a certain temperature and return to their solid state upon cooling. Among so many advantages that this method has, compared to other surface structuring methods, the low cost for embossing tools, the ability to pattern structures in large scale with a high-throughput, and simple operation and high replication accuracy are the most important.

This method involves creating a template from a hard metallic surface and using this template to reproduce its reverse pattern on polymeric surfaces. The template topography and morphology can be created through different ways, such as anodizing aluminum oxide (AAO), E-beam lithography, and casting natural superhydrophobic surfaces (lotus leaf) onto the template substrate. As it was mentioned above, femtosecond pulsed laser ablation is an effective method to produce controlled patterns on the surface of materials. As a result, high quality micro/nano structuring of the templates without thermal damage of the surroundings could be achieved.

Hofmeister et al created nano-holes in a template using femtosecond laser and replicated the nanoholes by casting a polymer solution onto the template [97]. In another work, by Psarski et al., laser ablated aluminum substrates were used as the template to imprint hierarchical topographies onto epoxy nanocomposite [98]. Laser ablated silicon templates were imprinted into sol–gel films; the sol–gel films contact angle was increased up to 160° [99][100]. Nuutinen et al. imprinted the laser ablated stainless templates onto poly caprolacton (PC) substrate to obtain CA of 150°. In some other works, nano/micro structures of laser ablated stainless steel

templates were imprinted onto the surface of polymeric substrates without improving the wetting sensitivity of the imprinted surfaces [101][102][103].

Micro/nano structured PLA surfaces have found enormous applications in biomedical engineering due to their high level of biocompatibility with human tissue [104][105][19] [106][107][108][109][110][111][112]. Few methods are reported in literature to create micro/nano patterns on PLA surface. One method is solvent-casting of PLLA/dioxane solutions onto a previously structured template e.g. using nonporous anodic aluminum oxide (AAO) templates[109]. Micro/nano structured PLA is mostly fabricated through phase inversion-based methods[107][113][114][115]. There are also reports on preparing micro/nano structured PLA through hot embossing. However, none of the above mentioned reports has reported superhydrophobic PLA or a structured PLA surface with water CA (WCA) of more than 130°. It is challenging to fabricate a truly superhydrophobic substrates from polylactic acid and in general from biodegradable polymers, due to their relatively hydrophilic ester bonds and flexible molecular chains.

Medical-grade poly vinyl chloride (M-PVC), is used as intravenous fluid bags and tubing, blood and plasma bags, enteral feeding and dialysis equipment, and catheters [116]. It has been suggested that creating superhydrophobic patterns or coatings might be useful to efficiently prevent or reduce thrombosis and biofouling formation on the surface of biomedicals. In order to study this hypothesis, very few scientist recently investigated the effect of superhydrophobic coatings on medical-grade PVC for antibacterial and anti-thrombosis application[117][118]. To the best of our knowledge, no studies were reported on fabricating a superhydrophobic M-PVC by adding roughness.

2.7 Superhydrophobic Anti-biofouling Surfaces

Antibacterial surfaces can be classified as either antibiofouling or bactericidal [119]. Bactericidal substrates may prevent the bacteria adhesion by inactivating any bacteria cell coming into contact with the substrate, causing cell death. Anti-biofouling surfaces may resist or prevent initial attachment of bacteria due to the presence of an unfavorable surface chemistry or surface topography with respect to the nature and size of the microorganisms [120].

The possibility of adhesion between a substrate and a bacterial cell is a complex process which is governed by the physico-chemical properties of the substrate [121][122]. Thus, surface chemical modification and surface physical modification are two possible methods to resist bacteria adhesion to surface.

Surface chemistry is an important characteristic in designing biomedical substrates as it determines the available functional groups on the surface to interact with biomolecules. Therefore, the most direct way to affect living micro-organisms attachment to the surface is to modify the surface chemistry [123][124]. The most typical example of surface chemical modification is incorporating of ultra-thin organic films onto the surface, such as self-assembled monolayers (SAMs) and Langmuir-Blodgett (LB) films[125]. Plasma modification techniques and chemical graft modification are other methods to modify surface chemistry[126][127][128]. Tunable functional groups such as CH3, NH2, COOH, peptide, and proteins are known to be able to interact with certain cell structures and accordingly trigger specific behaviors of the surface[123][124]. By tailoring the available functional groups of the sample's surface, the surface free energy and consequently wettability are changed[124][129].

While a substantial amount of research has been conducted on the effects of surface chemistry on microorganisms adhesion, recent studies are towards surface topography and roughness[121]. The main reason for this shift of focus arises from the inconsistencies in microorganisms' attachment rates of chemically similar, topographically different surfaces. Two chemically similar surfaces might exhibit very different adhesion behaviour due to differences in their surface topographies. Altering the surface topography changes the surface wettability; the wettability of a surface is a function of surface energy of the material and existence of nanostructure within the micrometer scale patterns (the so-called hierarchical structure) [130][131][132][133][134].

Nature presents several examples of superhydrophobic surfaces that show contamination resistance properties (as discussed earlier) such as lotus leaf [58], butterfly wing [49], and water strider leg [135]. The "self-cleaning" property of these superhydrophobic plants and animals remaining remarkably clean of fouling in highly bacteria-rich aquatic environments. The observations from nature have stimulated significant research activity in this area as

superhydrophobicity can be a potential solution to increase the microorganisms' resistance of temporary polymeric and metallic medical tools such as guide wires, catheters, and surgery tools.

Much of the research undertaken in this area was aiming in finding ways of inhibiting the initial adhesion of bacterial cells on the surfaces by manipulating the surface topography. A number of investigations on Gram positive bacteria (e.g., *S. aurous*) and Gram-negetive bacterial (e.g., *E. coli*) adhesion on the surfaces with a wide range of wettabilities revealed that the superhydrophobic surfaces adhered the least amount of bacteria [19][106][136]. However, along with these reports, conflicting results are published too. The origin of these conflicts are raised from the fact that the bacteria–surface interactions are largely influenced by the stability of superhydrophobic surfaces (transition from Casie-Baxter to Wenzel). In other words stability is the ability of the surface to exist for long time without significant deterioration of its wetting properties. Details of surface topology have a great impact on the superhydrophobicity durability and stability and has to be addressed in future investigations.

Investigations into bacteria adhesion on hierarchical superhydrophobic surfaces have been generally undertaken in an effort to understand the potential of these surfaces for minimizing or preventing bacteria initial attachment[137]. Ma et al. investigated the adhesion of bacteria cells on the natural hierarchical surface of taro leaves and found that structures on the surface resist bacterial attachment [138]. Fadeeva et al. studied the extent of bacterial retention on femtosecond laser ablated titanium substrates that had been modified to mimic the structure of lotus leaf [139]. The surface consisted of microscale, grain-like, bumps which varied from 10 μm–20 μm covered with nanoscale features of 200 nm or less. The results highlighted that the *Staphylococcus aureus* cells were able to attach to the surface and successfully colonize there.

Tang et al. studied the adhesion of *Staphylococcus aureus (s. aureus)* on a TiO2 nanotube based superhydrophobic surface after 2 h and 4 h. They reported that although bacteria were not totally absent on the superhydrophobic surfaces and the amount of adhered cells increased with time, they were much less in quantity compared to the smooth hydrophobic surface [140]. Privett et al. [141] demonstrated that the adhesion of *Staphylococcus aureus* bacteria was reduced considerably on the superhydrophobic coating manufactured from fluorinated silica colloids. Moazzam et al [16], studied the adsorption of Bovine Serum Albumin (BSA) and adhesion of *Staphylococcus aureus* cells on the superhydrophobic surface of Aluminum. Results confirm that

the BSA protein static/dynamic adsorption capacity and the relative bacterial attachment reduced significantly after the superhydrophobic modification. Crick et al.[137] reported reduced *Staphylococcus aureus* and *Escherichia coli* adhesion on a superhydrophobic glass surfaces with contact angle of 165° compared with an uncoated plain glass (water contact angle of 60°) . Additionally, Freschauf et al. reported a significant reduction on *Escherichia coli* growth on their shrink-induced superhydrophobic polystyrene (PS), polycarbonate (PC) and polyethylene (PE) surfaces. They also demonstrated the effectiveness of rinsing on removing the adhered bacterial cells. Rinsing removed almost all the bacteria cells with less than 0.1% of the initial bacterial cells remaining on the superhydrophobic surface[136].

On the other hand, Fadeeva et al.[139] found that *Staphylococcus aureus* cells were adhered and also colonized on the laser ablated superhydrophobic Ti surface after 18 h. Sousa et al.[106] also reported *Staphylococcus aureus* cells adhered and colonized on superhydrophobic poly (L-lactic acid) surface after 24 h. Furthermore, rinsing the substrates with large amount of water didn't remove the bacteria cells from the superhydrophobic surfaces.

2.8 Protein Adsorption on Superhydrophobic Surfaces

Blood plasma is a complex matrix of molecules with different characteristics and functionalities. Dissolved proteins (i.e.—serum albumins, globulins, and fibrinogen) are one of the main constituents of blood plasma. The adsorption of blood plasma proteins to blood contacting biomaterial surfaces is usually a rapid process that happens within seconds and generates a biologically active layer with a thickness of 2-10 nm which is capable of interacting with other blood borne mechanisms. The protein coating can serve as a substrate for cell and platelet adhesion. The adsorbed layer is capable of initiating thrombogenic and immunologic responses including inflammation and platelet adhesion and activation respectively [142][143][144][145]. Therefore, for blood contacting biomaterials, the protein response can ultimately lead to the biomaterial failure (mainly in temporary blood contacting implants), while in some biomaterial applications, protein adsorption can be a desired result (mostly, in tissue connecting permanent implants, e.g. orthopedic implants). Hence, in temporary blood contacting implants the ability of the surface to minimize protein adsorption is believed to be part of the biomaterial biocompatibility (i.e. in central venous catheters (CVCs), also known as a central line). The

interactions between the surface of the biomaterial and plasma proteins directly dictate the biocompatibility or failure of these biomaterials.

The behavior of proteins at the surface of biomaterials and the surface properties of the biomaterials play a vital role in determining the nature of the blood-biomaterial interface. Adsorbed proteins largely affect blood coagulation and bacterial and cell adhesion. Additionally, adsorbed proteins can affect biomaterial surface properties and degradation. The properties of both the protein and the surface with which the proteins are interacting, influence the adsorption behavior.

Size and Primary structure of the proteins (the sequence of amino acids) affects protein-surface interactions. Larger molecules are more likely to interact with surfaces due to their higher number of contact sites. For example, an albumin molecule (67 kDa) forms about 77 contact sites with a silica substrate, while a fibrinogen molecule with the size of 340 kDa forms about 703 contact sites per molecule. Protein charge, as well as the distribution of charge on the protein surface, largely affect protein adsorption to the surface as well. Charged regions (polar and/or hydrophilic regions) can greatly contribute to how that protein interacts with other molecules and surfaces, However, proteins often show greater surface activity near their isoelectric point (the pH at which the molecule exhibits zero electrical charge)[146]. Proteins are constantly in competition with one another over binding to a surface. The "Vroman Effect", developed by Leo Vroman, hypothesizes that small and abundant molecules will arrive first to coat and cover a surface. However, over time, bigger molecules with higher affinity for that particular surface will replace them[147]. This is often seen in materials that contact the blood where albumin and fibronogen, which are usually abundant, will bind to the surface first and over time will be replaced by larger proteins.

Once proteins present at the surface, they can interact with the substrate via intermolecular forces and interactions, such as ionic or electrostatic bonding, hydrophobic interaction (largely entropically driven), and interactions of charge-transfer or particle electron donor/acceptor type. In contrast to its importance in stabilizing protein structure, hydrogen bonding does not play a major role in protein-surface interactions [148].

The tendency for proteins to remain attached to a surface also greatly depends on the material's surface properties such as surface energy, texture, and relative charge distribution. The surface

properties of the blood contacting biomaterials determine its interactions and response to the surrounding host tissue. In addition to chemistry, it has been demonstrated that presence of nano/micro roughness which is closely related to surface wettability, has important influence on dictating protein adsorption to the surface as well. The adsorption can be more pronounced on the nano/micro rough substrate due to existence of more active sites as a consequence of bigger surface area. However, the existence of nano/micro structures on the surface of low- energy material could make a significant change in the exposed surface area; superhydrophobic surfaces which are stable at Cassie-Baxter. The entrapment of air pockets makes the fraction of the solid surface which is contact with surrounding liquid limited. This may result into the reduction of the adsorbed protein onto the biomaterial surface.

Chapter 3: Thesis Objectives and Organization

3.1 Thesis Statement and Objectives

The effect of femtosecond laser processing parameters such as laser fluence, scan speed, and laser beam overlaps on the micro/nano structures of PTFE substrates are systematically investigated. Two different methods are being utilized to scan the surface of PTFE, namely uniaxial scan, and biaxial scan. The water behaviour of the laser-structured surfaces was determined by measuring their contact angle(s) (CA) and their corresponding contact angle hysteresis (CAH).

Along with an advanced surface roughening technology (femtosecond laser ablation) used on PTFE, a cost efficient technique (imprinting through hot-embossing) was used to create different types of bioinspired superhydrophobic/s superomniphobic patterns and more complicated structures on a wide range of polymers.

The designed hierarchical bioinspired superhydrophobic patterns might be a solution to increase hemocompatibility and decrease the failure of temporary blood and urine contacting medical devices such as central blood lines and urinary catheters. In blood contacting devices, this happens through preventing and decreasing the chance of protein adsorption and the consequent platelet adhesion to the surface. In urinary catheters, it happens through preventing the initial attachment of bacteria to the surface and decrease the chance of biofouling. The various developed and fabricated polymeric substrates were tested in two protein solutions, blood plasma, and two different bacteria cultures.

In summary the objectives of the present thesis are:

1- Design and develop artificial surfaces by mimicking micro/nano structures of different plants and animals on polymeric surfaces such as PTFE and PU using ultra short laser ablation.

2- Develop micro/nano patterns on various polymers (PLA, HDPE, Medical PVC) using imprinting technique such as hot embossing. Femtosecond laser ablated Stainless Steel (SS) substrates were used as templates.
3- Study the wettability of micro/nano patterns and identify relationships between the fabricated micro/nano patterns and wettability through measuring and analysing contact angle and contact angle hysteresis.
4- Evaluate the protein adsorption and bacteria adhesion of the laser ablated superhydrophobic PTFE surfaces.
5- Evaluate the stability of superhydrophobic surfaces incubated in bacteria cultures and protein solutions.

3.2 Thesis Organization

This thesis is organized as follows. Chapter 1 briefly describes the introduction to urinary catheters and central blood lines which are the most common indwelling devices and their high risk of infection. Superhydrophobicity hypothetically was introduced as a potential solution for this matter, as it can significantly lower the risk of biofilm formation on the surface. Chapter 2 is a literature review on the wettability of rough surfaces and the two related wetting models of Wenzel and Cassie-Baxter. Also, it reviews the femtosecond laser ablation method and thermal imprinting (hot embossing) methods for nanoimprinting patterns on soft solids such as polymers. Related studies about anti-biofouling and anti-thrombosis properties of superhydrophobic surfaces in literature are also discussed. Part of these reviews have been published in a review paper in the journal of Reviews of Adhesion and Adhesives (RAA). The thesis statement, objectives and the organization of this thesis are presented in chapter 3. Material and methodology used for laser ablation and thermal imprinting, as well as protein/bacteria adhesion are described in chapter 4. Chapter 5 presents the experimental results on laser ablation of PTFE utilizing two methods (uniaxial and biaxial) and reports the wetting behaviour of the fabricated substrates. This chapter has been published in the Journals of Applied Surface Science (S. Toosi, S. Moradi, S. Kamal, and S. G. Hatzikiriakos, “Superhydrophobic Laser Ablated PTFE Substrates,” J. Applied Surface Sci., 349, 715-723 (2015)). Chapter 6 presents results obtained on morphology and wettability of imprinted nano/micro structures from laser ablated SS

templates onto polymeric films through hot embossing. This chapter has been published in Applied Surface Science (S. Toosi, S. Moradi, M. Ebrahimi, and S.G. Hatzikiriakos: Microfabrication of polymeric surfaces with Extreme Wettability using Hot Embossing," Applied Surface Science, 378, 426-434 (2016)). Results on protein/bacteria adhesion onto superhydrophobic samples placed into protein solutions, plasma proteins, Gram-positive bacteria, Gram-negative bacteria are presented in chapter 6. Based on the results reported in this chapter a manuscript has been prepared to be submitted (Effect of superhydrophobic modifications on bacteria adhesion of PTFE surface.). Finally, chapter 7 summarizes the main findings and concluding remarks of this thesis and recommendations for future works.

Chapter 4: Materials, Methodology, and Experimental Setup

4.1 Materials

The 2 mm thick Teflon discs purchased from McMasters Carr with approximate density of 2.15 g/cm^3 were used as substrates. Also, 1 mm thick polyurethane films were used. Stainless steel 316L with 1mm thickness were used as template substrate for hot embossing imprinting. A blow molding grade of high density polyethylene (HDPE) with Tm of 140°C was received from Kautex Corporation. Commercial PLA with the grade number of PLA 2002D, with Tg and Tm of 56.5°C and 152.4°C, molecular weight of 106.9 kg/mol, and polydispersity of about 1.8, as obtained from NatureWorks LLC. Medical grade PVC plasticized with tris(2-ethylhexy) trimellitate films with thickness of 1 mm of were donated by Renolit. One-millimeter-thick sheets of HDPE and PLA were fabricated by compression molding using hot press at pressure of 7.0 MPa and temperature of 145° and 180° respectively.

4.2 Methodology and Experiment Set up

4.2.1 Laser ablation

A schematic diagram for the laser ablation of PTFE substrates is shown in Figure 4-1 [149]. In this particular setup, ultra-short (femtosecond) laser pulses are generated by an amplified all solid-state Ti:Sapphire laser [34-36] . The laser system produces amplified femtosecond laser pulses with center wavelength of 800 nm. The repetition rate of laser pulses used was 1 kHz with pulse duration of 140 fs and maximum power of about 2W. The beam has a Gaussian distribution with a beam waist of 10mm. In order to attenuate and adjust the energy of the laser beam, a set of neutral density (ND) filters and a lens with 300 mm focal length was used to focus the beam on the sample. The spot size of beam at the focal point ($2\omega_0$) was calculated to be 30 μm by using the following equation:

$$2\omega_0 = \left(\frac{4\lambda}{\pi}\right).\left(\frac{F}{D}\right) \quad (7)$$

Where λ is laser wavelength, *F* is the focal length of the lens (300mm in this set up) and *D* is the beam waist before focal lens (here, 10mm).

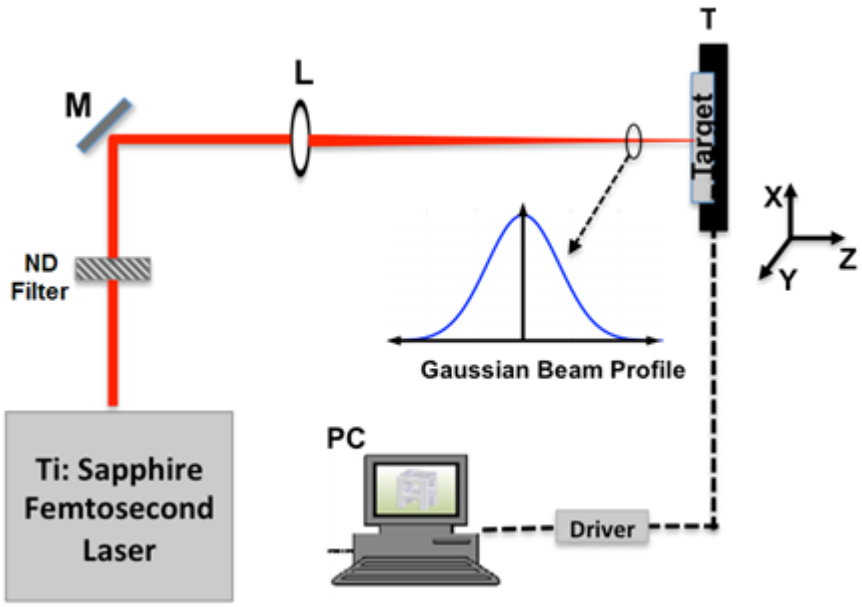

Figure 4.1. Schematic diagram of the laser irradiation set-up, M:Mirror, L: laser, T:Target [150]

Laser fluence Φ_o, is one of the most important laser ablation parameters defined in terms of laser pulse energy:

$$\Phi_o \equiv 2E_p / \pi\omega_o^2 \tag{7}$$

Where ω_o is the Gaussian beam radius *and* E_p is the ratio of laser power to pulse repetition rate (f). In order to obtain the best results and precise ablation, the distance between focal plane and the target surface should be in the Rayleigh range. Beyond the Rayleigh range, the laser beam becomes convergent or divergent. The Rayleigh range in this set-up ($2z_R$) was 1.8 mm as obtained from the following equation:

$$2z_R = \frac{2\pi\omega_0^{\,2}}{\lambda} \tag{8}$$

In order to move the samples under the laser beam, the sample is fixed on a computer-controlled ZABER T-LS80 X-Y stage with step resolution of less than 0.1 μm and a maximum linear speed

of 4000 $\mu m.s^{-1}$. The ratio of forward distance (in Y-direction) between two consecutive X-direction scans to the laser beam spot size (= $2\omega_o$=30μm) is defined as "overlap" (see Figure 4-2). For instance, an overlap of 50% (Figure 4-2a) corresponds to a Y-translation of 15 μm (=ω_o,) between two consecutive laser scans. An overlap of 0% (Figure 4-2b) corresponds to a vertical translation of 30 μm ($2\omega_o$) in Y-direction between two X consecutive scans. Finally a negative overlap of 50% (Figure 4-2c) corresponds to a vertical translation of 45 μm ($3\omega_o$) in Y direction between two consecutive scans. In this case, there is a clear distance of 15 μm between the edges of the two beams.

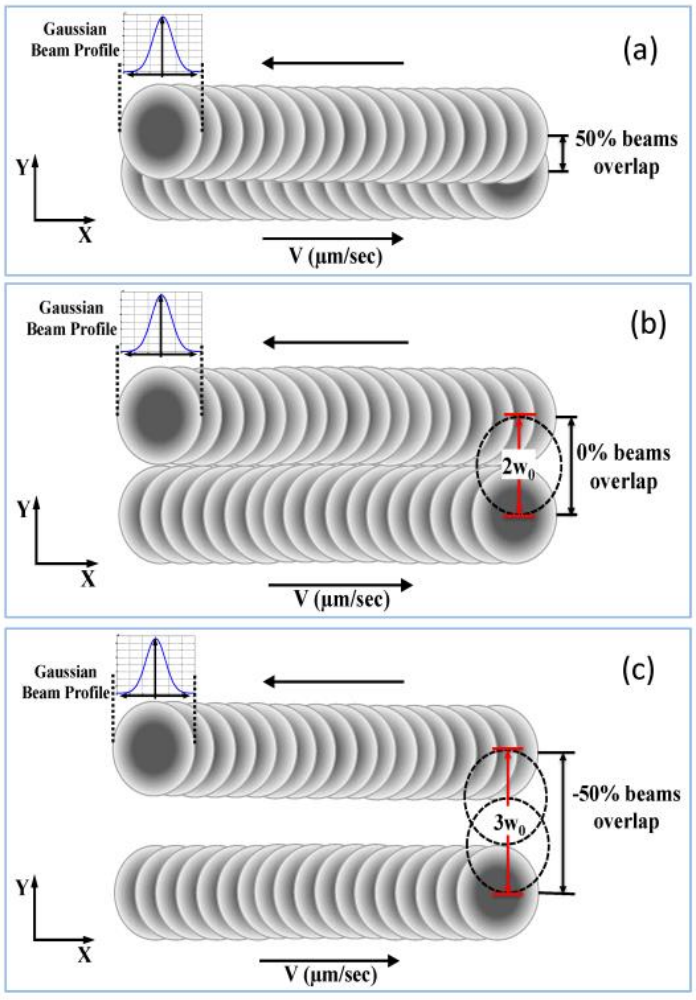

Figure 4.2. Definitions of beams overlaps in the Y-direction between two consecutive X-direction laser scans [149]

4.2.2 Thermal imprinting through hot-embossing

4.2.2.1 Template fabrication

The surface of the SS discs was ablated with femtosecond laser pulses. Three distinctly different patterns fabricated by changing the applied laser fluence and laser scan speed namely are paraboloidal, triple roughness and cauliflowered. The created parabolic pillared patterns were manufactured with a constant scanning speed of 930 $\mu m.s^{-1}$ and changing the laser fluence from 10 $J.cm^{-2}$ to 92 $J.cm^{-2}$. The triple structure has been formed by laser fluence of 480 $J.cm^{-2}$ and scanning speed of 1850 $\mu m.s^{-1}$. The ablated cauliflowered structure has been formed by laser fluence of 465 $J.cm^{-2}$ and scanning speed of 370 $\mu m.s^{-1}$. It seems that overall the cauliflowered nano/micro-structured pattern is the most superhydrophobic compared to the other nano-patterns manufactured on SS in this work. Details of the methodology to obtain these micro/nano-patterns by changing the laser fluence (Φ), scanning speed (V) and beam overlap can be found elsewhere [37][151] [150].

4.2.2.2 Hot embossing

Three morphologically and topographically different laser ablated stainless steel templates were used to duplicate their reverse patterns onto the surface of three different polymers; PLA, HDPE, and medial-PVC. Patterns were imprinted onto the surfaces of PLA and HDPE at two different temperatures, below and above the melting point of the polymers by applying low to medium embossing pressure. Processing conditions of each experimental run are listed in Table 4-1. At higher temperatures, when T_{emboss} is higher than $T_{melting}$, low embossing pressure was applied, due to the low viscosity of the molten polymers (zero and 3MPa to PLA and HDPE respectively). However, the embossing pressure must be increased when imprinting is taking place at temperatures between T_g and $T_{melting}$ of the polymers (10 MPa).

Fabricated polymer sheets with thickness of 1 mm were cut into 2.5 cm diameter discs (similar to the dimensions of the SS templates). As it can be seen in Fig 4-3, the laser ablated SS template was placed inside a metallic mold and the polymeric film disc followed by a 5 cm thick PTFE disc as a lid were placed on top. The mold was placed inside a heated hotplate with temperature equal to T_{emboss}; after 45 min the upper plate was pushed against the PTFE lid with pressure of

P_{emboss}. After applying pressure for 10 min at high temperature, the hotplate was cooled down to 10°C, while the pressure was still applied for another 30 min. After this period of time, the polymer films were pealed off easily from the template without destroying the morphology of the pattern.

Table 4.1. Materials and processing conditions for the hot embossing of PLLA, HDPE, and Medical-PVC

Material	Tg (°C)	Tm (°C)	Embossing temperature (°C)	Cooling temperature (°C)	Embossing pressure (Mpa)	Hold time (min)	Viscosity at the embossing T (Pa.s)
PLA	55	150	180	10	N/a	10	$0.02x10^5$
PLA	55	150	110	10	10	10	N/a
HDPE	-80	140	170	10	3-3.5	10	$4.25x10^5$
HDPE	-80	140	100	10	10	10	N/a
Medical PVC	-40	N/a	140	10	12	10	N/a

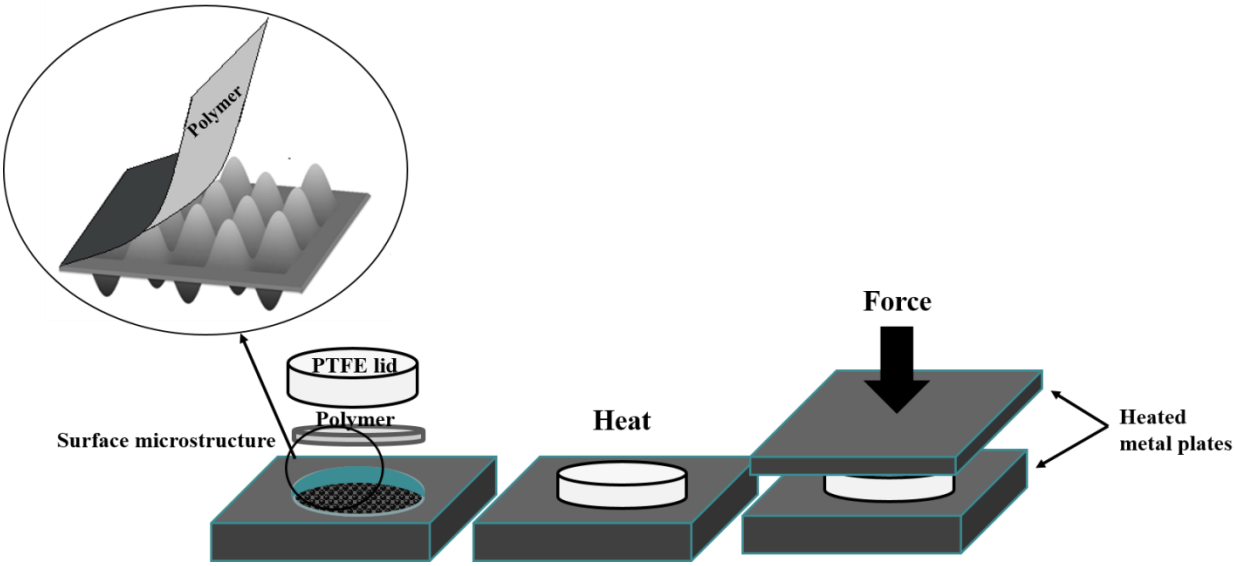

Figure 4.3. Schematic picture of the thermal imprinting through hot embossing technique used to microreplicate nanopatterns on polymeric films

4.2.3 Bacteria adhesion onto the laser ablated SH PTFE

In order to evaluate bacteria adhesion on to superhydrophobic and smooth (control) PTFE surfaces, they were incubated in Gram-positive (*Staphylococcus aureus*) and Gram-negative bacteria (*Escherichia coli*) solutions for 4 hrs at 37°C and under 80-100 rpm. Superhydrophobic samples which were used for these runs are presented in Table 4-2.

Table 4.2. Laser ablation processing conditions of PTFE samples used for bacteria adhesion and protein adsorption test. All samples were laser ablated with scan speed of 0.5 mm/s.

Sample No.	Method of ablation	Laser power of first scan (mW)	Laser power of second scan (mW)	Overlap of the first scan %	Overlap of the second scan %
1	Uniaxial	120	N/A	50	N/A
2	Uniaxial	220	N/A	50	N/A
3	Uniaxial	320	N/A	50	N/A
4	Biaxial	120	50	50	0
5	Biaxial	220	50	50	0
6	Biaxial	320	50	50	0

4.2.3.1 Bacteria inoculum preparation

Two different bacteria namely "*Staphylococcus aureus"* and "*Escherichia coli"* were purchased from Perkin Elmer (*S. aureus*-Xen29 and *E. Coli*-Xen14). *S. aureus* is a Gram positive spherical coccus and, and *E. coli* is a cylindrical Gram negative bacillus. *S. aureus* was transferred from frozen stocks into Luria broth and incubated for 10 hour at 37 °C without shaking. The bacteria were sub-cultured again in Luria broth and the optical density (OD) of the culture was measured at 595 nm after 8 hours. Knowing that an OD of 0.1 represents 1×10^8 CFU/mL of *S. aureus*, a bacteria inoculum containing 1×10^6 CFU/mL was prepared. The final concentration was verified by serial dilution and spotting on agar plate, too. All sample preparation and bacteria adhesion experiments for them were performed under aseptic conditions.

4.2.3.2 Evaluation of bacterial adhesion

Imaging of adhered bacteria: In each experimental repeat, 5×5 mm laser ablated PTFE and flat PTFE samples, immersed in 70% ethanol (prepared from anhydrous ethanol, P016EAAN, Commercial Alcohols) for 10 minutes and washed five times with sterile phosphate-buffered saline (PBS). The samples were stored in sterile containers and left under a biological safety cabinet overnight for drying. Each sample was fitted in the bottom of one well of a sterile 48-well plate. Coupons were placed with the rough surface facing up, except for the control. In the case of *S. aureus*, one milliliter of $1x10^6$ CFUs/mL bacteria inoculum was added to each well and incubated at 37°C for 4 hrs under shaking with 80 rpm. In case of Escherichia coli, one milliliter of $1x10^8$ CFUs/mL bacteria inoculum was added to each well and incubated at 37°C for 6 hrs under shaking with 80 rpm. Each coupon was thoroughly rinsed by consecutive immersion in five sterile PBS vials, 1 minute in each. For fluorescence microscopy, samples were stained with green fluorescent nucleic acid stain (Syto 9; one of the stains included in LIVE/DEAD Bac light bacterial viability kit, L7012, Molecular Probes Inc.) according to the manufacturer's instructions. Syto 9 is a nucleic acid stain that can penetrate both viable and nonviable bacteria.

Coupons were rinsed with distilled water and analyzed with a fluorescence microscope with an FITC filter (Axioskop 2 plus, Carl ZeissMicroimaging, Inc.). For SEM imaging, the coupons were fixed in a 2.5% (vol/vol) glutaraldehyde solution (diluted with distilled water from glutaraldehyde 25%, Sigma-Aldrich G6257) for 1 hour, rinsed with water, and dehydrated with graded ethanol concentrations (30, 60, 85, and 100%). Coupons were stored in a desiccator and coated with gold before imaging.

Bacterial adhesion behaviors were investigated within 4 and 6 hrs (for *S. aureus* and *E. coli* respectively), and each test was repeated three times. Each time two samples with the same patterns were incubated; one sample was used for SEM imaging and the other sample for fluorescence microscopy and fluorescene confocal microscopy. Details of these methods and typical interpretation of these images are discussed in Chapter 6.

4.2.4 Protein adsorption of the laser ablated Superhydrophobic PTFE

In order to evaluate protein adsorption on superhydrophobic PTFE and smooth (control) PTFE surfaces, the surfaces were incubated in BSA and IgG protein solutions and also in blood plasma

proteins for 4 hrs at 37°C and under 80-100 rpm. Superhydrophobic samples which were used for these runs are presented in Table 4-2.

To investigate protein adsorption, bovine serum albumin (BSA) conjugated to fluorescent tags and Immunoglobulin G (IgG2a-FITC), from mouse plasma conjugated to fluorescent tags were purchased from Sigma Aldrich. These two proteins were chosen as model proteins. After placing the PTFE (laser ablated and smooth) samples in 6-well culture plates (Corning Inc.), 2 mL of phosphate-buffered solution (PBS, pH 7.4) was added into each well. In order to let the samples to rich equilibrium, samples were left in PBS for 30 min. After removing the samples from PBS, the samples were incubated in BSA solution (1 $mg.mL^{-1}$ BSA in PBS) at 80-100 rpm and 37 °C in a humidified 5% CO2 atmosphere. After 4 hrs of incubation, PTFE samples were dipped into PBS for three times and dried in the air. The same protocol was used for the other protein test, simply instead of BSA solution, IgG solution was made and applied on the PTFE samples.

The interaction of human plasma proteins with superhydrophobic PTFE surfaces in vitro was evaluated by preparing blood plasma from fresh human whole blood. The fresh venous blood was collected from two healthy volunteered adults. The protocol was approved by the University of British Columbia clinical ethical committee. Blood plasma was prepared by centrifuging citrate anticoagulated (using sodium citrate:blood 1:9) blood at 800 rpm for 15 minutes at room temperature.

4.3 Surface Characterization

The wetting behavior of the laser ablated and imprinted samples was evaluated by measuring their contact angle with distilled, deionized water. To evaluate the wettability, the samples were first ultrasonically cleaned in the mixture of water and acetone, and then their CAs were measured using the static sessile drop method.

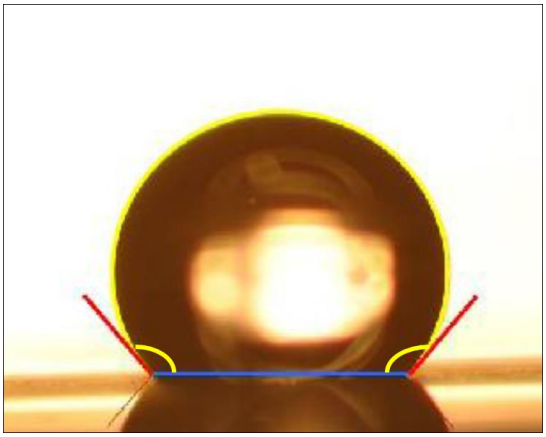

Figure 4.4. A typical droplet image and the measurement of contact angle

Droplets of water of volume 4-5 μL were dispensed on the respective surfaces with a pipette. Digital images of the water droplet on the surfaces were taken with a Nikon D90 digital camera. The CAs were determined by analyzing droplet images with the image processing methods of ImageJ.

Contact angle hysteresis (CAH) measurements were performed using dynamic sessile droplet method. This method determines the advancing and receding contact angles by growing and shrinking a water droplet on the surface. The camera was set to capture three images per second for advancing and receding contact angle analysis. The difference between the advancing and receding angle is the contact angle hysteresis.

The morphology of the nano/micro structured surfaces were analyzed by taking SEM (Scanning Electron Microscopy) images. The topography and roughness of the patterns was measured using a Wyko NT3300 Optical Profilometer. Roughness factors and height of the peaks and depth of the valleys were determined with an optical profilometer. To evaluate the wettability, the samples were first ultrasonically rinsed with mixture of water and acetone, and then their static and dynamic CAs were measured using the sessile drop method. Water droplets with volume of 4μl were placed on the laser ablated and micro/nano imprinted surfaces. The water CAs of the samples were determined by analyzing droplet images with the ImageJ's image processing methods.

The CA and CAH of uniaxially scanned surfaces are highly dependent to the direction of the channels. Hence, the CAs and CAHs of all uniaxially scanned surfaces were measured along the direction of the channels.

X-ray photoelectron spectroscopy (XPS) located in AMPEL "Advanced Materials Process Engineering Laboratory" was used to compare the surface chemistry of smooth and laser ablated PTFE. Also, it was used to determine if laser ablation has affected the molecular structure (chemistry) of the top layer of PTFE sample. XPS analysis suggested that the chemistry of smooth and ablated PTFE surfaces was practically similar.

In order to quantify the bacteria adhesion and protein adsorption on the surface, five random images were taken from each sample using a fluorescent light microscope with FITC filter (Zeiss Axioskop 2 plus, Carl Zeiss Microimaging Inc.). The adherent protein/bacterias were quantified based on the surface fluorescent light intensity of images using ImageJ software. Results were normalized to the flat surface of PTFE (control substrates) for comparison. Also in order to have a better understanding of bacteria adhesion onto different layers of hierarchical surface of PTFE samples, 3D images using confocal microscopy were taken. In order to determine plasma protein adsorption on to the surface of superhydrophobic PTFE and smooth, fluorescent microscopy and ATR-FTIR were used.

ATR-FTIR was used to determine plasma protein adsorption onto PTFE samples. FTIR spectroscopy is one of the classical methods for structure determination of small molecules, such as protein structure. It provides information about the secondary structure content of proteins. FTIR spectroscopy operates by emitting infrared radiation on a sample and detecting which wavelengths of radiation in the infrared region of the spectrum are absorbed by the sample. Each compound has a specific set of characteristic absorption bands in its infrared spectrum. Characteristic bands found in the infrared spectra of proteins and polypeptides include 9 characteristic bands named amide A, B, I, II ... VII. Amide I and amide II bands are two major bands of the protein infrared spectrum and they arise from the amide bonds that link the amino acids. The amide I band is mainly associated with the C=O stretching vibration and is directly related to the backbone conformation. Amide I band is found between 1600 and 1700 cm^{-1}, near 1650 cm-1. Amide II results from the N-H bending vibration and from the C-N stretching vibration. This band is found in the 1510 and 1580 cm^{-1} region, near 1540 cm^{-1}. The presence of amide I and amide II bands at 1650 cm^{-1} and 1540 cm^{-1}, respectively, is an indicative that protein was onto samples surface after the adsorption experiment.

One drawback of infrared spectroscopy of protein adsorbed samples is the strong absorbance of water in the mid-infrared spectral region (near 1645 cm-1) which overlaps the important amide I band. In order to avoid this conflict, the samples have to be perfectly dried prior to FTIR.

Chapter 5: Ultra-short Laser Ablation

PTFE is a well-known polymer with very low surface energy which makes this polymer suitable for developing superhydrophobic surfaces for manufacturing smart materials and biomaterials. There are several methods for micromachining of PTFE without altering the bulk composition such as ultrashort pulsed laser ablation. Femtosecond laser ablation is an accurate and effective method to produce controlled roughness on the surface of PTFE due to the negligible heat conduction produced during laser irradiation and the minimized energy loss into the sample.

Laser parameters such as laser peak fluence, scan speed and two consecutive laser beam overlap strongly affect the geometrical details of the morphology of the irradiated PTFE surface. Laser parameters determine the energy density that the surface receive. The minimum energy density required to initiate material removal is called the ablation threshold, Φ_{th}. In order to initiate laser ablation, energy density has to be above the ablation threshold. Laser ablation just above the fluence threshold is called "gentle ablation". At this point, the ablation rate is quite low and the created patterns are nearly smooth. At higher laser fluence, "strong ablation" occurs and regular surface roughness starts appearing[152].

A systematic, detailed experimental study on the effects of laser parameters on the fabricated morphology of uniaxially scanned PTFE substrates was performed. The effect of laser fluence, ablating speed, and laser overlap was studied in this work. While several investigations have used femtosecond laser ablation to create superhydrophobic surfaces on PTFE successfully, for the first time, we managed to find an effective way to produce uniform morphology in all directions on a laser ablated PTFE surface through biaxial scanning the PTFE surface. In addition, the effect of these uniaxial and biaxial patterns on the surface wetting behaviour is investigated by varying the laser parameters to identify the patterns that maximize the superhydrophobicity of PTFE surface.

Essentially the XPS analysis of laser ablated PTFE sample is explained in section 5.1. The uniaxial laser scanning of PTFE is studied in chapter 5.2. The effects of laser parameters on the laser ablated surface morphology was investigated; laser fluence and laser scan speed in section 5.2.1, and laser beams overlap in section 5.2.2. In section 5.3 biaxial laser scanning of PTFE was

studied. Two different types of biaxial scanning were applied. Each was studied in a separate section, 1- biaxial laser ablation with identical scans in section 5.3.1, and 2- Biaxial laser ablation with non- identical scans in section 5.3.2. Wetting behaviour of the uniaxial scanned PTFE is reported in section 5.4.1, and wetting behaviour of biaxial scanned PTFE is reported in section 5.4.2. In section 5.5 the laser ablation of poly urethane films is briefly explained.

5.1 XPS Analysis

First the surface chemistry of PTFE surface was examined after laser ablation in order to check for chemical changes. XPS analysis suggested that laser ablation doesn't change the chemical properties of the PTFE surface. The chemistry of the ablated and flat (untreated) PTFE surfaces were nearly similar. The results are summarized in Table 5-1. The C 1s spectra for both treated (laser ablated PTFE) and untreated PTFE (flat) show the presence of couple of distinct types of C species. The first peak centered at ~284.5 eV is related to the surface contaminations (C–C and –CH2 groups), while the second peak which is centered at 292.5 eV is assigned to the backbone of the PTFE macromolecule (a carbon with two fluorine, part of –CF2 carbon groups). While the concentration of –CF2– groups was increased in the laser ablated samples (25.6%) compared to the untreated material (27.2%), the total percentage of the C 1s peaks was decreased in the ablated PTFE from 48.9% to 46.7%.

Table 5-1. Atomic ratios of untreated and laser ablated samples.

PTFE sample	F1s %	C_{-CF2-}	C_{-CH2-}	C1s %	O_2%	F/C_{-CF2-}
Flat	40.2	25.6	23.3	48.9	7.6	1.57
Laser ablated at laser fluence of 31.0 J/cm^3	44.3	27.2	19.5	46.7	7.4	1.63

Due to surface etching, the percentage of undesired –CH2– groups were lowered in the ablated surface compared to flat surface (23.3% decreased to 19.5%). Also, the atomic percentage of fluorine peak (centered at 677–695 eV) was increased from 40.2% in the untreated PTFE to 44.3% in the ablated PTFE. As result, F/C atomic ratio stayed constant at about 1.6 before and after laser ablation. XPS results confirms that that the chemistry of flat and laser ablated surfaces

of PTFE were similar, which means that the superhydrophobicity promoted by the ablated rough surface is only due to topographic features and not to any changes in the surface chemistry.

5.2 Effect of Uniaxial Scan on Surface Morphology

5.2.1 Effect of laser fluence and scan speed on the surface morphology

Figure 5-1 shows SEM images uniaxial scanned PTFE samples (laser lines are parallel). Laser peak fluence was set to be in the range of 5.7–51.0 J/cm^2 (laser power of 40–360 mW), while the scanning speed and laser overlap of the scans were kept constant at 0.25 mm/s and 50% respectively. Depending on the laser fluence (while other laser parameters are constant), channels of different width and height are formed. At the low laser peak fluences of 5.7 J/cm^2 and 11.3 J/cm^2 (Fig. 5-1-a and -b), only fine microstructures are formed (gentle ablation), as material is slightly removed from the PTFE. The height of the formed channels/grooves is of the order of a few tens of microns and the scanned area is still relatively smooth. However, increasing the laser fluence at constant scan speed, develops deeper ablated grooves and more well-defined channel (with the height of around 100 µm, (Fig. 5-1c)). These channels were also partially covered with submicron and nano scale grains.

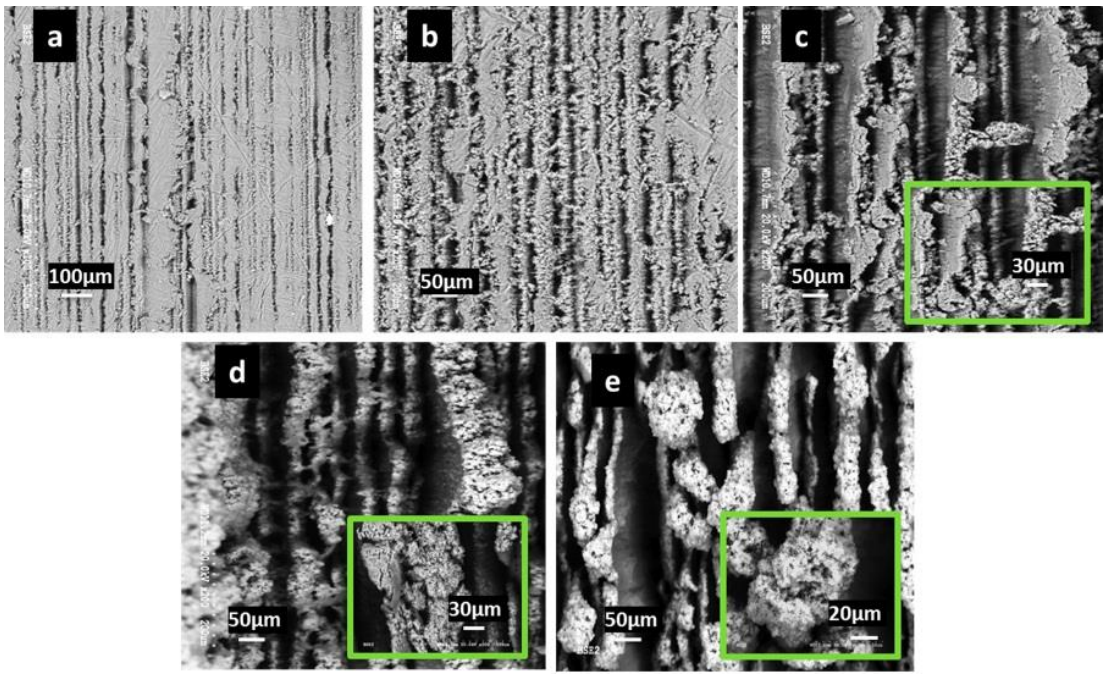

Figure 5.1. SEM images of the various fabricated PTFE substrates using different levels of laser fluence at constant scanning speed and laser overlap (V=0.25 µm/s and overlap=50%) (a) Φ_0=5.7 J/cm^2, (b) Φ_0= 11.3 J/cm^2, (c) Φ_0=17.0 J/cm^2 (d) Φ_0=34.0 J/cm^2, (e) Φ_0=51.0 J/cm^2

Further increase of the laser fluence to higher numbers e.g., 51.0 J/cm^2, (Fig. 5-1-e), develops channels with heights in the order of few hundreds of microns (340 µm) in combination with submicron and nano scale roughness, which forms on the top and sides of the micro-channels.

Figure 5-2 depicts SEM images of laser ablated PTFE samples uniaxial scanned at the constant laser fluence of 34.0 J/cm^2 (power of 240 mW) and constant beam overlap of 50% (as explained in Fig 4-2), while the laser scan speed varies in the range of 0.25–2.0 mm/s. Increasing the laser scan speed basically decreases the number of pulses received per spot. Decreasing the number of pulses per spot, decreases the received laser energy of the spot and this has a direct effect on the height and shape of the roughness. For example, at the laser fluence of the 34.0 J/cm^2, increasing the scan speed from V = 0.25 mm/s to V = 2.0 mm/s, decreases the height of the channels from 180 µm to 45µm.

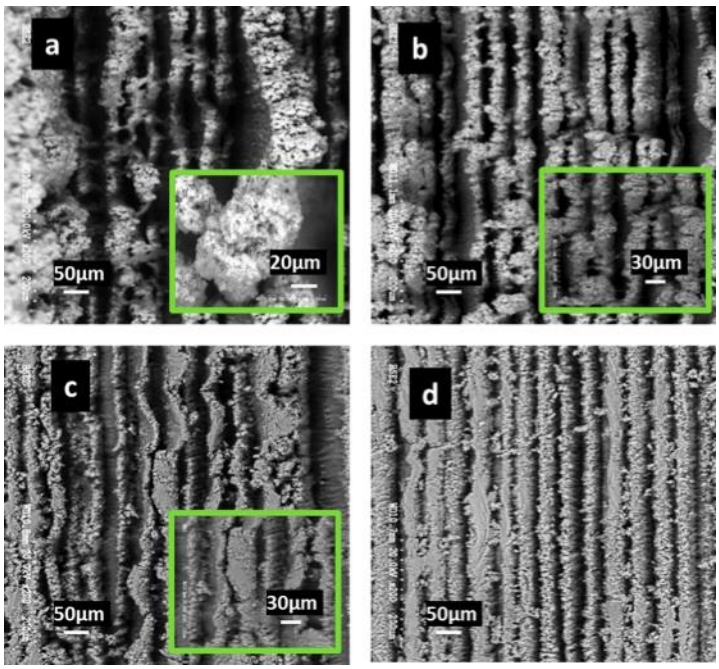

Figure 5-2. The effect of increasing the laser scan speed, while keeping the laser fluence and overlap constant at Φ_0=34 J/cm^2 and 50%, respectively; (a) *V*=0.25mm/s, (b) *V*=0.5mm/s, (c) *V*=1.0mm/s, (d) *V*=2.0mm/s.

Figure 5-3 summarizes the SEM pictures of laser ablated PTFE samples on a single graph in terms of the laser fluence and the laser scan speed at constant 50% beam overlap. The SEM images were captured under the magnification of 200X. The effects of increasing the laser

fluence and decreasing the scan speed are similar as both increase the laser energy received per spot and result into the formation of more well-defined channels with bigger height. The morphology and topography of the laser ablated patterns have a significant impact on the wettability of the surface as discussed below.

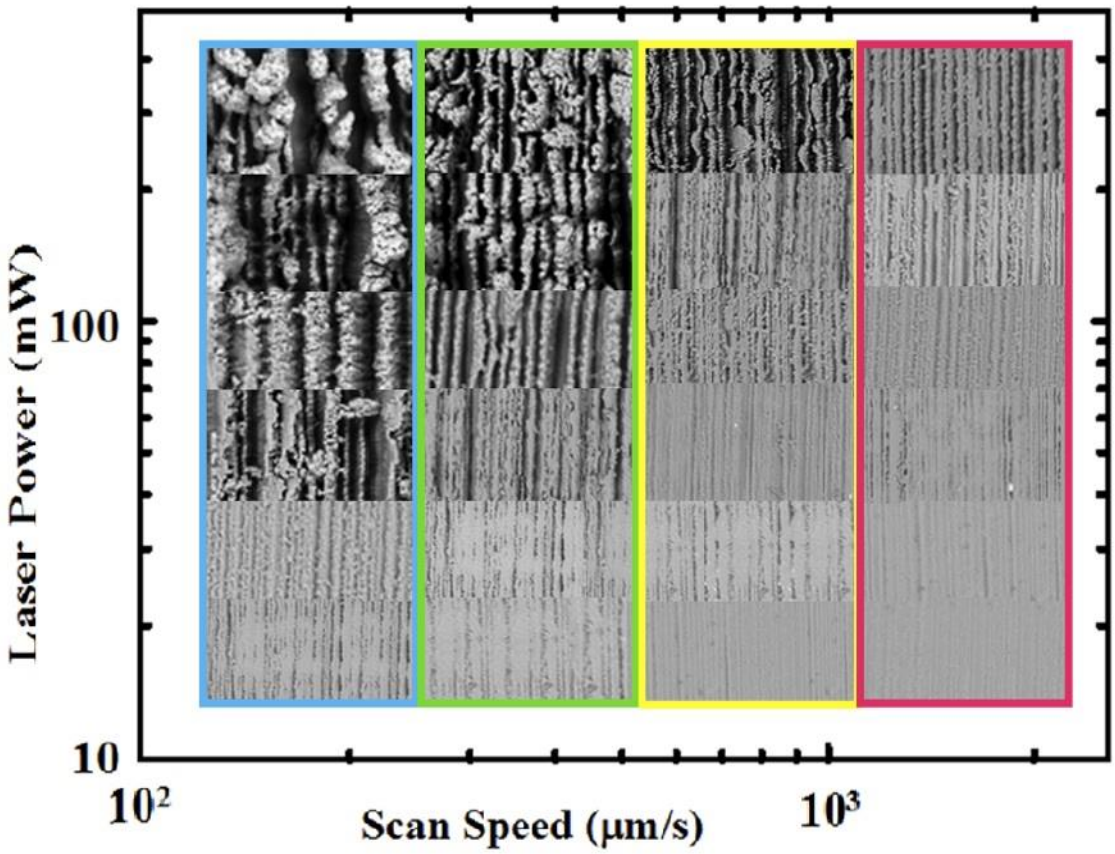

Figure 5-3. Formation of micro/nano-patterns on PTFE substrates using different laser powers and scanning speeds at constant 50% overlap

5.2.2 Effect of overlap on the surface morphology

Decreasing the overlap between two consecutive laser beams has significant effects on the morphology and topography of the created patterns. Changing the overlap has direct effects on the channels' height, distance between the channels, and the size of the dual scale roughness appearing on top of the channels. This can be explained by the fact that decrease of the overlap, causes a decrease in the amount of energy absorbed by the surface. At high laser beams overlaps, some parts of the surfaces are scanned twice. Fig 5-4 displays the effect of decreasing the two

consecutive beam overlap from 50% to 0%, and then to −50% (as defined in Fig 4-2) at two different levels of the laser peak fluence while the scan speed is constant.

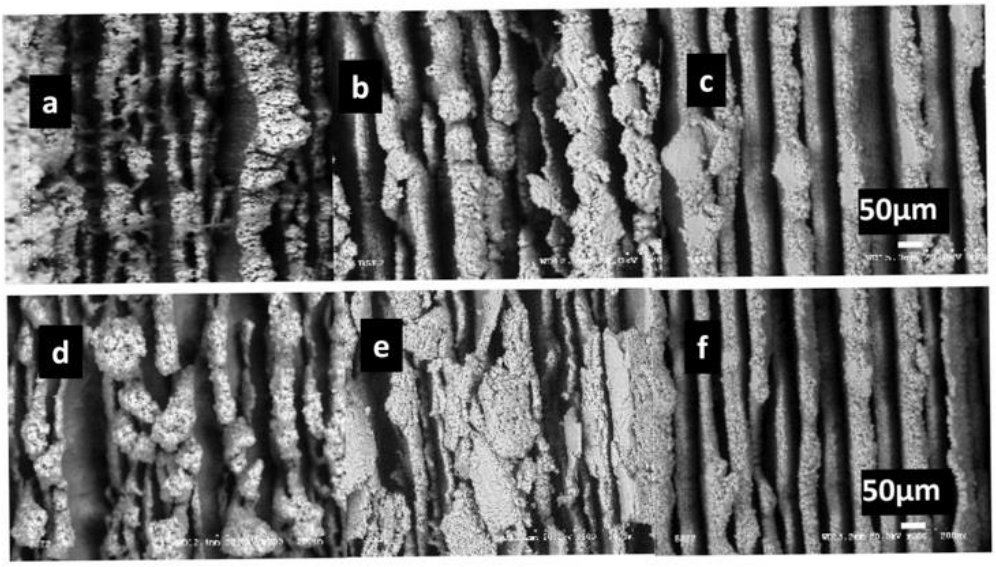

Figure 5-4. The effect of decreasing the overlap on the laser ablated surface of PTFE. For the upper images (a-c), Φ_0=34.0 J/cm^2, V=0.25 mm/s (a) Overlap= 50% (b) Overlap= 0% (c) Overlap= -50%. For lower images (d-f), Φ_0= 51.0 J/cm^2, V=0.25 mm/s (d) Overlap= 50% (e) Overlap= 0% (f) Overlap=-50%

5 .3. Effect of Biaxial Scan on Surface Morphology

As was shown above, with scanning in a single direction (uniaxial scan), channeled morphology with anisotropic wetting behaviour may be developed. These surface morphologies are presenting direction-dependent wettability i.e. parallel versus vertical to the channels. To produce a homogeneous morphology which presents uniform wettability independent of direction, biaxial scanning is examined in this section. The scans in the horizontal and vertical directions are named as pass 1 and pass 2 respectively as shown in Figure 5-5. Biaxial scan creates pillared morphology with outstanding non-wetting behaviour in all directions. Two different types of biaxial scans were performed on PTFE substrates; identical and non-identical laser fluence for pass 1 and 2.

5.3. 1 Biaxial laser ablation with identical scans

The first set of samples were fabricated by biaxial scans using identical laser parameters values (laser fluence, scan speed, and overlap) for both passes (1 and 2). The SEM images of the created

morphologies are displayed in Figure 5-5. The laser peak fluence was set to be in the range of 11.3 to 51.0 J/cm^2 (laser power of 80 to 360 mW), while the scan speed and overlap were set to be constant at of 1.0 mm/s and -100% respectively. As the laser fluence of passes 1 and 2 increases (to a same level), pass 2 overwrites the morphology already ablated by pass 1.

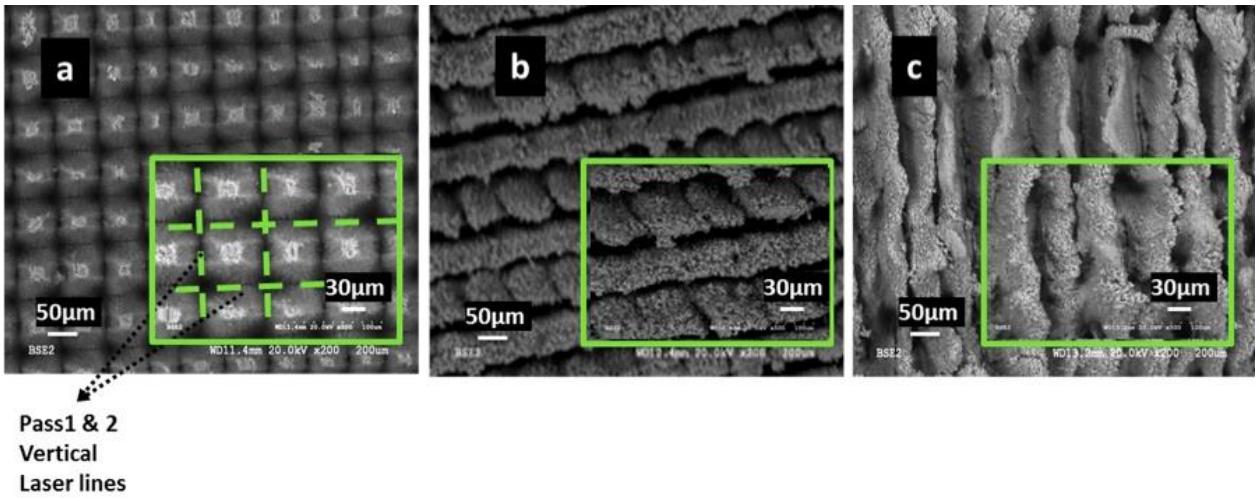

Figure5-5. The effect of biaxial scan (same laser peak fluence for both scans) on the formed micro-nano patterns on PTFE substrates using (a) Φ_0=11.3 J/cm^2, (b) Φ_0=34 J/cm^2 (c) Φ_0=51.0 J/cm^2, and scan speed, V=1.0 mm/s and overlap=-100% respectively for all images.

The effect of identical biaxial scan at lower laser fluence is presented in Figure 5-5, in which channels in both vertical and horizontal directions forming a pillared morphology with rounded tops. Figure 5-5-b and 5-5-c show clearly channels only in the vertical direction, as pass 2 has overwritten the channels created during the horizontal –pass 1 scan. Therefore, in order to preserve the morphology created by the first pass, a lower laser fluence should be applied in the second scan. It is noted that in all three SEM pictures depicted in Figure 5-6, the laser overlaps of both passes are unchanged.

Figure 5-6 presents the effect of two consecutive beam overlap on the morphology of biaxial scanned PTFE. At negative values of beam overlaps (e.g., -50% or-100%, when there is a gap between two consecutive laser lines), biaxial scan creates a mesh-like structure of squared pillars on the surface, as shown in Figure 5-6-b and -c. As it is presented in Figures 5-6, overlap between the scan lines determines the size of the square-shaped pillars with rounded tops. At the constant laser fluence of 11.3 J/cm^2 and scan speed of 1.0 mm/s, when the overlap between the two laser lines decreases from 0% to -50%, the height and the side length of the squares are

about 40μm and 42 μm respectively. By further increasing the distance between the laser lines from -50% to -100%, a very well defined square-shaped pillared structure is created on the surface. While the height of the squares doesn't change much, their side length increases from 40 to 50-60 μm.

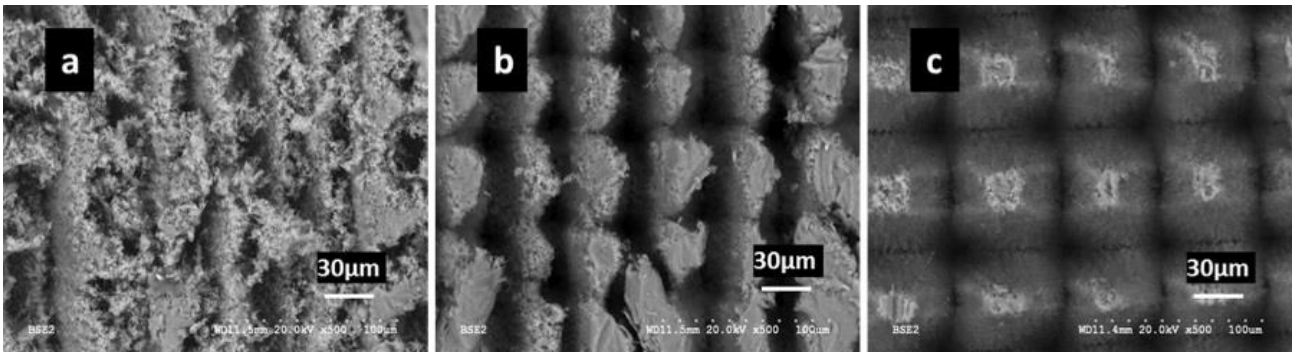

Figure 5.6. The effect of the beam overlap on the characteristic dimensions of micro patterns formed on PTFE using biaxial scan at the constant laser fluence of Φ_0=11.3 J/cm^2 and scan speed of V=1mm/s (a) overlap=0%, (b) overlap=-50%, (c) overlap=-100%

5.3. 2 Biaxial laser ablation with non- identical scans

In the second series of biaxial scanned surfaces, the laser fluence of pass 1 and pass 2 are set to be different. In order to avoid the overwriting of the morphology created during pass 1, laser fluence of the second scan was set to be smaller than that of the first scan. For all these runs, the laser fluence of pass 2 is kept constant at the low level of 7.1 J/cm^2, while the laser fluence of pass 1 was changing between 11.3 and 51.0 J/cm^2. Reducing the laser fluence of the second pass dramatically increases the level of nano and submicron scale roughness on the micro channels and creates a porous structure on the surface. The high density of nano-grains (as it can be seen in Figure 5-7) results into superhydrophobicity by promoting Cassie-Baxter state. This affects superhydrophobicity dramatically as it will be discussed below.

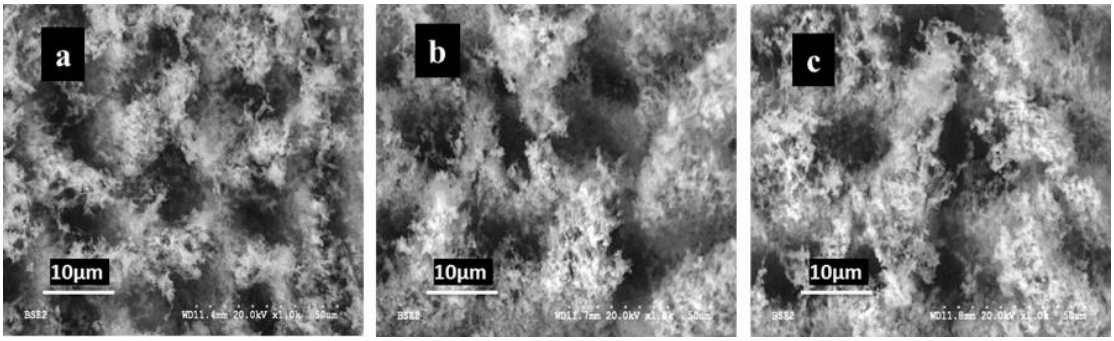

Figure 5-7. The effect of biaxial scan using a low fluence laser beam of pass 2 on the formed PTFE surface morphology. The laser fluence of pass 2, scan speed of pass 1 and 2, and overlap of pass 1 and 2 are kept constant at Φ_0, pass 2=7.1 J/cm^2, 1.0 mm/s

5.4 Surface Wettability

5.4.1 Wettability of the uniaxially scanned samples

The effect of laser parameters on the wetting behaviour of the laser ablated PTFE was systematically studied. Results confirm that by increasing the laser fluence, the obtained CA

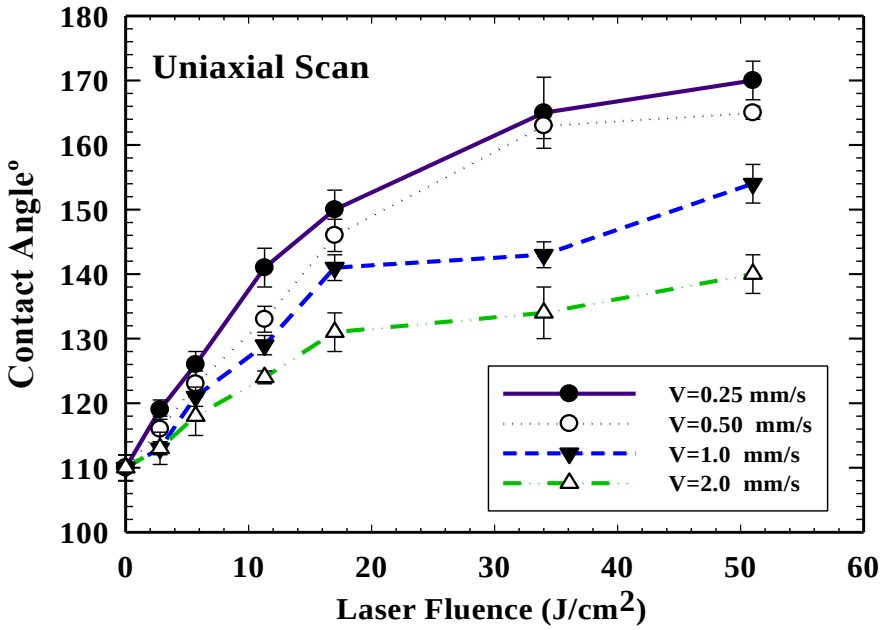

increases as well.

Figure 5.8. The contact angle of the laser ablated PTFE surface as function of laser power and scan speed at beam overlap of 50%.

The appearance of the sub micron and nano- scale features on top of channels is responsible for the increased CA. The nano/micro dual scale structure on the substrate facilitates the formation of Cassie–Baxter states. The effect of laser fluence on the contact angle (CA) of uniaxially scanned PTFE substrates scanned at different scan speeds and constant overlap (50%) is displayed in Figure 5-8. It is shown that in a uniaxial scan, when the laser fluence is above 28 J/cm^2 (200 mW) and scan speed is below 0.5 mm/s, the obtained CA can be as high as 160°.

For uniaxially scanned substrates, the contact angle hysteresis (CAH) in the direction of the channels is different from CAH in other directions. The CAH along the channels direction dramatically decreases with increase of the laser fluence. Increasing the laser fluence from 5.7 to 17.0 J/cm^2, decreases the CAH from 70° to almost 14° (at the constant scan speed of 0.25 mm/s). Although further increase of the laser fluence still increases the CA of the samples, it does not decrease the CAH anymore. At high laser fluence of 34 and 51.0 J/cm^2, the measured CAH were 16° and 19° respectively. The high depth of the channels, which cause droplet pinning is "blamed" for the increase of the CAH (Figure 5-9).

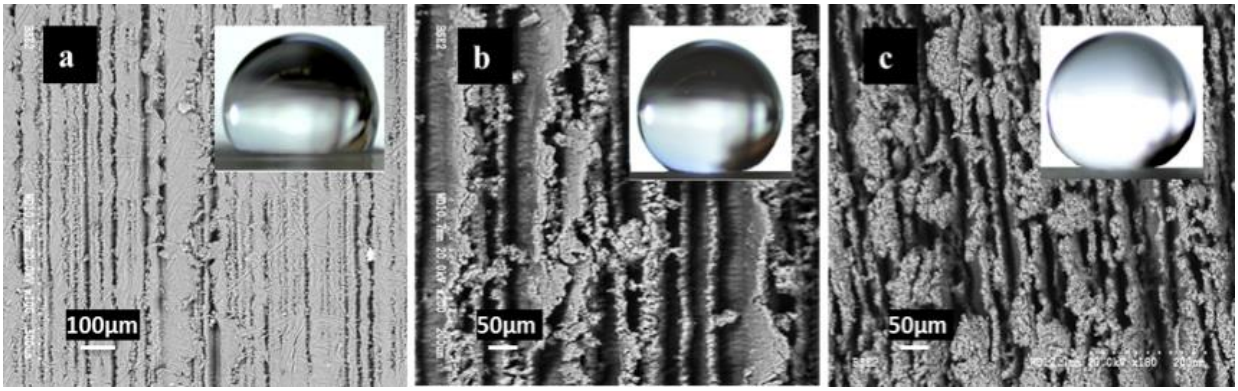

Figure 5-9. The effect of channel height on the wettability of PTFE samples (a) Φ_0= 5.7 J/cm^2, V= 0.25 mm/s, channel depth= 31µm, CA=130°, CAH > 70° (b) Φ_0 = 17.0 J/cm^2, V=0.25 mm/s, channel depth=145µm, CA=150°, CAH=10°, (c) Φ_0 = 51.0 J/cm^2 , V= 0.5 m

Table 5-2 shows the effect of overlap on the CAH of laser ablated PTFE samples for laser fluence higher than 14.0 J/cm2 (laser power of 100 mW). The beam overlap is decreased from 50% to -50%, while the laser fluence and the scan speed are kept constant. Increase of the distance between the laser lines (decrease of the overlap) from 15µm (50% overlap) to 45µm (-50% overlap), keeps the CA of the samples almost untouched, while it dramatically increases the

CAH. The high CAH can be explained by the fact that the wide channels may trap the small droplets, preventing easy roll of the droplet off the surface. Also, it can be described by considering the un-scanned area between the channels which increases by decrease of the scan overlap and it is responsible for droplet pinning onto the surface.

Table 5.2. The effect of laser beam overlap on the Contact Angle (CA) and Contact Angle Hysteresis (CAH) (the latter in the parenthesis) of the laser ablated PTFE surfaces at different levels of laser power/fluence at the constant scan speed of 0.25 mm/s.

Laser Power (mW) **(Lase Fluence J/cm^2)**	**120** **(17.0)**	**240** **(34.0)**	**360** **(51.0)**
Overlap 50% (ω_0)	CA=146±2 CAH=14 ±1	CA=153±3 CAH=16 ±2	CA=160±1 CAH=19 ±1
Overlap 0% ($2\omega_0$)	CA=150±1 CAH=22 ±2	CA=157± 2 CAH=27 ±1	CA=164±2 CAH=29 ±2
Overlap -50% ($3\omega_0$)	CA=160±3 CAH= 25 ±3	CA=163±1 CAH=37 ±4	CA=170±2 CAH=46 ±3

5.4.2 Wettability of biaxial scanned samples

Uniaxial scan creates channeled morphology on the surface of polymeric materials. As a result, the produced superhydrophobicity is anisotropic and wetting behaviour depends on the water droplet moving direction. One of the main advantages of biaxial scan over uniaxial scan (for polymeric substrates) is the creation of isotropic patterns with high CAs and low CAH similar in all directions. As explained earlier, biaxial scan creates micro pillars covered with high level of sub micron and nano scale features, which increases the amount of air trapped in the interface under the droplet, thus forming Cassie-Baxter states easier. Figure 5-10 displays the CAH of laser ablated PTFE surfaces fabricated by using identical laser characteristics (laser fluence, scan speed, and laser line overlaps) for both passes.

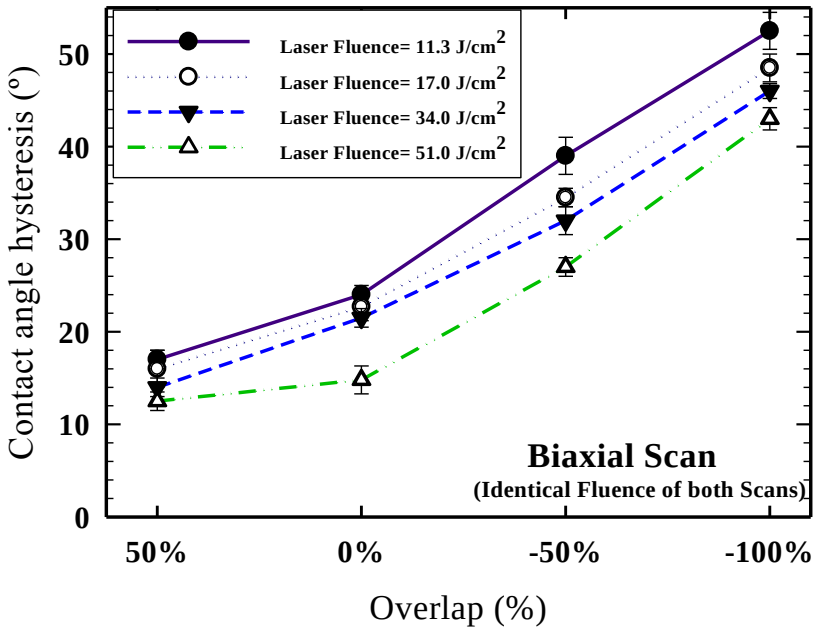

Figure 5.10. The contact angle hysteresis (CAH) of PTFE biaxially scanned using different levels of laser power (same for both scans) and overlap.

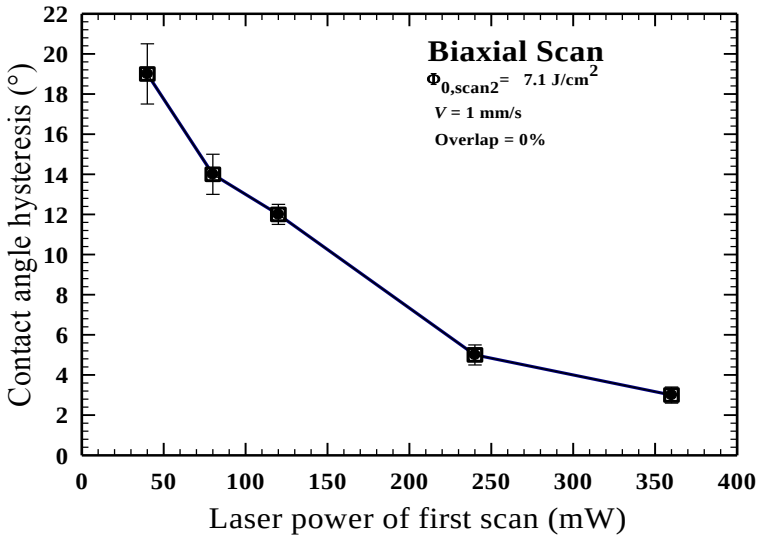

Figure 5-11. The contact angle hysteresis of biaxial scanned PTFE substrates, with constant laser fluence of pass 2 at 7.1 J/cm^2; the overlap and scan speeds of both passes are set to 0% and 1.0 mm/s respectively

In this type of biaxial scanned samples (identical), the laser fluence (power) and overlap vary in the range of 7.1 J/cm^2 to 51.0 J/cm^2 (50 mW to 360 mW) and 50% to -100% respectively (scan speed was kept constant at 1 mm/s). Unlike uniaxial scans, biaxial scans are capable of

presenting very high CA even at low levels of laser fluence. It can be seen from Figure 5-10 that even at the low laser fluence of 7.1 J/cm^2 (laser power of 50 mW) and high scan speed of 1 mm/s, with the overlap of 50%, the CA can be as high as 155º. It is noted that under the similar ablation conditions, the contact angle for uniaxial scan did not exceed 125º. Although, identical-fluence biaxial scan decreased the CAH of the PTFE to lower numbers compared to uniaxial scan, it was not possible to lower the CAH to below 10º. At laser fluence of 51.0 J/cm^2 (laser power of 360 mW) and overlap of 50%, CAH of identical biaxial scanned PTFE is as low as 12º, while under the same conditions, CAH for uniaxial scan is 19º. Besides the laser fluence, the scan overlap also has a dramatic effect on CA and particularly CAH of biaxial scanned polymer and thus should be carefully selected. Increase of the overlap in biaxial scan has very similar effects on the surface wettability as it does in uniaxial scan. Decreasing the overlap from 50% to −100% largely increases the CAH, while didn't change the CA noticably. This is again due to the un-scanned area between the channels which increases by decrease of the scan overlap and it is responsible for droplet pinning onto the surface.

In biaxial scan, using a lower laser fluence in the second pass (to avoid overwriting the morphology ablated by the first scan) would considerably increase the level of nano/micro dual scale structure on the surface, which in return increases the amount of air trapped in the interface under the droplet, and promotes Cassie-Baxter states. As a result, the level of superhydrophobicity significantly increases as well.

The contact angles of non-identical biaxial scanned samples (with low-fluence second pass) are extremely high. In this method, by scanning the PTFE surface while the laser fluence of first pass is higher than 14 J/cm^2 (laser powers of 100 mW) and the laser fluence of second pass is around 7.1 J/cm^2 (laser power of 50 mW), CAs with values higher than 160° are obtained. The CAH of these samples are significantly lower compared to ant other laser ablated PTFE sample. Figure 5-11 shows the CAH for non-identical biaxial scanned PTFE samples as a function of the laser fluence of the first scan. As seen in the graph, the CAH of the biaxially scanned samples can reach values as low as 3°. This is due to the increased amount of nano-scale features; which air pockets get trapped within them. This results into decreasing the pinning strength of the droplet to the surface which stimulates the water droplet rolling on the surface.

Figure 5-12 compares the three laser ablated PTFE samples scanned with three above mentioned methods (uniaxial, identical biaxial, and non-identical biaxial) under the same laser fluence, laser

scan speed, and overlap. By switching from uniaxial scan to identical biaxial scan to non-identical biaxial scan, the CA of PTFE substrates significantly increases and CAH of the samples dramatically decreases. This figure shows the significantly different morphologies as well as the significantly different wettability of the PTFE surfaces which decreases by changing the channel structure into the mesh-like structure.

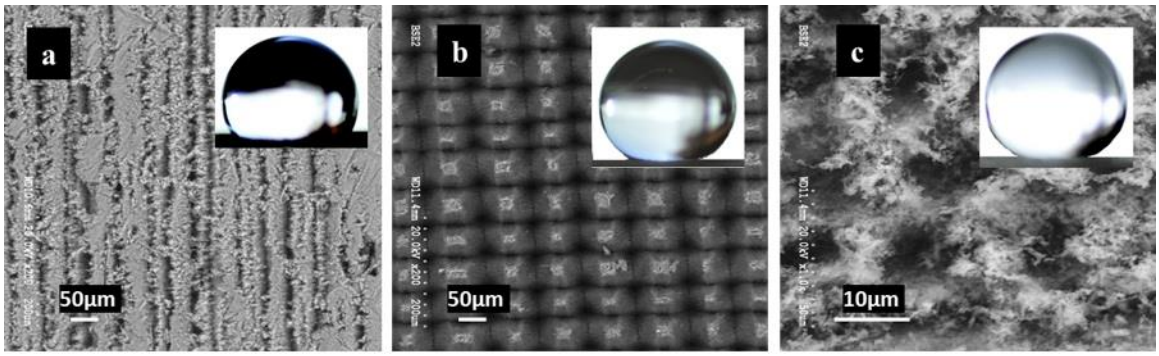

Figure 5.12. Comparison between the superhydrophobicity of PTFE surface containing (a) uniaxial channelled morphology, Φ_0 = 11.3 J/cm^2, V= 1000 µm/s, CA=135°, CAH > 60°, (b) Mesh-like pattern/ identical laser characteristics for the two passes, $\Phi_{0,\,scan\,1} = \Phi_{0,\,scan\,2}$ = 11.3 J/cm^2, V = 1000 mm/s, overlap =−100%, CA = 152°, CAH≈30°, (c) mesh-like pattern/non-identical laser characteristics for the two passes, $\Phi_{0,\,scan\,1}$ = 11.3 J/cm^2, $\Phi_{0,\,scan\,2}$ = 7.1 J/cm^2, V = 1000 mm/s, CA > 160° and CAH < 12°

5.5 Femtosecond Laser Ablation of Polyurethane

Superhydrophobicity cannot always be obtained through adding roughness and without applying low surface energy modifications such as fluoroalkylsilane coatings. Usually hydrophilic polymers e.g. PMMA and polyurethane are not stable at Cassie-Baxter state under some circumstances as later is explained for the case of medical grade PVC.

Polyurethane films with different laser powers (varied from 15 to 150mW), were exposed to laser beams with constant laser scan speed of 1.0 mm/s, beam overlap of 50% (equal to 15µm between two consecutive lines), and pulse repetition of 1 KHz. All ablation experiments were conducted in air. Fig. 5-13 shows SEM images of PU films laser scanned in the one direction (uniaxial scan) by applying laser power in the above mentioned range at two different magnifications. SEM images indicate that the geometrical details of the morphology of the laser ablated patterns, is largely influenced by the laser power (laser peak fluence). Increasing the laser power applied to the surface, increases the laser energy that each spot receives. This would cause

the micro channels to become deeper, wider, and slightly covered with submicron and nano scale features, which appear on the top and sides of the micro-channels as the laser energy increases.

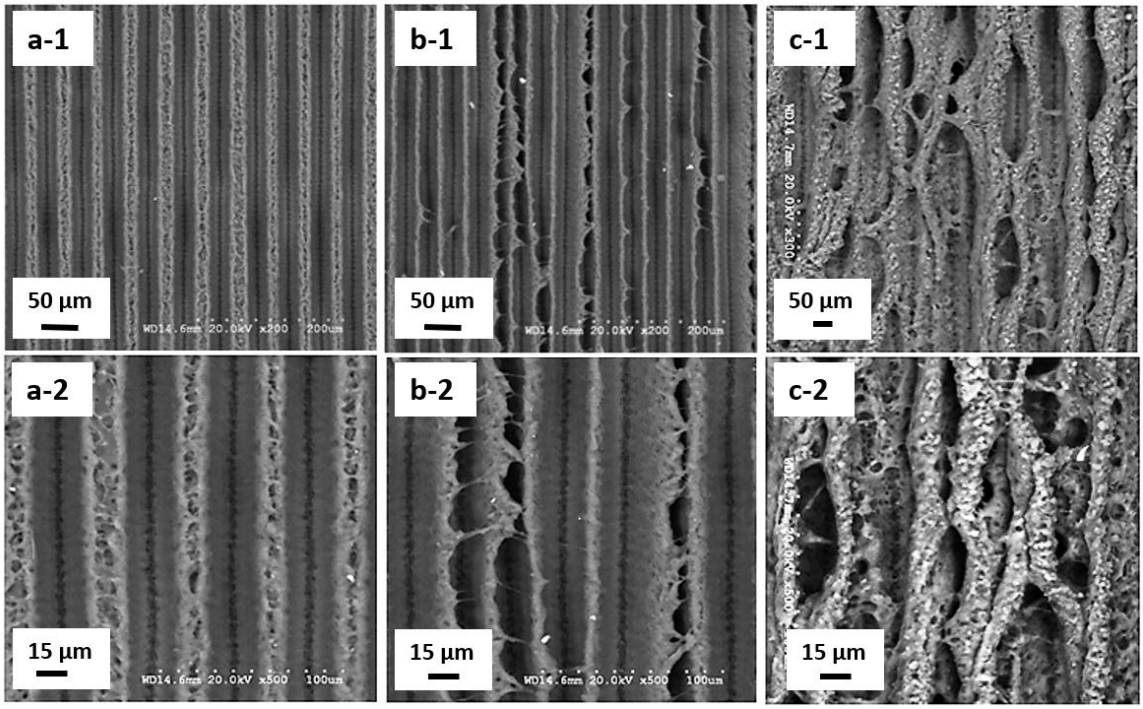

Figure 5.13. Laser ablated surface of PU at different magnifications scanned with laser scan speed of 1.0 mm/s, and overlap of 50% and laser power of a) 15mW, b) 50mW, c) 100mW

By increasing the laser power to 100mW, the opaque color of the polyurethane film at the lasered area turned yellow, while by further increasing the power to 150mW, the color change to dark brown, possibly due to severe degradation.

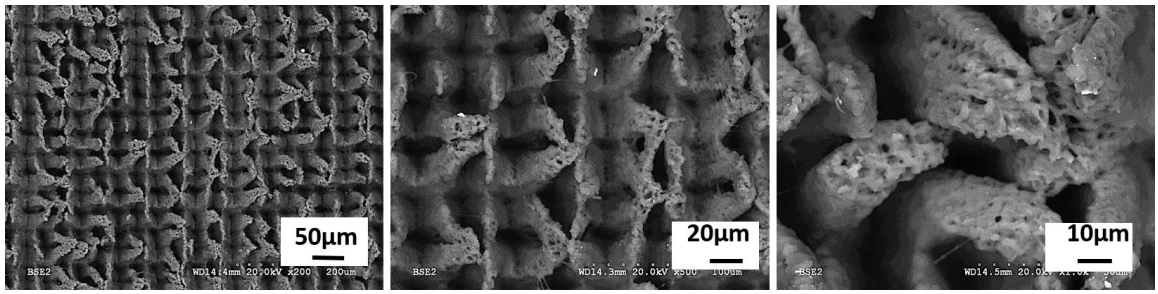

Figure 5.14. Biaxial laser ablated surface of PU at different magnifications with scan scan speen of 1.0mm, overlap of 50% and laser power of 60 mW for both passes

PU samples uniaxilay scanned with laser power above 100mW, display much higher water CA (as high as 144º ±2) compared to PU films ablated with 15 to 100mW with water CAs in the

range of 111º to 132º respectively. This is due to the fact that the micro channels are covered with submicron scale features at the laser powers above 100mW. However, the high CAs of PU samples are not beneficial since the polymer films are already thermally degraded at these high laser fluences.

PU surface scanned with two perpendicular laser lines (biaxial scan, as explained for PTFE before) show relatively higher water contact angle compared to uniaxial scanned PU surface. However, PU surface scanned with laser power lower than 100 mW barely show any superhydrophobic behaviour. SEM images are shown in Figure 5-14.

5.6 Effect of Laser Parameters on Micro/Nano-Patterning

The fluence profile for a Gaussian beam, Φ(r) , is defined as the below equation:

$$\Phi(r) = \Phi_0 e^{-2r^2/\omega_0^2} \tag{9}$$

where, ω_0 referred to as the Gaussian beam radius, *r* is the distance from the beam centerline and is the peak fluence of beam, given by:

$$\Phi_0 = \frac{2E_p}{\pi\omega_0^2} \tag{10}$$

Where *EP* is the laser beam pulse energy, which is ratio of power to pulse frequency (repetition rate). For laser ablation with a Gaussian spatial intensity beam profile, a simple relation has been derived between the diameter of an ablated crater, *D*, and the peak fluence in the beam (Jiang and Tsai, 2003):

$$D^2 = 2\omega_0^2 \ln\frac{\Phi_0}{\Phi_{th}} \tag{11}$$

.

Where Φ_{th} is the material surface ablation threshold, and $\omega_{0\ is}$ the laser Gaussian beam radius[153].

5.7 Summary

Femtosecond laser ablation method is proposed for fabricating dual scale roughness on PTFE in order to develop superhydrophobic surface. The effect of femtosecond laser irradiation parameters (fluence, scanning speed and beam overlap) on the morphology, topography, and

wettability of the resulted micro/nano-patterns was studied in details. Two distinctly different methods were used to ablate the PTFE surface; uniaxial and biaxial patterns.

Scanning electron microscopy images show that the uniaxial laser ablation of the surface creates micro-channels partially covered with sub micron- and nano-scale features. Uniaxial laser scanning of PTFE surface, could increase the CA of PTFE surface up to 160° and decrease the CAH as low as 12°.

Based on our study, it is not possible to fabricate truly superhydrophobic PTFE substrates with extremely low CAH which presents self-cleaning properties in all directions through biaxial laser ablation. For the first time, a novel method of laser scanning (biaxial scanning) has been proposed which could decrease the CAH of the PTFE surface to below 3°, while the CA can be as high as 170º. Biaxial scanning creates uniform pillared morphology (square pillars with rounded tops uniformly distanced) which its wetting behaviour is not anisotropic. Biaxial scanning of PTFE surface with non-identical laser fluences (laser fluence of first scan and second scan are not equal) increases the superhydrophobicity of PTFE surfaces into extremely high levels. For these laser ablated PTFE samples, the high density of nano-features is responsible for the air-trapping and long term.

Chapter 6: Imprinting Hot Embossing

Fabrication of nano/micro roughness utilizing femtosecond laser ablation is a maskless, simple, single step process which benefits from many advantages including accurate and clean patterning, controlled morphology and topography, creating dual scale roughness, and minimum thermal damaging of the surrounding. At the same time, this method suffers from some drawbacks as well. In addition to it's time consuming and costly process, femtosecond laser ablation can only create limited morphologies (channeled morphology and mesh-like pillared morphology) on polymeric substrates, although this is not applied to femtosecond laser ablation of metals such as stainless steel. Femtosecond laser ablation of metals (for instance SS) creates diverse complicated morphologies with wide range of varieties of shape and size, depending on the laser parameters. In order to create such advanced and diverse morphologies on large polymeric substrates, imprinting method was used and the results are presented in this chapter.

Essentially the thermal imprinting of nano/micro-structured stainless steel (SS) templates fabricated by means of femtosecond laser ablation were imprinted onto three different polymeric surfaces (HDPE, PLA and medical-grade PVC) through hot-embossing. These three polymers were chosen on the basis that they find applications as superhydrophobic biomaterials in biomedical and tissue engineering. Section 6.1. explains the template morphologies on Stainless steel that were used to microreplicate their negative morphologies on polymeric substrates. The results (morphology and wetting behaviour) of this microreplication technique are presented in section 6.2 for HDPE and PLA, and in section 6.3 for medical-PVC. Periodic arrays of grooved and pillared patterns with dimensions ranging from submicron to several microns alter the wettability of the polymeric substrates significantly. In section 6.3, a simple strategy developed to create re-entrant superomniphobic structures on HDPE surface was explained. The fibrous hook-like structure of the fabricated HDPE is very similar to the skin's roughness of a superoleophobic fish. Interestingly, the HDPE surface is capable of repelling water and also organic solvents solutions which have much lower surface tensions than water. This section is one of the main accomplishments of this PhD work.

6.1 Template Morphology

The stainless steel templates surface are ablated with ultra-short laser pulses generated by an amplified Ti:Sapphire laser with center wavelength of 800 nm, repetition rate of 1 kHz, pulse duration of 140 fs, maximum output power of about 2 W, and focal point of 30 µm to create nano-patterns. Laser parameters have significant influence on the morphology of the laser ablated SS. The morphologies were tuned by varying the laser fluence, scanning speed and beam overlap. The imprinted patterns in terms of diameter and height of the peaks and valleys (pillars and bumps), pitch size and density/amount of nano-scale features which cover the micro-pillars are different from each other. Figure 6-1 depicts the SEM pictures of SS laser ablated substrates which were used as templates in this work. The presented morphologies on stainless steel are referred to as paraboloidal, triple roughness and cauliflowered. The micro-pillars dimensions are in the range of 18.5 to 50.3 µm and feature heights of 17.0 to 120.5 µm. The micro-scale features are covered with recesses of submicron and nano scale size. Laser fluence was increased from paraboloidal pattern to trippled to cauliflowered. So, the height of the pillars (peak to valley) and the concentration of the nano-scale features would increase from pattern "a" to "c" in figure 6-1.

All three SS templates offer a common characteristic: symmetric patterns; meaning that the reverse patterns of the templates are very similar to the original one. Offering symmetric patterns makes these templates perfect for this purpose.

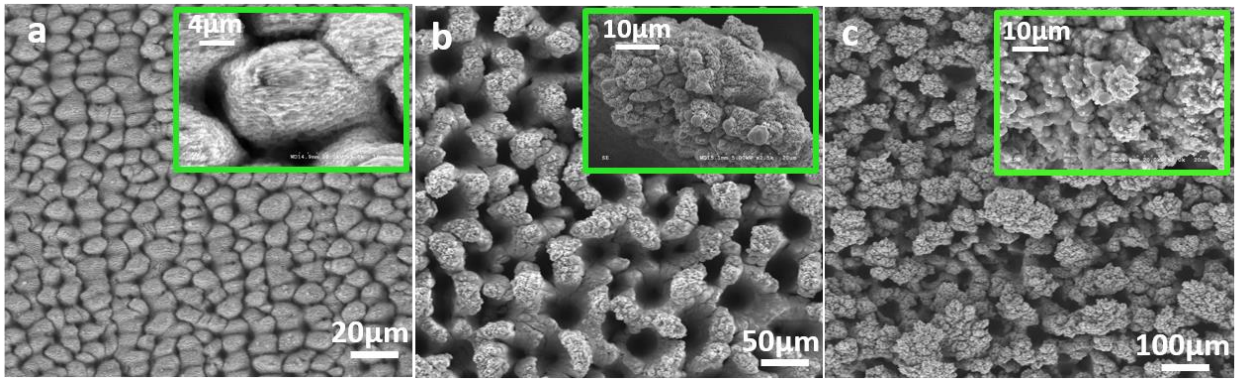

Figure 6.1. SEM pictures of patterns create on SS templated; a) Paraboloidal patterns, b)Trippled, c) Cauliflowered.

6.2 HDPE and PLA Embossing

In order to avoid the pattern deformation of the imprinted substrates due to elastic recovery and chain relaxation, the embossing temperature, T_{emboss}, was set to be slightly higher than the peak melting point, T_m, of the polymer. During the hot embossing process, the SS template is readily stamped onto the softened/molten polymer film. Pressure forces drive the soften/molten polymer to fill in the gaps between the micro-scale pillars and nano-scale grains, and create the reverse pattern of the template on the polymeric film. SEM pictures of the imprinted morphologies on Polylactic polymer (PLA) are shown in Figure 6-2 for the three patterns (paraboloidal, triple roughness, and cauliflowered). Very similar nano/micro structures were also obtained from imprinting the templates onto HDPE substrates. The SEM images illustrate that the submicron-scale features (ripples or bumps) are clearly formed on the polymeric substrates. This confirm that at temperatures above the polymer melting point, the polymer chains can easily flow and fill in the nano/micro structures of the SS patterns.

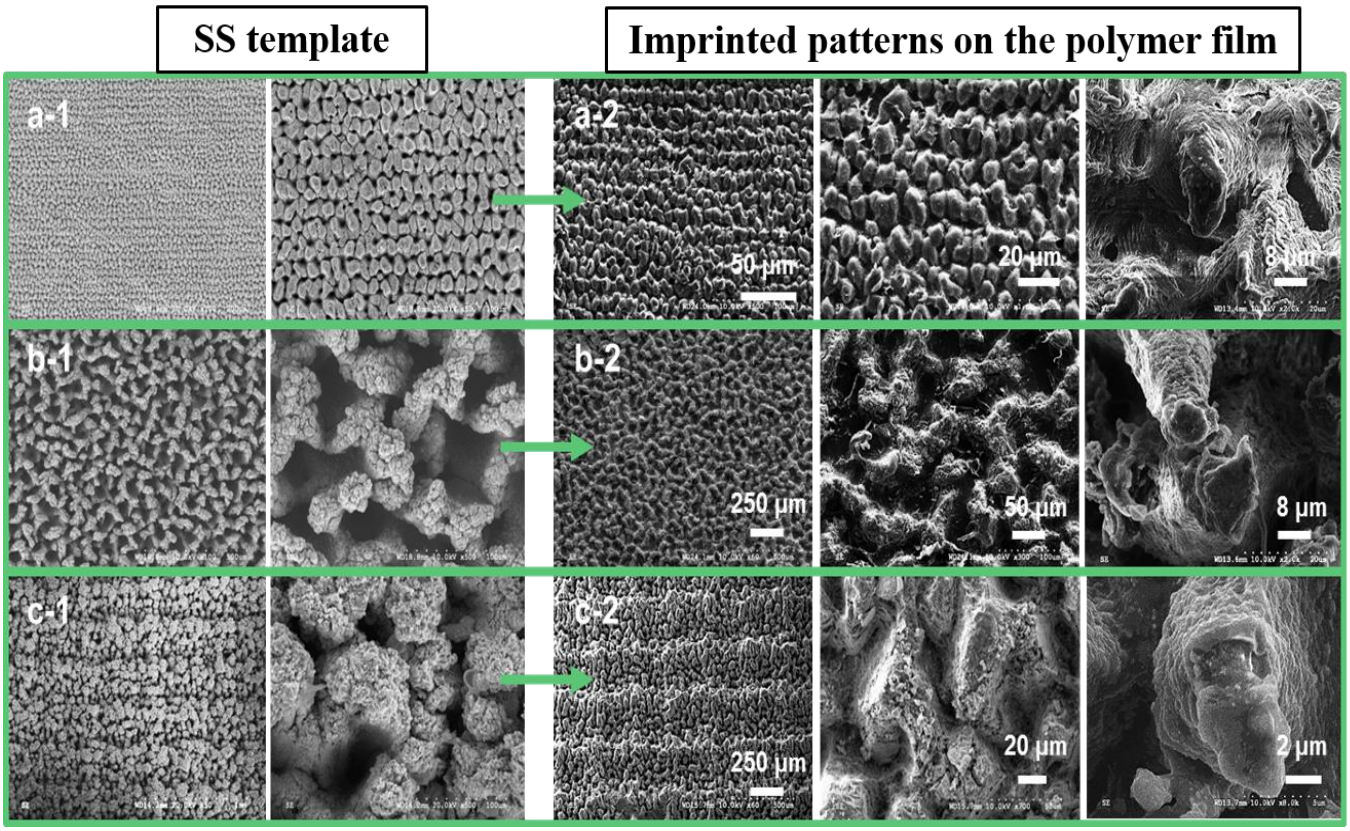

Figure 6.2. SEM pictures of stainless steel templates and the corresponding imprinted PLA surfaces with different nano/micro structures; a) Paraboloidal, b) Tripled roughness, and c) Cauliflowered.

The imprinted structures on the polymeric films are very similar to the original structures on the SS templates in shape, size, and density of the micro-pillars and second order roughness. In addition to the surface morphology, topography of the imprinted samples is also studied. The average height of the pillars (peak to valley, H) and the average diameter of the micro-bumps (D) were measured using optical profilometery. The SS and the imprinted polymeric films had similar aspect ratios (the ratio of H over D, H/D) and roughness averages (R_a). For example, Figure 6-2a depicts the paraboloidal SS pattern (6,2a-1) that was imprinted on a PLA film (Figure 6-2a-2). This pattern presents the smallest aspect ratio among the three patterns (height-to-diameter ratio of the pillars, H/D≈0.7) and also the least amount of sub-micron features on top of the micro-pillars. The second imprinted structure, "trippled roughness", is a symmetric pattern with the largest aspect ratio among the three patterns (H/D≈3.0) (Figure 6-2b). This structure is partially covered with sub-micron features. Finally, the third imprinted pattern (Figure 6-2c) is also a symmetric structure with relatively large aspect ratio of about 2.5. The surfaces of the SS template and imprinted PLA both are densely covered with sub-micron grains. The combination of high aspect ratio and high density of submicron and nano-scale features renders the imprinted tripled and cauliflowered polymeric substrates superhydrophobic.

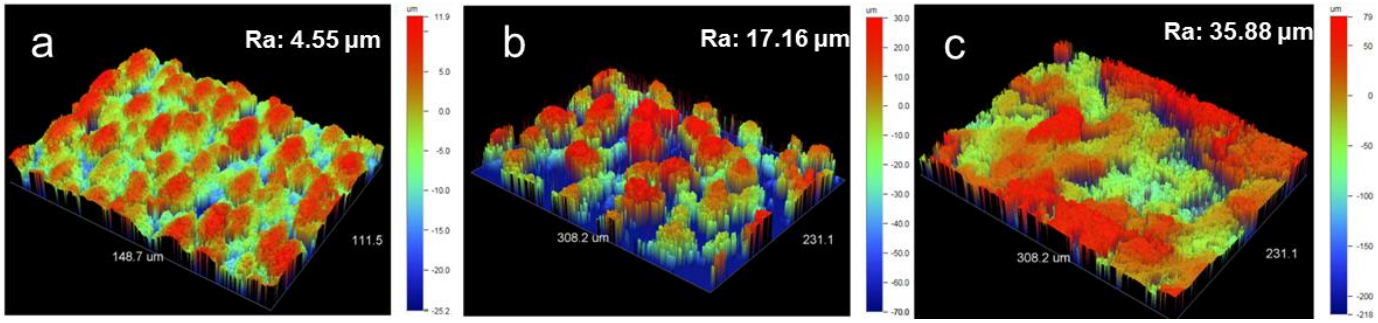

Figure 6.3. Profilometery 3-D images of imprinted HDPE substrates; a) Paraboloidal, b) Trippled, and c) Cauliflowered structure.

Figure 6.3 presents 3-D images taken by optical profilometry from the imprinted HDPE substrates. The average roughness (R_a), is a representation of the surface roughness. Colors on the 3-D pictures present the dimensions of the individual heights (asperities) and depths. Profilometry results suggest that the tripled and cauliflowered substrates possess favorable

geometrical characteristics for superhydrophobicity. This is due to their much higher roughness average.

6.2.1 Wetting behaviour of imprinted polymeric surfaces when $T_{emboss} > T_m$

The following figures of 6-4-a and 6-4-b depict the effect of the imprinted geometrical details on the water contact angle (WCA) and water contact angle hysteresis (WCAH) of the replicated substrates (PLA and HDPE). As expected, cauliflowered pattern possesses the highest WCA between all three patterns; this particular pattern having the highest R_a value possessing micro-scale pillars which extensively are covered with sub-micron, nano-scale grains. The dual scale structure of this pattern is highly capable of holding the Cassie–Baxter states [154].

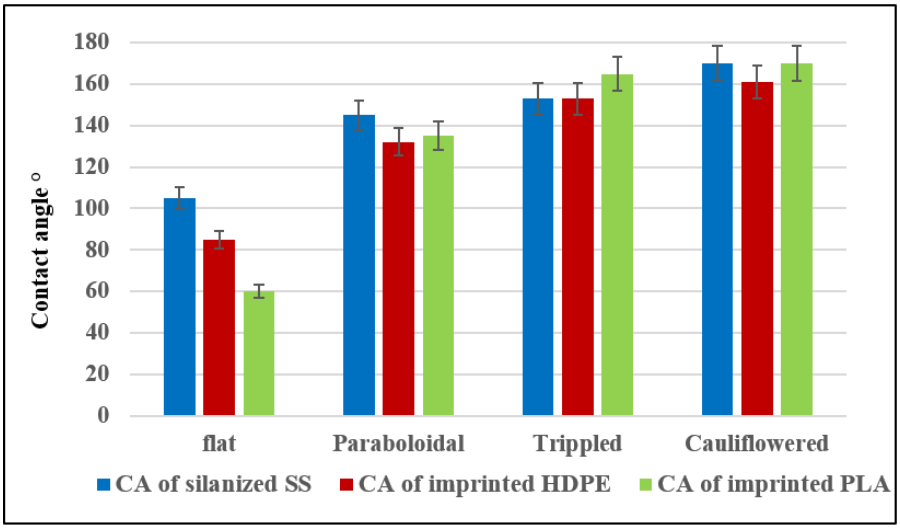

Figure 6.4.a. Water contact angle measurements for SS templates and the related imprinted polymers

Despite its less hydrophobic intrinsic nature of PLA compared to HDPE (flat CA of PLA is lower than that of HDPE), the imprinted surface of PLA exhibits higher WCA and lower WCAH compared to their HDPE counterparts. One important reason is the lower melt viscosity of PLA which makes the duplication and formation of micron and sub-micron features easier. This causes more accurate micro-replication of the dual roughness in the case of PLA. Figure 6-5 depicts the complex viscosity of HDPE and PLA at their corresponding processing temperatures of 170°C and 180°C respectively. The considerably lower viscosity of PLA plays an important role on the quantity and quality of the imprinted nano-micro geometrical details. Another very

important aspect is the relatively high glass transition (T_g) value of PLA (55°C), which locks the formed geometrical details of the patterns at temperatures below 55°C, during the cooling process.

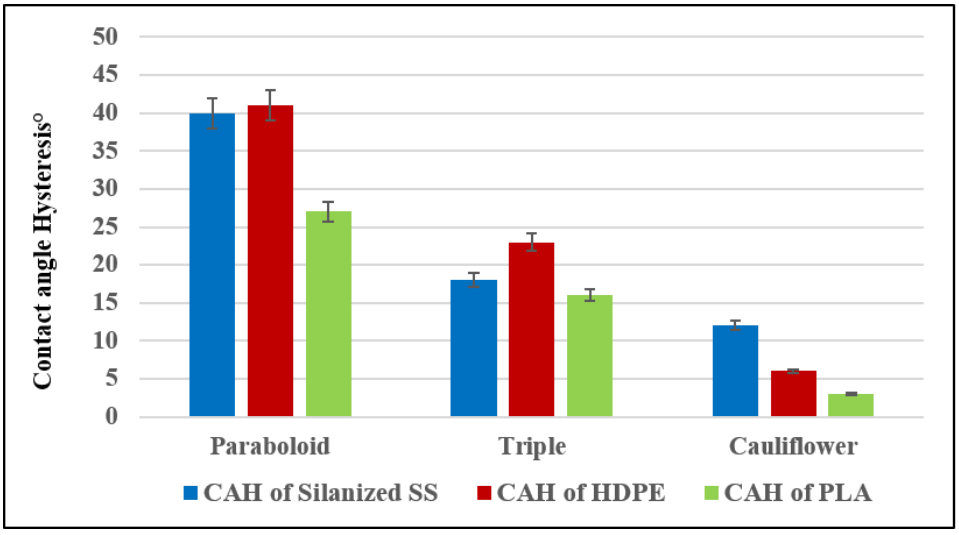

Figure 6.4.b. Water contact angle hysteresis measurements for SS templates and the related imprinted polymers

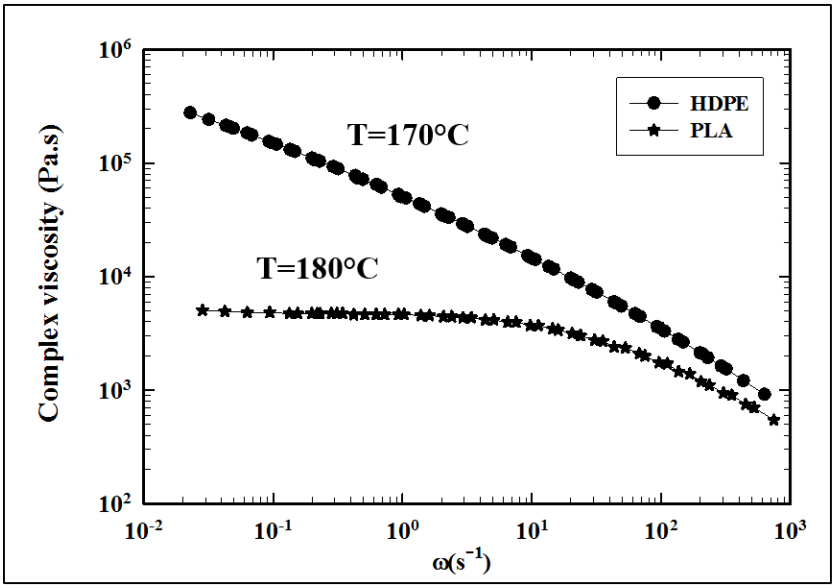

Figure 6.5. Viscosity curves of PLA and HDPE at 180°C and 170°C respectively

6.2.2 Wetting behaviour of imprinted polymeric surfaces when $T_{emboss} < T_m$

In order to study the effect of embossing temperature on the wetting behavior of the replicated polymeric substrates, T_{emboss} was lowered to below the melting point (T_m) of the polymer. To compensate for the lower temperature, the embossing pressure, P_{emboss}, was increased to about 10 MPa (referred to table 4-1). The higher embossing pressure forces the soften polymer to fill the micro gaps of the template. While the WCA and WCAH of the PLA and HDPE samples imprinted at temperatures above T_m are well above 160° and below 10° respectively, these values drop to below 140° and increased to above 40° for these new imprinted samples (imprinted at temperatures below $T_{m)}$. The CA and CAH measurements of the PLA substrates replicated from SS templates at two temperatures of 110°C (below $T_{m)}$ and 180°C (above $T_{m)}$ are presented in Figure 6-6.

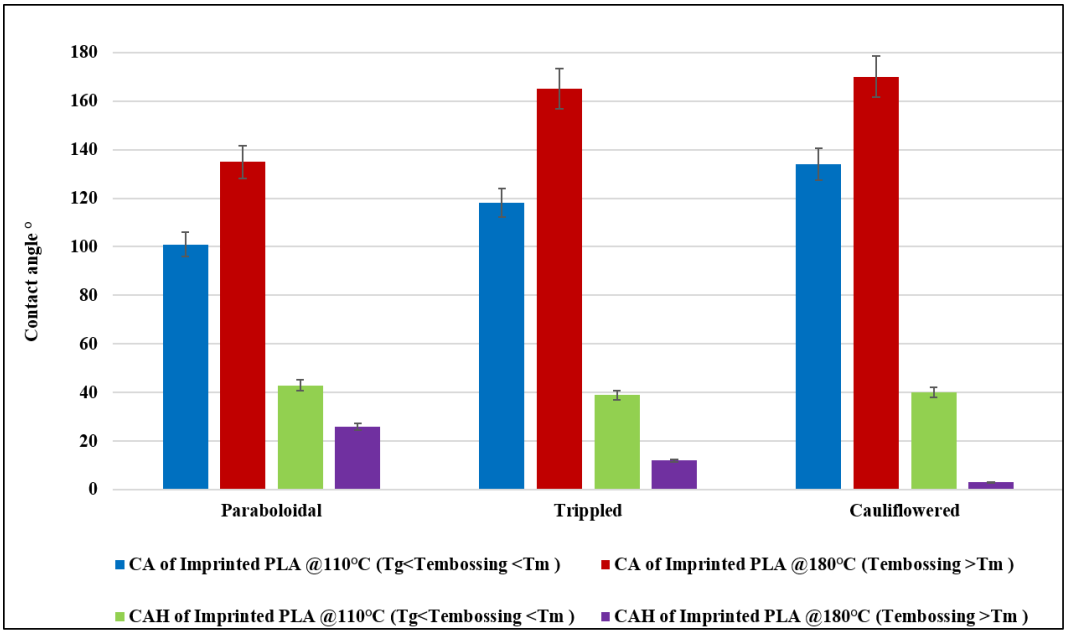

Figure 6.6. Water contact angle (°) of PLA substrates imprinted under different temperatures and pressures

In the production of superhydrophobic polymeric surfaces, it is important to ensure that Cassie-Baxter is the dominant state of the surface and has lower energy than Wenzel state. Main surface properties that affect the stability of the Cassie-Baxetr state are organization of nanoscale features and intrinsic hydrophobicity of the polymer. It is argued in the literature that the efficiency and robustness of superhydrophobic surfaces are increased through combination of

micro and nano scale structures. Structured surfaces with grooves at the micro, sub-micro, and nano scales are the most stable ones at the Cassie-Baxter state [155].

The different WCA and WCAH obtained from imprinting the SS patterns on the surface of PLA and HDPE at different temperatures are in perfect alignment with literature; when the embossing temperature is below the melting point of the polymer, polymer is still in the solid state. However, since the T_{emboss} is above T_g polymer chains have some limited mobility which is only enough to fill the micro holes and not enough to penetrate into the nano recesses. In order to force the polymer to penetrate into the nano recesses, much higher pressures are required. This work, however, does not cover high pressure imprinting. Optical profilometer proofs that the height of the micro-pillars is similar for both cases ($T_{embossin}$ below and above Tm).

Non-wetting superhydrophobic behavior of HDPE and PLA films imprinted at $T_{emboss}>T_m$ can be justified with their lower viscosity at their molten state, which allows the chains to easily flow filling in the micro hallows as well as penetrate into the submicron recesses and form dual scale structure (submicron grooves on top of the micro pillars). Figure 6-7 shows the SEM images of PLA and HDPE films imprinted at temperature below the polymer's melting point versus the ones imprinted at temperatures above the polymer's melting point.

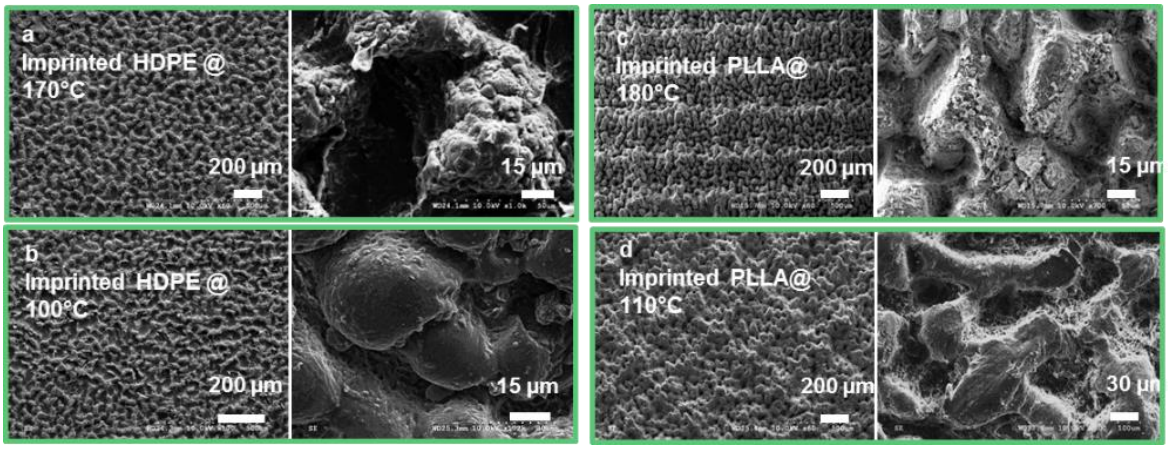

Figure 6.7. SEM images of trippled-roughness SS pattern imprinted on a) HDPE at 170°C, and b) HDPE at 100°C; and cauliflowered SS patterns imprinted on c) PLA at 180°C, and b) PLA at 110°C

The SEM images display that when $T_g<T_{emboss}<T_m$, the imprinted micro-scale features are not covered with sufficient amount of submicron grains required for Cassie-Baxter state to promote superhydrophobicity.

6.3 Medical Grade PVC Hot Embossing

Medical-PVC is a plasticized polymer contain high amount of tris (2-ethylhexyl) trimellitate (TOTM) plasticizer. DSC doesn't show a melting point for this polymer. In order to obtain the best imprinting results for this polymer, the embossing temperature was set at high temperatures where the polymer can easily flow without the application of excess pressure. In this regard, the T_{emboss} was set at 170°C which is slightly lower than the degradation temperature of the polymer. Thermogravimetric analysis (TGA) revealed that the degradation starts at 185°C. Figure 6-8 shows the SEM images of the three patterns (paraboloidal, triple roughness and cauliflowered) imprinted on medical- PVC at 170^{o}C and 12 MPa. The SEM images indicate that the submicron-features of the SS templates were not completely duplicated onto the PVC film.

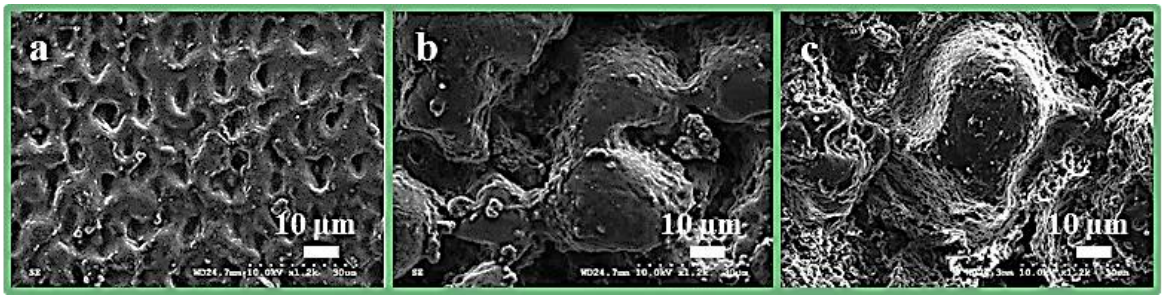

Figure 6.8. SEM pictures of imprinted medical-PVC replicated from femtosecond laser ablated SS, a) Paraboloidal, b)Trippled, and c) Cauliflowered patterns

The water contact angle of samples (a) to (c) in Figure 6-8 respectively were 112°, 134°, and 148°. The contact angle hysteresis of all these three samples were higher than 90°. The wetting behaviour of imprinted cauliflowered surface can be seen in Figure 6-9. The high CAH values typically indicate strong adhesion forces between the surface and the liquid droplets.

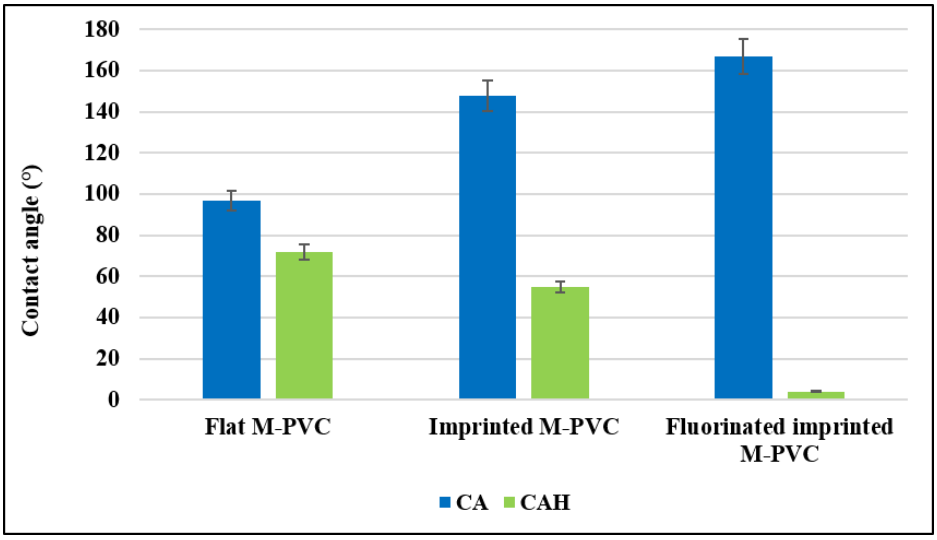

Figure 6.9. Water contact angle and water contact angle hysteresis of medical-PVC i) a flat surface, ii) Cauliflowered imprinted surface, and iii) fluoroalkylsilane coated, cauliflowered imprinted surface

For the imprinted medical-PVC with "paraboloidal" and "tripled roughness" patterns, water droplet would pin to the surface even when the substrate is tilted upside down. This raised the question that what parameters do increased the contact angle hysteresis of imprinted medical-PVC during the hot embossing process.

PVC is an amorphous polymer with relatively hydrophobic behavior with water contact angle of 80° for its flat surface. This grade of medical PVC is plasticised with Tris (2-ethylhexyl) trimellitate (TOTM) plasticizer which is hydrophilic, mostly due its to non- symmetrically arranged polar covalent bonds (C=O) (Figure 6-10).

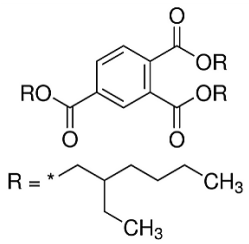

Figure 6.10. Chemical formulation of Tris (2-ethylhexyl) trimellitate (TOTM), non-symmetric

The wetting behaviour of medical-PVC is influenced by the hydrophobic nature of PVC as well as the hydrophilic nature of its plasticizer. After the hot embossing process, XPS analysis showed higher amounts of TOTM plasticizer on the surface. The plasticiser leached out to the

surface under the high temperature and pressure. This causes separation of the plasticizer moieties from the PVC matrix, which results in fractal morphology and separates the surface into two phases. The presence of hydrophilic defects in hydrophobic substrate would decrease the receding contact angle and elevate the contact angle hysteresis [156]. Also, in a fractal morphology, the borders between the soft domains (plasticizer) and the main matrix (medical-PVC surface) tend to retain liquid stronger than a homogeneous surface might. The tendency of decreasing receding contact angle increases with increasing the percentage of these soft domains[157].

Also, since the imprinted medical-PVC surfaces exhibited penetration of the water droplets into their grooves (due to lack of sufficient sub-micron and nano-scale features), they follow the Wenzel model. For the surfaces that are stable at the Wenzel state, the receding contact angle tended to follow the predictions of the Wenzel equation and decrease with decreasing the roughness. This results into higher contact angle hysteresis [158].

In order to decrease the adhesion forces between the surface and the water droplet, the surface chemistry has to be altered; a thin layer of fluoro alkyl silane coating was deposited on the surface of the imprinted medical-PVC by using a chemical vapor deposition (CVD) technique. As it is illustrated in Figure 6-9, the wetting behaviour (WCA and WCAH) of the silane-coated PVC significantly improved.

6.4 Superomniphobic HDPE Surface

Generally, the thermal imprinting process is consisted of three steps: (i) fabrication of a master metallic (SS) template with desired feature size and shape; (ii) replication of the metallic template under high temperature and pressure; and (iii) cooling and removal of the template. Altering the parameters of each step could be a source of significant change on the appearance and performance of the final replicated features. In the previous section, imprinting three geometrically different patterns at two different temperatures and pressures onto the polymeric substrates, the impact of steps (i) and (ii) parameters on the wettability behavior of the imprinted polymeric surface was investigated. In this section, it is being shown that the cooling details and the template removal off the replicated substrate has a significant impact on the roughness shape and size of the final pattern as well as on its wetting behavior.

A strategy was developed to utilize thermal imprinting process to create re-entrant micro-structures on polymeric surfaces and particular on HDPE. In the embossing procedure explained earlier, after the embossing pressure was applied to the heated polymeric substrate, the system was cooled down under pressure to completely lock the microdetails formed. In the case of superomniphobic replication, the polymeric substrate was detached from the template at higher temperatures without complete cooling (at *T* in the range of 85°C to 100°C); at this temperature the relaxation of the polymer chains are not completed and chains are strongly adsorbed on high surface energy substrates such as SS. During the peeling process, the directional applied peeling force causes each existing micro-adhesion between the apex of a pillar on the template and the polymer surface to create an angled micro-fiber. Adhesion between the polymer and the template is required to allow proper re-entrant micro-fibril structure formation. The type and appearance of the pillars on the SS template, and HDPE fibrous characteristic play important roles in creating such hook-like structures on the surface of HDPE. Typical SEM images of these structures exhibited in Figure 6.11.

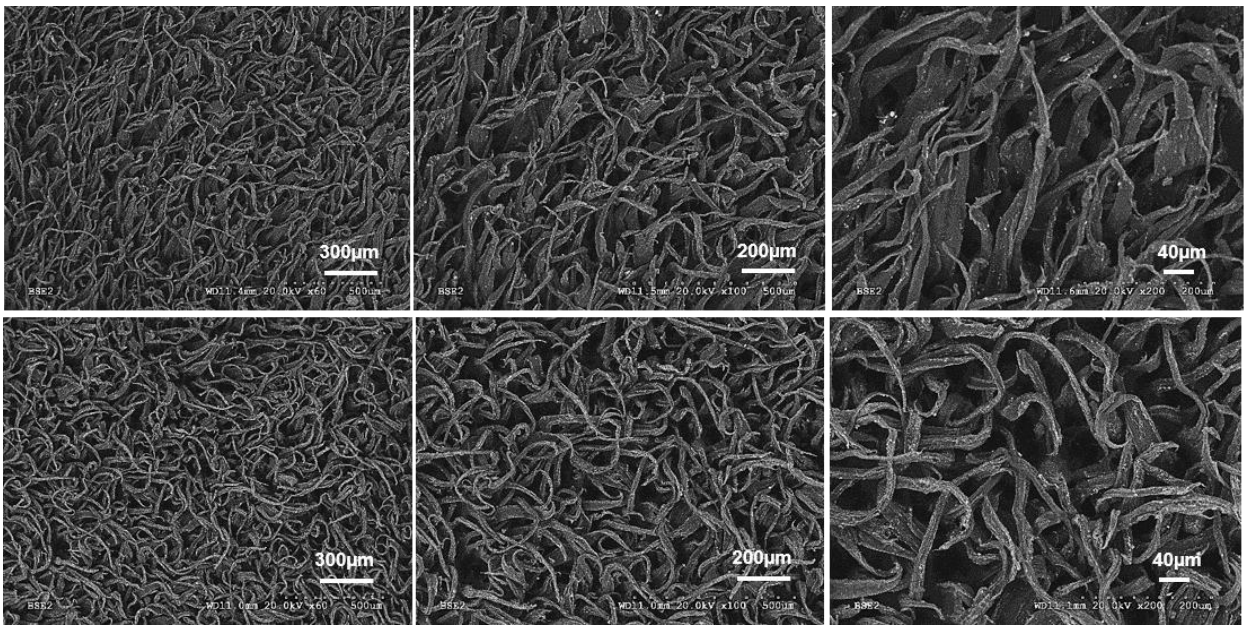

Figure 6.11. SEM images of superomniphobic fibrous rough structures of HDPE, T_{emboss}=170°C, T of template removal=75°C; Upper row images: Tripled roughness structure was used as template. Lower row images: Cauliflowered structure was used as template

A simple technique in removing the laser ablated template resulted in creating novel bioinspired superomniphobic surfaces. Superomniphobic surfaces are defined as superhydrophobic non-adhesive surfaces that can repel virtually any liquid, even very low surface tension organic solvents or blood or highly concentrated acids.

The fibrous hook-like structure of the fabricated HDPE is very similar to the skin's roughness of a superoleophobic fish. The filefish is one the sea creatures that its skin exhibit extreme water and oil repellency. Instead of the common flaky scales seen on most fishes, this fish has sandpapery bony skin (Figure 6-12). In oil-spilled sea areas, this fish is observed to be free from oil contaminations, which indicate the superoleophobic nature of its skin [50]. In addition, the rough skin of the filefish benefits from anisotropic properties; the liquid droplets tend to roll off along a head-to-tail (HT) direction, but pin to the skin in the opposite direction. This anisotropicity is due to the oriented hook-like spines arrayed on one direction on the fish skin (Figure 6-11). Similar hook-like fibers and the same anistropic behavior were seen in the fabricated superomniphobic HDPE, and will be investigated in detail in the future works of out research group.

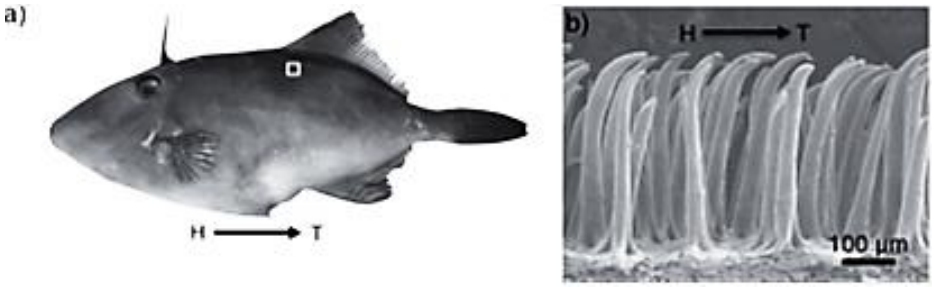

Figure 6.12. a) Picture of filefish N. septentrionalis , b) The SEM picture of the superoleophobic skin of the fish; arrow directing from head (H) to tail (T) indicates the oriented direction of hook-like spines (image adopted from reference [50] with permission)

Various liquids and solutions with different surface tensions were used to measure the wetting properties of the fibrous structure (Table 6.1).

Results confirm that the structure is highly superhydrophobic and superomniphobic. The water contact angle of the micro-fibrous surface can become as high as 170°, while the contact angle

hysteresis is below 3° (extremely high superhydrophobic properties). By using organic solutions with considerably lower surface tensions than water, the surface exhibited similar liquid repellant behavior and Cassie-Baxter was still the dominant stable state. The contact angle and contact angle hysteresis of several low surface tension liquids (Table 6.1) are plotted in Figure 6.13. X-axis id the wt% of the organic solvents (acetone, methanol, and 2-propanol) in water. The results confirm the superomniphobic behavior of the imprinted surface in contact with organic solutions. Based on Figure 6.13, the CA and CAH of all three organic solvent solutions below 50 wt% meet the superomniphobic criteria.

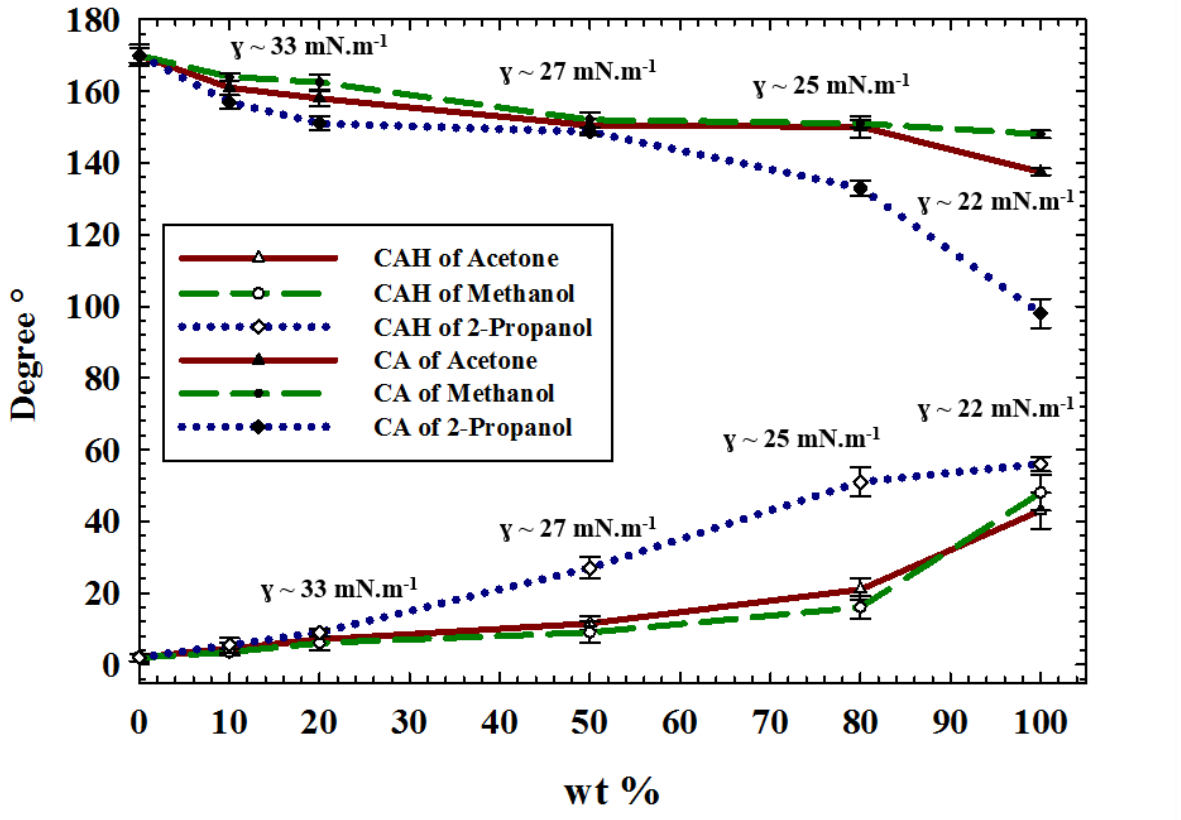

Figure 6.13. Contact angle (CA) and contact angle hysteresis (CAH) of solutions of methanol, acetone, and 2-propanol with HDPE micro-fibrous rough surface.

Table 6.1. The surface tension ɣ ($mN.m^{-1}$) at T=20°C of aqueous solutions of methanol, acetone, and 2-propanol solutions at 20^0C [159][160]

wt %	0	10	20	50	80	100
Acetone	72.75	39.69	32.96	27.63	25.14	23.68
Methanol	72.75	56.87	47.86	33.37	25.98	22.95
2-propanol	72.75	41.21	31.16	24.78	22.62	21.74

6.5 Summary

Femtosecond laser ablated SS templates were used to imprint dual scale patterns onto three different thermoplastics (PLA, HDPE, and medical-PVC) through hot embossing. In order to speed up the imprinting process and create stable patterns which experience the least deformation due to elastic recovery and relaxation, the embossing temperature was set to be slightly higher than the peak melting point of the polymers. PLA and HDPE imprinted substrates became superhydrophobic with water CA well above 160° and CAH below 5°. Despite its less hydrophobic intrinsic nature, the water repellency of PLA surface is higher compared to its HDPE counterpart. This is due to the more accurate micron/submicron replication of the dual roughness on PLA substrate that is mainly due to its lower viscosity.

The quality of removing the template from the replicated polymeric substrate has a significant impact on the roughness shape and size of the final pattern. A re-entrant structure with a fibrilar morphology was fabricated on the surface of HDPE by applying directional force while removing the template from the replicated surface at high temperatures. Fibrils were formed as a result of the micro-adhesion (chain adsorption) of HDPE chains on the metallic SS surface. This bioinspired morphology is highly liquid (water and other organic liquids of low surface tension) repellant, and thus possesses properties of superomniphobicity.

Imprinting dual scale structured SS on to the medical-PVC surfaces produced morphologies with high CA and high CAH due to the adhesion forces developed at the interface between the hydrophilic plasticizer and water droplets. Imprinting conditions cause microphase separation of

PVC matrix from the plasticizer moieties resulting in fractal morphology of the patterned medical-PVC. The concentration of polar (C=O) groups, originated from the plasticizer, on the surface of the imprinted substrate is high enough to ascertain high adhesion between water droplet and surface features. These substrates can become superhydrophobic by depositing a thin layer of fluoro-alkyl-silane coating using a chemical vapor deposition technique.

Chapter 7: Protein Adsorption and Bacteria Adhesion on Superhydrophobic PTFE Surface

One of the most promising potential applications of superhydrophobic surfaces is in the area of medical devices i.e. their interactions with biological systems. Significant research exists related to the initial interactions between proteins, cells, and bacteria with superhydrophobic substrates; however, much of these data appear contradictory, and no universal rules have yet been identified [19][62]. Most likely this is due to the complexity of interfacial interactions between the rough surface of these materials and biological adsorbents.

This chapter focuses on the reduction of bacterial adhesion and protein adsorption on superhydrophobic PTFE surfaces. Thus, it is important to describe how bacteria interact with a substrate and how surface physical properties affect bacterial adhesion.

Superhydrophobicity is obtained due to the combined effects of chemistry by additional topology effects. The hierarchical roughness of these superhydrophobic surfaces provide them with the capability to form trapped air pockets as long as the Cassie-Baxter state is the dominant wetting state of the system. The entrapment of air pockets makes the fraction of the solid surface in contact with the surrounding liquid limited (figure 7-1). This results into the reduction of the adsorbed protein and bacteria onto the biomaterial surface. [161][162][163][43][164] [17][18].

The influence of surface topography on protein adsorption and bacteria adhesion also depends on the presence or absence of shear forces within the system[165]. It has been shown that in dynamic systems, the introduction of a directional flow enabled the detachment of proteins/bacteria to a greater degree from superhydrophobic surfaces than from smoother one (Figure 7-2); in some cases even almost complete protein removal was achieved [166]. This is due to self-cleaning properties of superhydrophobic surfaces.

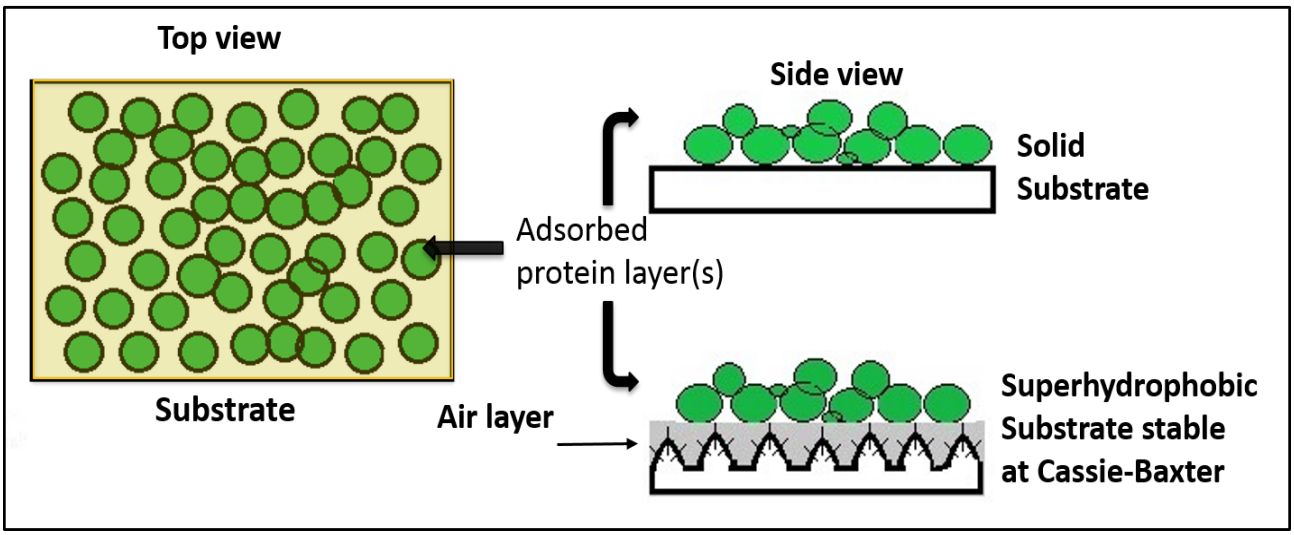

Figure 7.1. Effect of superhydrophobicity on protein/bacteria attachment on to the surface, when surface is stable at Cassie-Baxter state

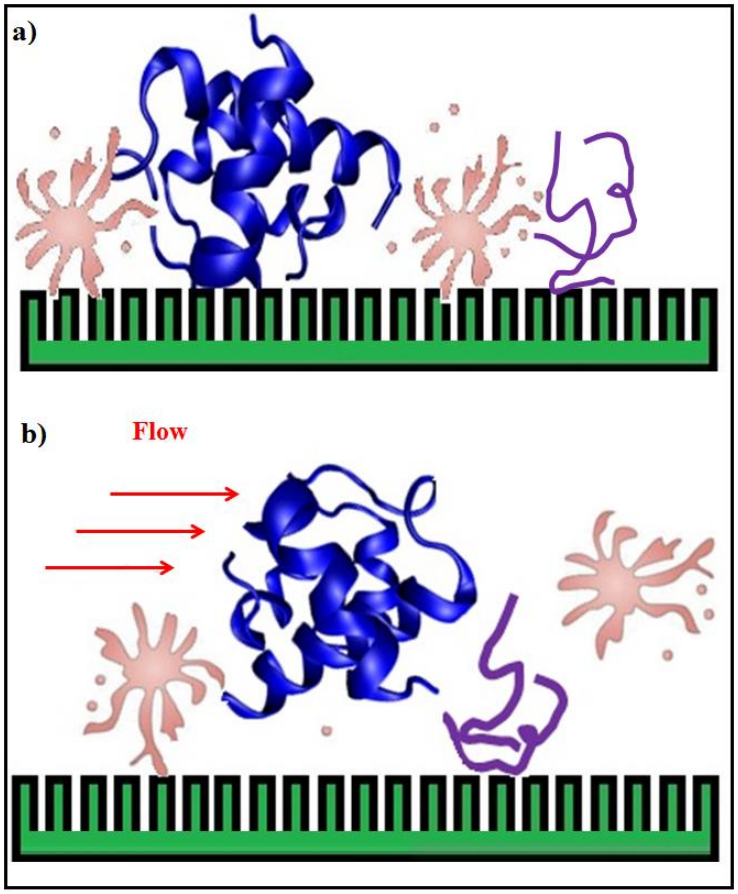

Figure 7.2. a) Biological species seat on top of the mico/nano grooves of a superhydrophobic surface in a static system, b) biological species detach from the superhydrophobic surface under the action of shear force (due to self-cleaning characteristic of superhydrophobic surfaces)

Figure 7.2 explains that only air can penetrate into the submicron and nano patters during the adhesion test, while the larger particles including the bacteria roll over the structure.

Several efforts to design a new generation of antibacterial surfaces based on mimicking the surface topography are recently reported[3][106][19][163]. The rational for these approaches was to design a topographically rough surface, which would reduce the attachment of bacteria through reducing the contact sites. It is generally accepted that the presence of nano-scale roughness limits the level of contact that occurs between the bacterium and the substratum; thus, there are fewer anchor points and as a result the force of adhesion is lower [167][168] .

The mechanism of bacteria adhesion into a substrate can be described as a two phase process. The initial phase is an instantaneous, reversible interaction which occurs under the effects of physical forces such as Brownian motion, van der Waals attraction forces, gravitational forces, the effect of electrostatic charge, and hydrophobic interactions. This initial stage of bacteria adhesion into a surface is so called "attachment". Attachment is more referred to physical contact than complicated cellular and chemical interactions, and is usually reversible. This initial attachment of bacteria into a substrate is the beginning of the adhesion stage (second phase), which make the molecular or cellular phase of adhesion possible. The second "adhesion" phase, is where bacteria adhere firmly to a substrate by time-dependent, irreversible chemical and cellular interactions. There is energy involved in the adhesion stage (second phase) between the bacteria and the substrate.

There are various factors influencing the bacteria adhesion process to a substrate, including some characteristics of bacteria themselves (the reason that two different types of bacteria are used), the target material surface, and the environmental factors such the absence or presence of plasma proteins. By changing the surface characteristics of the material and the relevant environmental factors, it would be possible for one to control the adhesion process of a unique bacteria to a surface.

Similar to tissue cells, bacteria growing in *in vitro* culture prefer to grow on available surface areas rather than in the surrounding aqueous phase. This fact is in complete alignment with many studies that indicate that the surface roughness increases the bacteria adhesion since the

depression in the roughened substrate provide more favorable sites for colonization (when the surface chemistry is unchanged). However, this fact is not applied to all roughened surfaces. The feasibility of applying superhydrophobic substrates to reduce bacterial adhesion has been studied by a number of researchers [161][162][163][43][164] [17][18]. However, the effect of details of the surface morphology and topology on the success of these surfaces over time has not received much attention.

In this study, we hypothesized that micron, submicron, and nano scale surface textures would prevent the initial attachment of bacteria through promoting superhydrophobicity and reducing the contact sites, therefore preventing the subsequence formation of a biofilm. PTFE surface fabricated in chapter 5 was used as a model substrate.

This study shows that in addition to water CA and CAH of the samples, surface topology also has to be closely studied to gain a better understanding on the factors affecting bacteria suppression. This would facilitate the fabrication of a stable superhydrophobic surface with antibacterial activity.

In this chapter, the effect of superhydrophobicity on bacteria adhesion and protein adsorption on to the surface of PTFE is studied. In section 7-1, three uniaxial scanned PTFE substrates were studied by capturing SEM and fluorescent microscopy after 4 hrs of incubation in *S. aureus* and *E. coli*. Fluorescent microscopy pictures were semi-quantified using Image J. The same study took place for three biaxial scanned PTFE samples; results are reported in section 7-2. Superhydrophobicity failure of the laser scanned PTFE sample, and also roughness characteristics of the scanned samples were studied in section 7-3. In order to verify the hypothesis mentioned in section 7.3, bacteria adhesion on a PTFE surface scanned with two different laser powers was studies (section 7-4). Also, protein adsorption on the surface of PTFE samples after 4 hrs of incubation in protein solutions and blood plasma was studied in section 7-5.

7.1 Uniaxially Scanned Surfaces; Superhydrophobicity and Bacteria Adhesion

Three superhydrophobic laser ablated PTFE samples with similar channel-like morphology, but different channel size (height and width) were incubated in *S.aureus* and *E.coli* culture for 4 hrs and 6 hrs respectively at 37° and under 80 rpm. SEM images of the ablated channels are depicted

in Figure 7-3. The wetting behaviour of the samples can be found in Figure 5-9 of chapter 5. The WCA of a, b, and c substrates are of 151°, 155°, and 162° respectively.

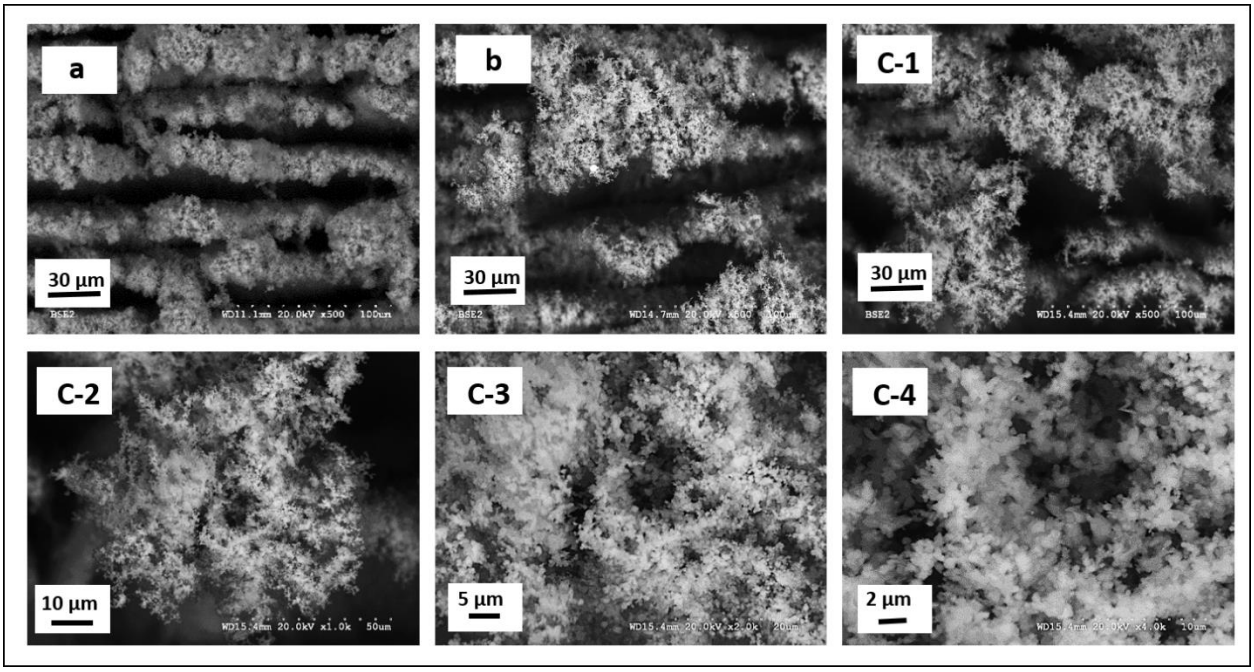

Figure 7.3. Low magnification SEM images of laser ablated PTFE surfaces scanned with and laser power of a) 120mW, b)220mW, and C-1) 320 mW. C-2, C-3, and C-4 are SEM images of PTFE surface ablated with laser power of 320mW at higher magnifications. The laser scan speed and overlap of all samples was constant at 0.5 mm/s and 50% respectively [149]

Results obtained from SEM and optical Profilometery of laser ablated PTFE samples indicate that the geometrical details of the morphology and topology of the irradiated micro/nano-structures strongly depend on the laser parameters, e.g. laser power. As the laser power increases, actual depth of the channels increase too. In addition to this, random pillars with larger heights are also formed along the side walls of the channels. The presence of these pillars on top and side of the walls increases the overall height of the walls even more. The appearance of these random pillars also dramatically decreases the spacing distance between the pillars (D). As a result, the H/D (height or depth to channels diameter ratio) parameter which is an indicating factor for superhydrophobicity increases by increasing the laser power [151].

Moreover, by increasing the laser power, the density of sub-micron and nanoscale features on the top and sides of the channels also increases. This phenomenon also affects the wetting behaviour of the samples and renders them more superhydrophobic (SH).

By placing the superhydrophobic PTFE samples in LB bacteria culture, a visible silver layer was formed on top of the ablated/superhydrophobic surface (Figure 7.4). The presence of the silver layer confirmed the presence of air pockets between the micro and nano structures of the ablated surface. This air layer prevents direct contact between bacteria and the surface. For the sample not stable at Cassie-Baxter state, the air layer developed narrower over the experiment time until it disappeared. These kind of samples (not stable at Cassie-Baxter) eventually failed and fully soaked with LB culture.

In the case of failed superhydrophobic surfaces, bacteria cells take advantage of the very large surface area of the hierarchal superhydrophobic surface and largely adhere and colonise on the surface. The rough surface would be bombarded with bacteria due to the higher surface area and offering hidding spots from the shear to the bacteria.

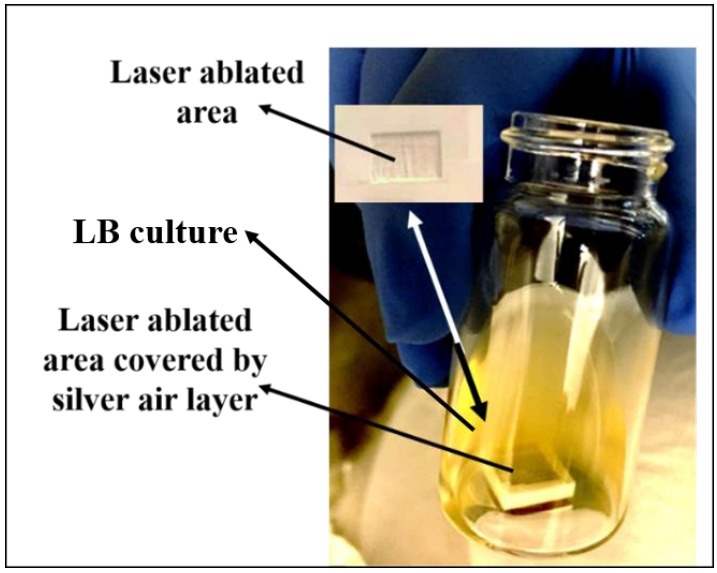

Figure7.4. Laser ablated placed in air and in LB bacteria culture, a silver air layer covered the superhydrophobic surface indicates the Cassie-Baxter state

Hence, the existence of air layer is essential for development of anti-biofouling properties of superhydrophobic surfaces. The stability of the air layer is key in maintaining durability of the superhydrophobic surface. The failure of the air layer results into the failure of the anti-

biofouling properties of the superhydrophobic surface. Thus, the silver air layer has to be closely examined upon placing the samples in the LB culture and also during the incubation. The silver air layer is a representative of the wetting state of the sample (Cassie-Baxter or Wenzel). When the SH samples are placed in LB culture, initially they are in Cassie-Baxter state.

While the silver layer of some PTFE substrates were stable towards the end of the experiment, the air layer of some others became visibly thinner during the incubation. The failure time greatly depends on the roughness properties of the SH PTFE surface.

When air layer failure takes place, the air pockets between the micro channels, as well as the air pockets between the sub-micron grooves, partially to fully, fail and only nano-scale pockets between the nano features remain. This failure is a source for a transition and coexistence between the Cassie-Baxter and Wenzel state. This transition state plays an important role in the adhesion of bacteria cells into the PTFE SH samples as explained below. After 4 hrs of incubation, samples were removed from the LB bacteria culture and prepared for SEM, fluorescent microscopy and confocal imaging. The results are presented in Figures 7-5 and 7-6.

As seen in Figures 7-5 and 7-6, bacteria adhesion (both type; *S.aureus* and *E.coli*) to all the superhydrophobic PTFE surfaces is extensively less compared to the smooth surface of PTFE (control- Figure7-5-a and 7-6-a). The SEM images of the flat PTFE surfaces show a significant number of bacteria, while SEM pictures of superhydrophobic samples noticeably show less bacteria attachment (figure 7-5-b,c, and d). More results obtained from the fluorescence microscopy as well as confocal microscopy show that the level of fluorescence correlates with bacteria population.

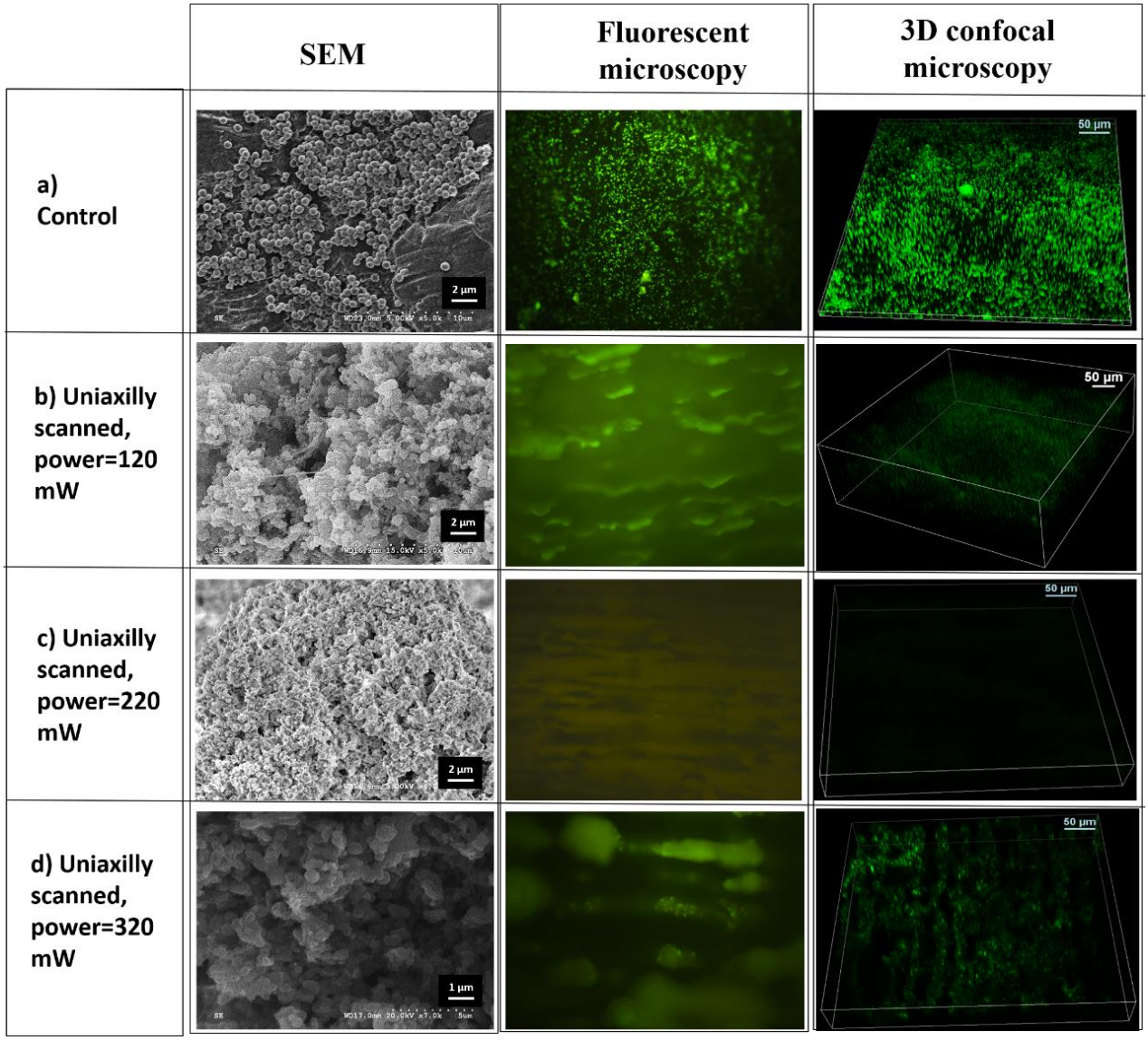

Figure 7.5. SEM images, fluorescent microscopy, and 3D fluorescent confocal images of Laser ablated and smooth PTFE samples incubated in LB *S. aureus* culture for 4hrs at 37°C

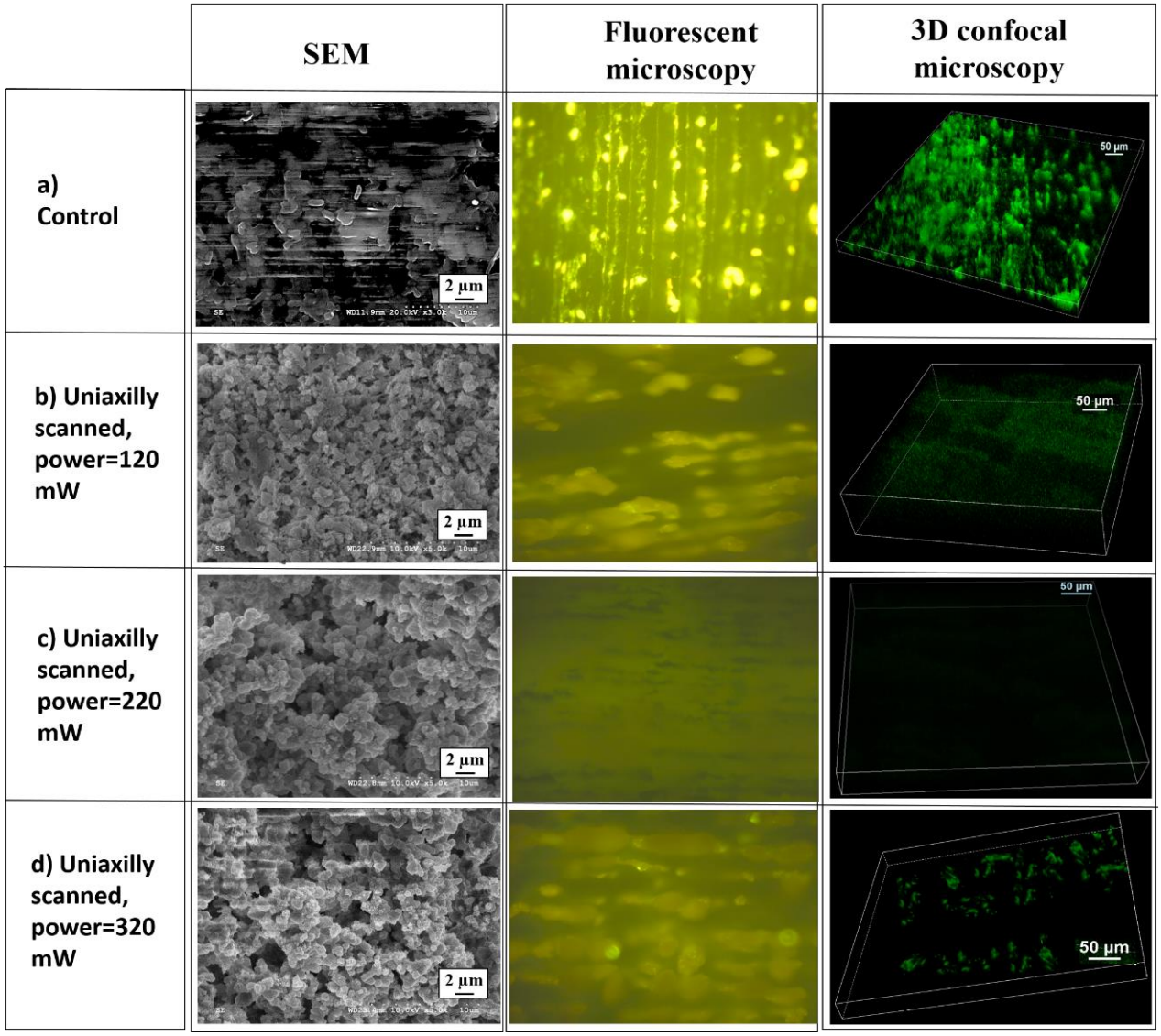

Figure 7-6. SEM images, fluorescent microscopy, and 3D fluorescent confocal images of Laser ablated and smooth PTFE samples incubated in LB *E. Coli* culture for 6 hrs at 37°

Figure 7-7 semi-quantifies the results obtained from the images shown in Figure 7-5 and 7-6. The level of adhered bacteria for each sample was quantified based on the surface fluorescent light intensity of images using ImageJ software. Results were normalized to the flat surface of PTFE (control substrates) and plotted in Figure 6. Contact angle and contact angle hysteresis are also listed for each sample. In figure 7-7, columns a, b, and c represent PTFE surface scanned with 120mW, 220mW, and 320mW respectively.

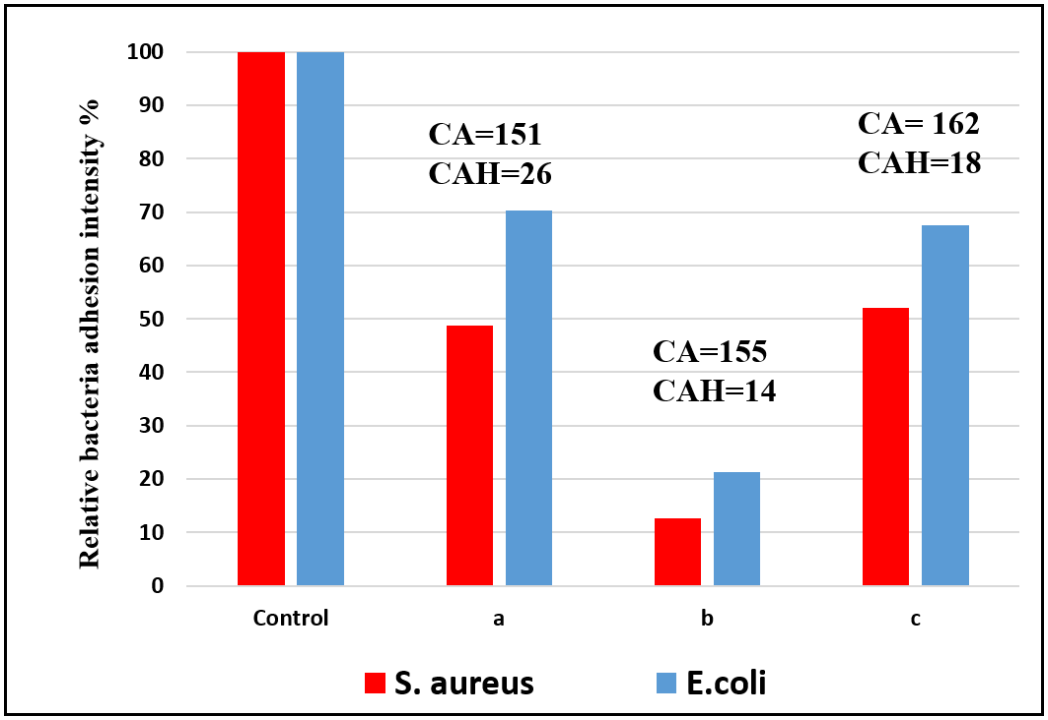

Figure 7.7. Relative *S.aureus* and *E.coli* bacteria adhesion intensity on flat and laser ablated PTFE surfaces scanned with different laser powers a)120mW, b)220mW, and c)320mW. Relative intensities of laser ablated PTFE surfaces have been determined with respect to the flat PTFE substrate

All superhydrophobic surfaces exhibit less bacteria adherence compared to the flat one. Bacteria adhesion significantly decreased from sample "a" to sample "b", due to higher CA and lower CAH (higher level of superhydrophobicity). However, there is a significant change in bacteria adhesion from sample "b" to sample "c" in the opposite direction, contrary to our expectation and indeed surprizing. Clearly PTFE sample lasered with 220mW (Figure 7-5-c and 7-6-c) exhibits less bacteria adhesion of all SH surfaces.

As the laser power of ablation increases, deeper channels (H) are created. Although developing deep channels increases the surface aspect ratio, it might increase the capillary effect of channels for LB culture as well. Increasing the capillary effect along with high contact angle hysteresis of these surfaces accelerate air pockets failure leading to transition state[169]. High contact angle hysteresis along with channel morphology results in loss of air pockets (transition from Cassie-Baxter to Wenzel); and even high CA cannot compensate for that. This is usually the case for uniaxial laser scanned polymeric surfaces scanned with non-optimized laser power.

In order to minimize the capillary effect and decrease the CAH, all three laser ablated substrates are laser scanned biaxially. By this method, pillared dual structured, truly superhydrophobic samples with high CA and low CAH are obtained (for more details see section 5-3-2). This gave us the opportunity to closely study the effect of roughness factors, without interfering effects of channeled morphology and wetting sensitivity.

7-2 Biaxial Scanned PTFE Surfaces and Suppression of Bacteria Adhesion

In order to prevent capillary effect and decrease the CAH, three uniaxially scanned PTFE surfaces were vertically laser scanned to create uniform pillared morphology. The laser scan speed and overlap for the second pass was set equal to 0.5 mm/s and 0% respectively. The laser power of the second scan is much smaller than the laser power of the first scan in order to avoid overwriting the morphology created during pass 1. The laser power of the second scan was set to 50mW for all three samples, while the laser power of first scan were 120, 220, and 320 mW.
The effect of biaxial scan using a low power laser beam for the second pass on the formed PTFE surface morphology is shown on Figure. 7-8 where clearly pillared morphology has been produced.

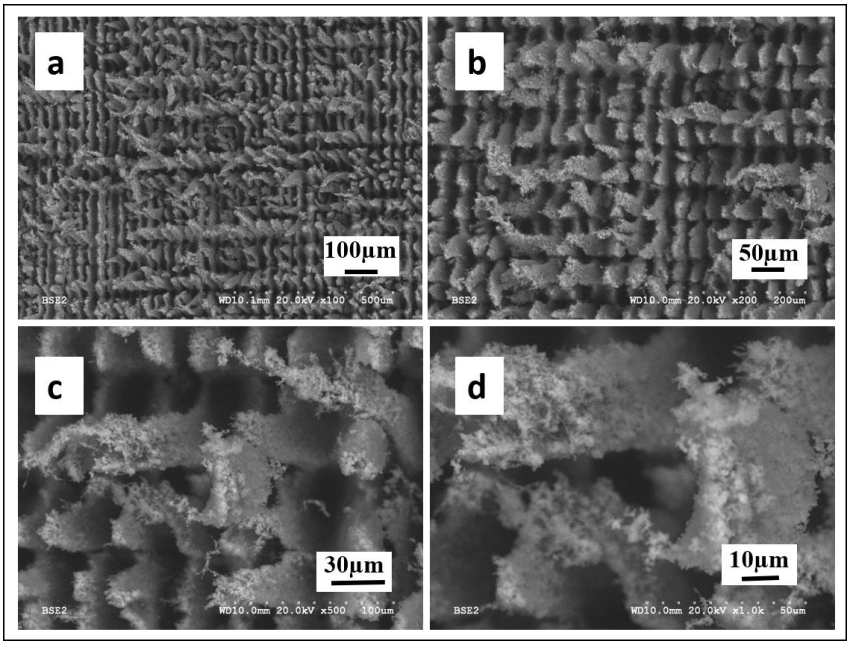

Figure 7.8. SEM pictures of biaxially scanned PTFE surface at various magnifications. The laser power for the first scan was 320mW and for the second scan was 50mW [149]

Reducing the laser power of the second pass dramatically increases the level of sub-micron and nano-scale roughness. This affects superhydrophobicity dramatically. As a result, the water contact angle of all three samples are above 160° and their hysteresis is less than 12°. As the laser power of first scan increases the CAH of the sample decreases; from 12° to 7° to 4° for 120, 220, and 320mW respectively. The contact angle and contact angle hysteresis indicates that samples are superhydrophobic in contact with water and LB bacteria culture. The wetting behaviour of the biaxially scanned samples are summarized in Table 7.1.

Table 7.1. Wetting behavior of biaxial scanned PTFE samples

Sample	**a'** **Pass 1: 120mW,50%overlap** **Pass 2: 50mW, 0% overlap**	**b'** **Pass 1:** **220mW,50%overlap** **Pass 2: 50mW, 0% overlap**	**c'** **Pass 1:** **320mW,50%overlap** **Pass 2: 50mW, 0% overlap**
CA°	162±2	162±2	162±2
CAH°	12±1	7±2	4±1

Biaxially scanned superhydrophobic PTFE surface were incubated in *S.aureus* and *E.coli* culture for 4hrs. Consequently, they were removed from the LB bacteria culture and prepared for SEM, and fluorescent microscopy as described before. Results are shown in Figure 7.9.

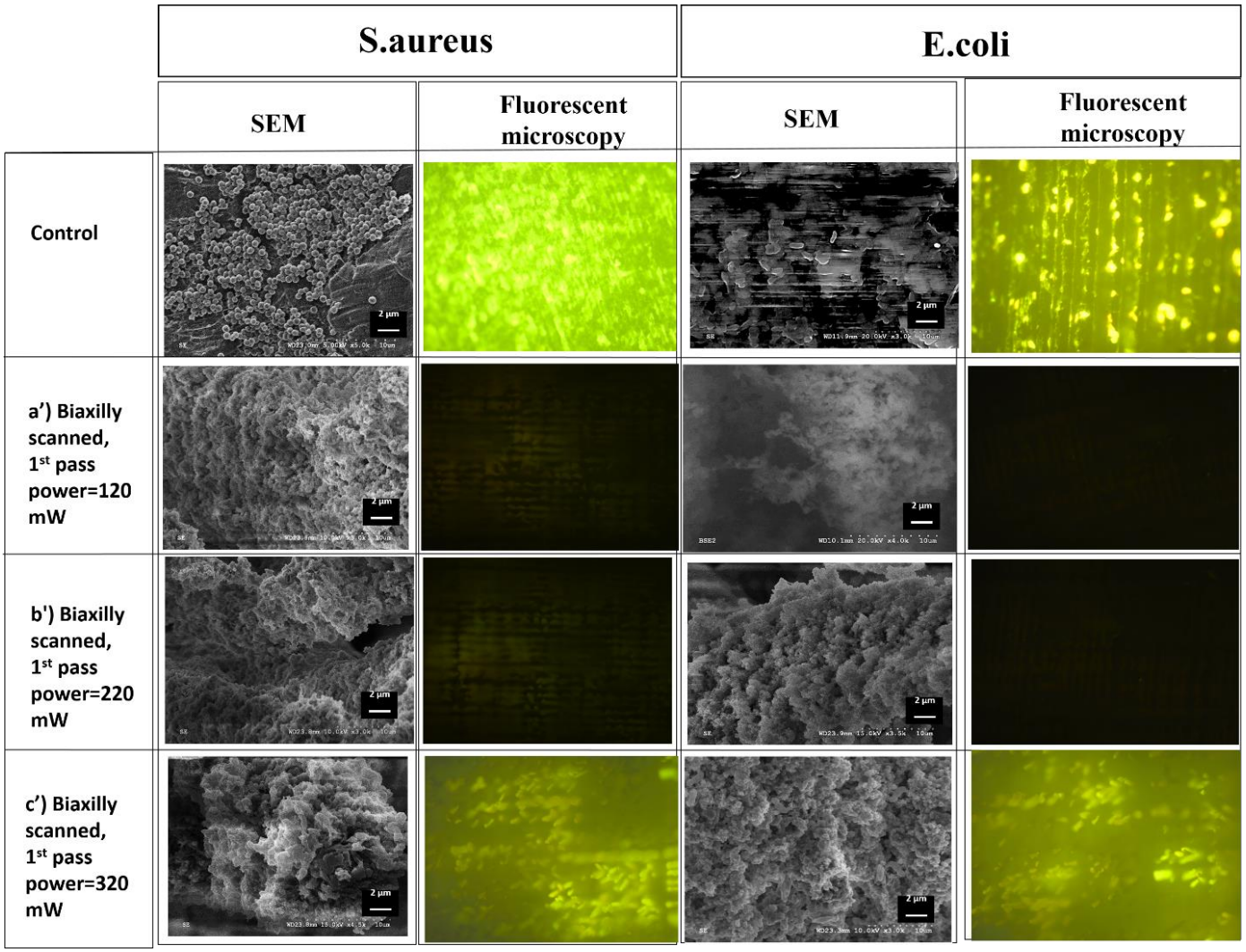

Figure 7.9. SEM images and fluorescent microscopy images of biaxially laser ablated and flat PTFE substrates incubated in LB *S.aureus* and LB *E. Coli* culture for 4hrs at 37°

The level of adhered bacteria for each sample was semi-quantified based on the surface fluorescent light intensity of images using ImageJ software. Results were normalized to the flat surface of PTFE (control substrates) and plotted in Figure 7-10.

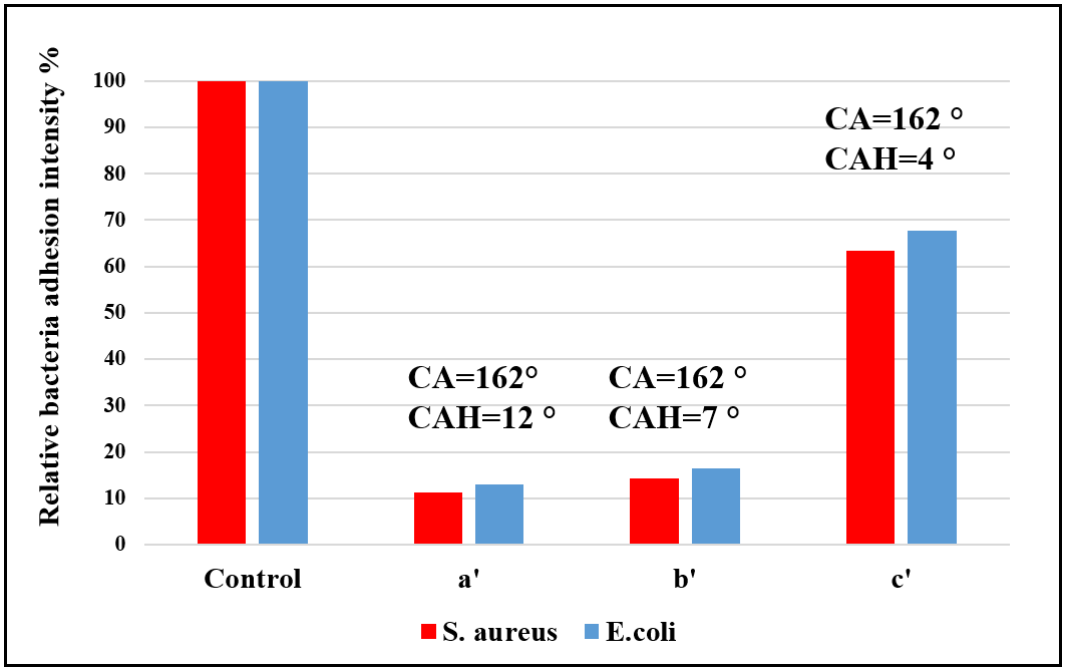

Figure 7.10. Relative S.aureus and E.coli bacteria adhesion intensity on flat and biaxial laser ablated surfaces of PTFE; first scanned with different laser powers a')120mW, b')220mW, and c')320mW and later vertically scanned with 50mW. Relative intensities of laser ablated PTFE surfaces have been performed with respect to the flat PTFE substrate

7.2.1 Biaxially scanned PTFE with 120 and 50 mW

SEM and Profilometery images show that the substrate depicted in Figure 7-9-a′ allow adhesion of significantly less amount of bacteria in both bacteria cultures compared to its uniaxially scanned counterpart (7-5- a and 7-6-a). The silver air pocket layer which created on top of the a′ substrates at the beginning of the tests, were still visible toward the end of the 4 hrs period (in both LB cultures). SEM and fluorescent images confirm that bacteria cells were not even attached onto the peak of the pillars, which are usually the first spots that exit the Cassie-Baxter state and enters the transition state. This shows that the surface was stable at Cassie-Baxter state or at early stages of transition state towards the end of 4 hours' incubation period. Low bacterial adhesion to this surface is in full agreement with its high water resistance and pillared morphology.

7.2.2 Biaxial scanned PTFE with 220 and 50 mW

Bacteria adhesion onto the PTFE samples scanned with 220mW with and without applying the vertical scan (Fig 7-9-b' and Fig 7-5-b & 7-6-b respectively) is similar. Silver air layer was still

visible in both uniaxial and biaxial scanned surfaces (in both LB cultures) towards the end of the four hours' test. By comparing sample b in fig 6 and sample b' in fig 7-10, it could be concluded that pillared morphology was in a better alignment with anti-bio fouling properties of superhydrophobic PTFE substrate.

7.2.3 Biaxial scanned PTFE with 320 and 50 mW

Despite the fact that the c' sample exhibits the highest CA and lowest CAH of all substrates fabricated, completely failed after less than 2 hrs of test in the *S.aureus* culture. At about the same time, the air pockets of c′ sample incubated in *E.coli* were disappeared too. After removing the samples from the LB cultures, c′ samples are entirely soaked and wet. Results obtained from fluorescent microscopy and SEM images depict large amount of bacterial adhesion on the surface of these superhydrophobic samples.

Due to outstanding wetting resistance behavior of this sample, it was expected to see the least amount of bacteria adhesion. Unexpectedly, this sample turned to fail faster in LB cultures among all 6 samples tested. Interestingly, c sample which scanned uniaxial with 320mW, also failed despite its excellent superhydrophobic properties (sample c in Figure 7-5, 7-6, and 7-7).

This shows that a closer look to roughness parameters is needed in order to determine those characteristics that play a significant role in suppressing bacteria and protein adsorption.

7.3 Roughness Characteristics of Laser Ablated PTFE and their Effect on Superhydrophobicity Durability

Figure 7-11 presents optical profilometry images of (a) uniaxially and (b) biaxially scanned PTFE surfaces at two levels of magnification. Diverse colors of the patterns represent peaks and valleys with different heights and depths. For the uniaxial scanned surfaces, various colors are seen along the walls of the channels which show the variety of heights along the wall (not all parts of a single wall have equal height). For biaxially scanned patterns also, the color of the pillars are different which confirms the height difference between the pillars.

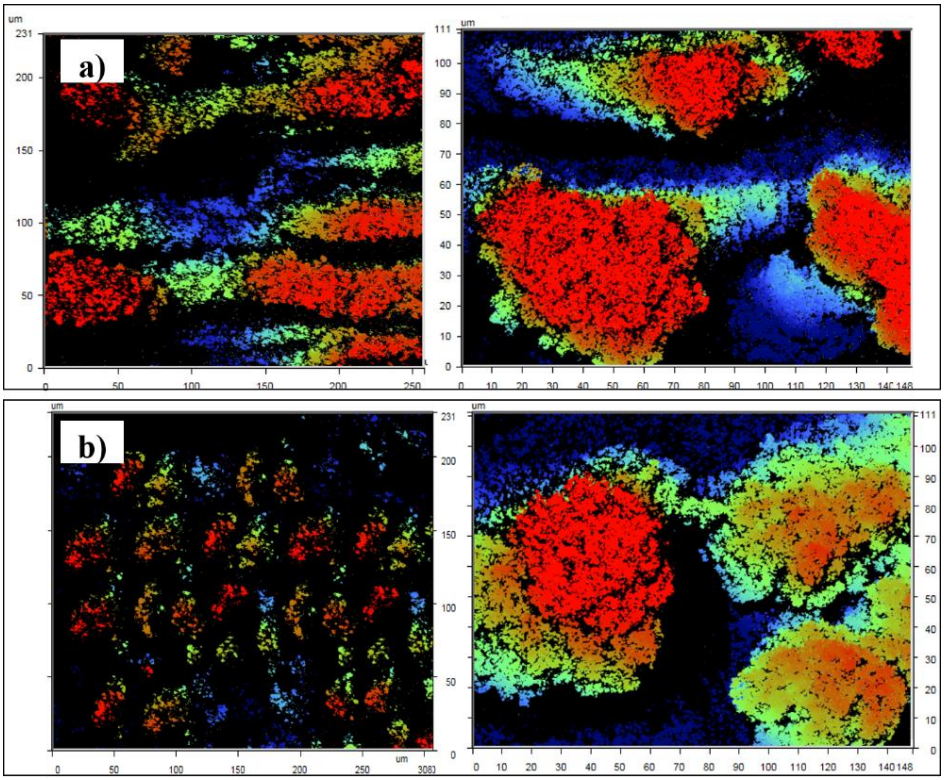

Figure 7.11. Profilometery images of a) Channeled-like uniaxial scanned PTFE with laser power of 220mW, scan speed of 0.5mm/s, and overlap of 50%, b) pillared biaxial scanned PTFE with laser power of 220mW and 50mW, scan speed of 0.5mm/s, and overlap of 50%, at two levels of magnification

From the SEM and profilometry images such those depicted in Fig 7-11, it was concluded that by increasing the laser power, more well-defined sub-micron grains are created on the surface in both morphologies (channelled and pillared). At higher laser powers, a larger number of grains with higher heights and less spacing are formed along the walls or pillars. This can be seen in Figure 7-12 which shows the roughness profile for two biaxially scanned PTFE substrates at two different laser powers. Sample "a" was biaxially scanned with 220 and 50mW, while sample "b" was biaxially scanned with 320 and 50mW.

The roughness profile of the substrates are shown along the X-direction (red line) and Y-direction (blue line). For the substrate ablated with the bigger laser power (320mW, sample "b"), the peaks are remarkably higher and valleys are much deeper compared to that ablated with the smaller laser power (220mW, "a"). The roughness profiles of both surfaces are distinctly different, in spite of their close "R_a" values displayed in Figure 7-12.

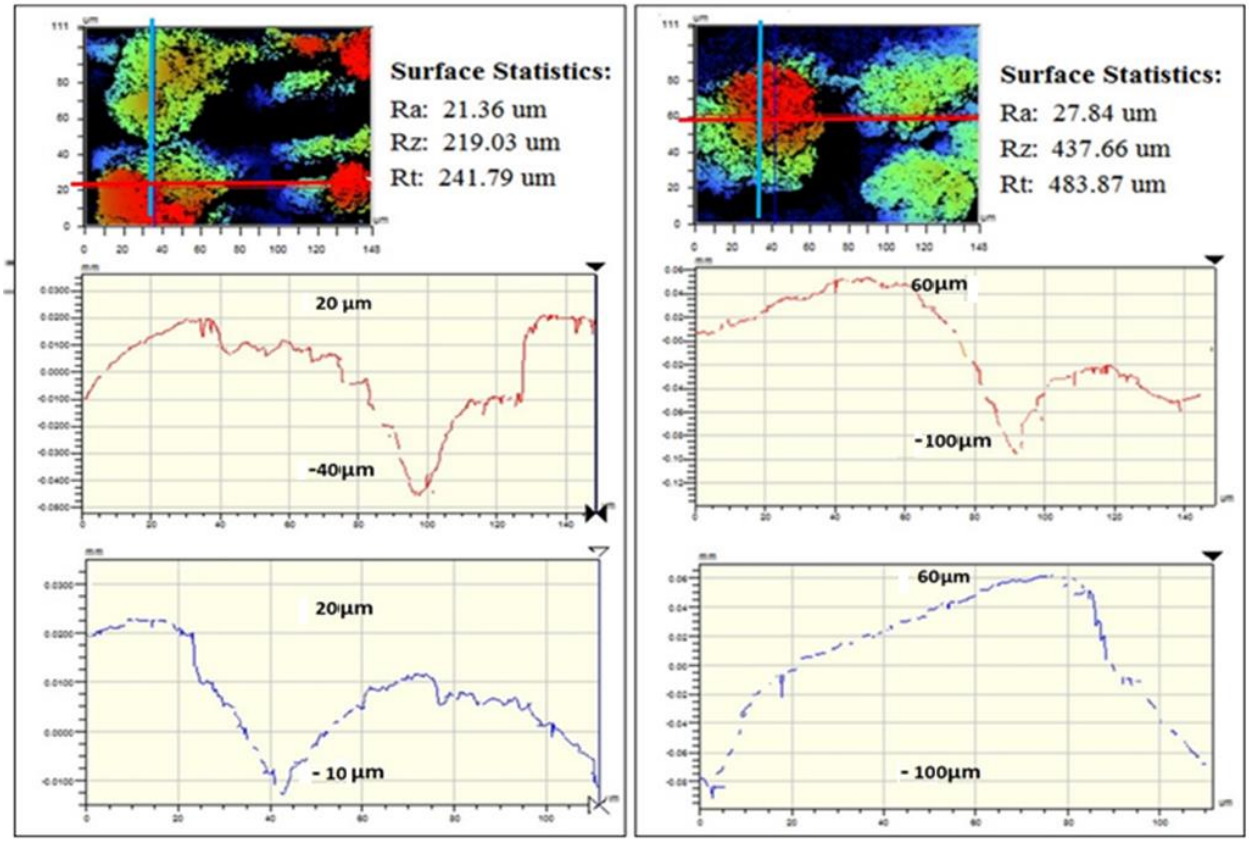

Figure7.12. Roughness profile of biaxial scanned PTFE surfaces obtained from optical Profilometery; a) Biaxial laser scanned PTFE with 220 and 50mW, b) biaxial laser scanned PTFE with 3320 and 50mW

While the CAs, CAHs, and roughness average of both samples, "a" and "b" in Figure 7-12 are similar, the question is what makes these two surfaces be so different in terms of bacterial adhesion? Therefore, a different quantification/measure of roughness is needed.

To quantify the roughness profile of a surface, three different measures of the roughness topography were used in this work. First R_a which is defined as the average roughness that is arithmetic average of absolute values of peak to valley heights; secondly R_z which is defined as the average of ten maximum heights of the profile; and finally Rt of the surface which is defined as the maximum height of the profile. The results for the various substrates are summarised in Table7-2. The reported values for each surfaces are the average of 5 measurements. By looking through the roughness factors of the samples, it is obvious that R_t and R_z of the samples laser scanned with 320mW (both uniaxial and biaxial) are significantly larger compared to other

samples, while their Ra are very similar. This results into a large difference between the R_z and R_a of the samples scanned with 320mW in both morphologies (uniaxial or biaxial).

The large difference between R_z and R_a reveals that the laser ablated surfaces contain a number of extended sub-micron grains (on top of the channel walls or on the micro pillars) whose average heights (R_z) are considerably larger than the average height of their surrounding walls or pillars (R_a). This leads to fast failure of the air pockets surrounded the tips of these sub-micron grains (due to the lack of sufficient support) thus allowing the transition from Cassie-Baxter to Wetzel state.

By investigating the CA, CAH, and Ra of the samples, it is not possible to attain enough information regarding the durability of the samples. By plotting bacteria adhesion versus CA or CAH, neither a trend nor any meaningful information would be obtained. Thus a new parameter is needed to correlate it with the level of bacteria adhesion.

Table 7.2. Roughness factors of laser ablated PTFE surfaces

Laser power (mW)	Type of laser patterning	R_a (roughness average, μm)	R_z (average of 5 maximum height of the Profile, μm)	R_z / R_a (The ratio between R_z and R_a)
120	Uniaxial	29.66	292.51	9.86
220	Uniaxial	31.98	312.26	9.79
320	Uniaxial	32.84	498.87	15.52
120, 50	Biaxial	20.69	229.51	10.70
220, 50	Biaxial	21.94	241.14	11.31
320, 50	Biaxial	24.48	447.66	18.22

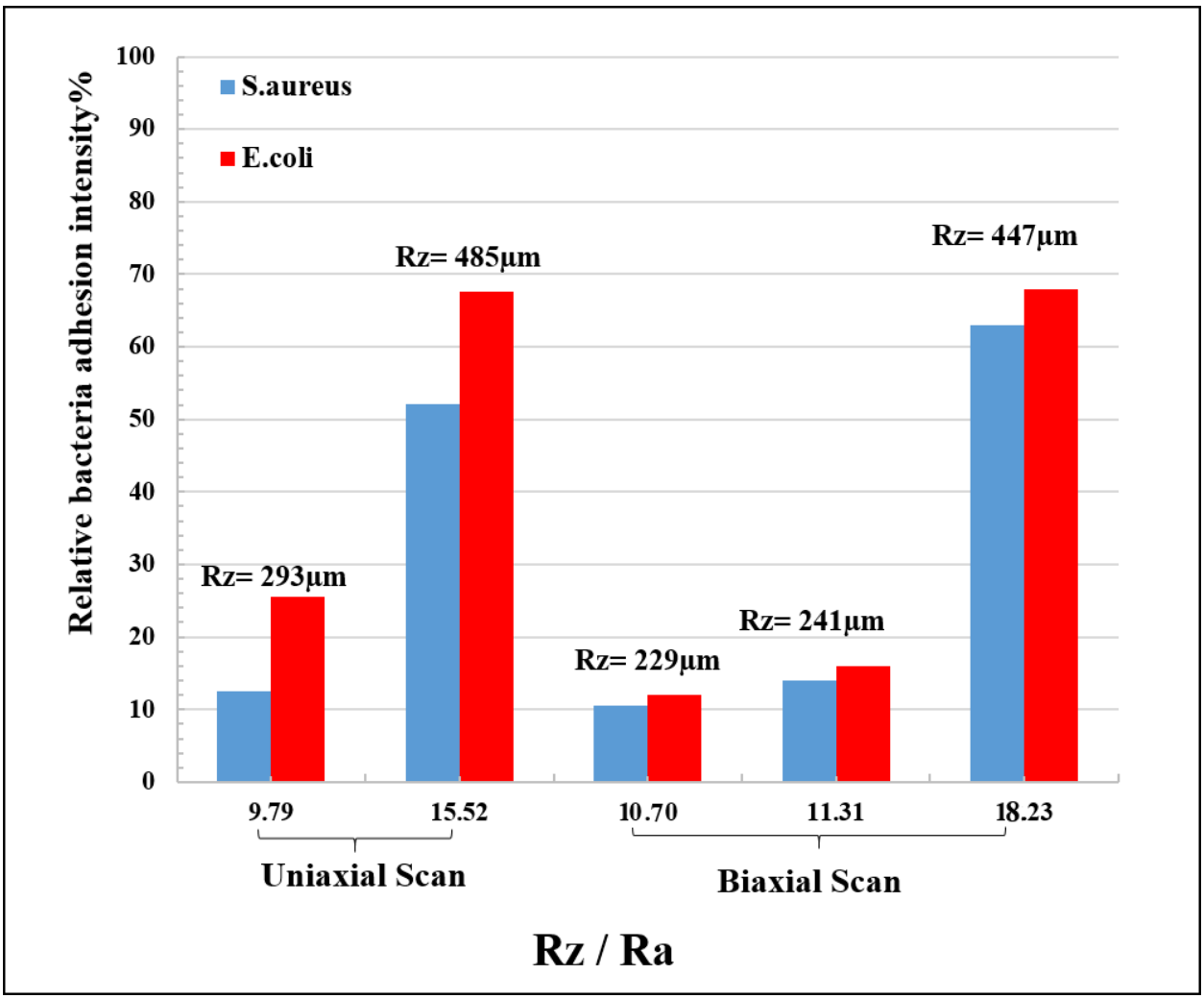

Figure 7.13. Relative Gram positive and Gram negative bacteria adhesion onto laser ablated PTFE surface after 4 hrs of incubation at 37° vs. the ratio of the average height of the 5 tallest peaks(R_z) to the roughness average (R_a) of the surface

Figure 7-13 plots, the relative bacteria adhesion over 4 hrs at 37° as a function of the ratio of the average height of the 5 tallest peaks of the surface (R_z) normalised by the average roughness (R_a). It was found that the relative adhesion of bacteria cells onto the superhydrophobic PTFE surface (the probability of Cassie-Baxter failure) correlates well with R_z/R_a ratio. In other words, bacteria adhesion considerably increases for the samples that their R_z/R_a ratio is significantly large, while CA and CAH remain the same PTFE surface biaxially scanned with 320 and 50mW allow adherence of the highest amount of bacteria due to its higher surface area.

7.4 Comparison of Bacteria Adhesion of Superhydrophobic PTFE Surface

In order to confirm the results obtained from bacteria adhesion test, a complimentary experiment was performed. A PTFE substrate was biaxially scanned with certain laser powers, such that the left half was laser scanned with 120 and 50mW and the right half was laser scanned with 320 and 50mW resulting different roughness characteristics. The sample was incubated in LB culture for 4 hrs at 37° under 80 rpm.

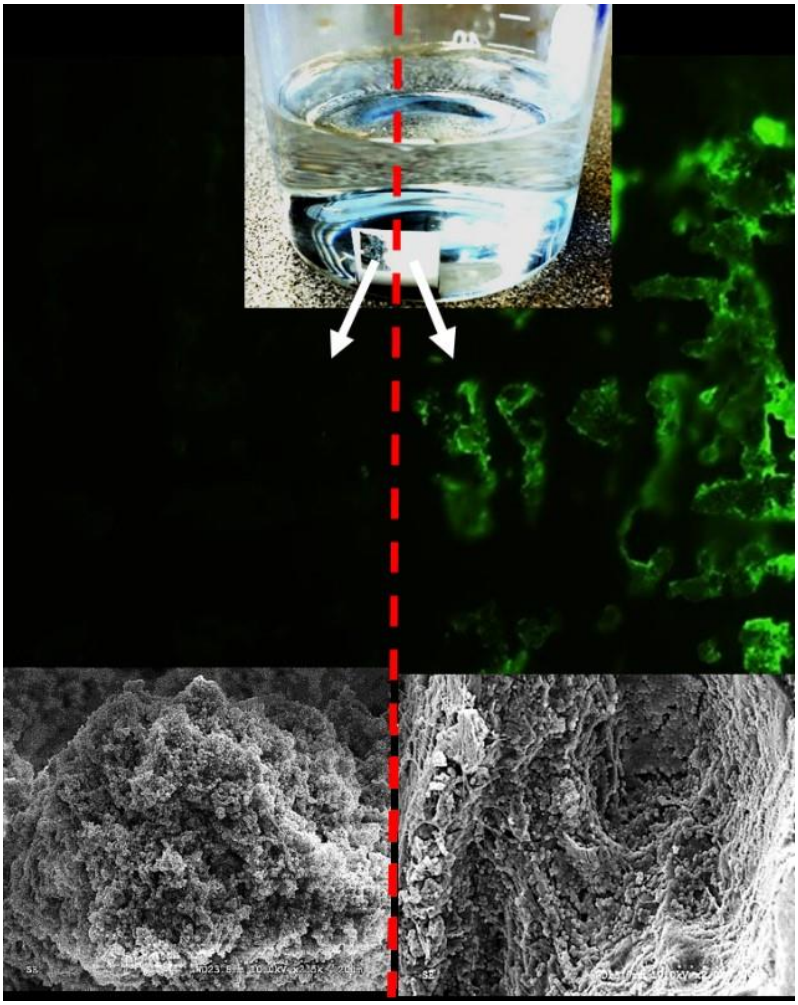

Figure7.14. PTFE superhydrophobic surface scanned with two different laser powers; the left half is biaxially scanned with 120 and 50mW, while the right side is biaxially scanned with320 and 50mW

The SEM and fluorescent microscopy pictures confirm that after 4 hrs, the half scanned with 320 and 50mW (R_z/R_a value equal to 18.3) is fully soaked and wet while the other half (R_z/R_a value

equal to 10.7) is still covered with air pockets that is seen as a visible silver air layer in Figure 7-14.

Fluorescent microscopy pictures and SEM images of Figure 7-14 have also shown that the left part of the sample was stable in Cassie-Baxter state towards the end of the incubation, while the right part entered into the transition and eventually became stable at Wenzel state at a time significantly less than 4 hrs. Figure 7-14 confirms that even superhydrophobic surfaces with the highest CAs and lowest CAHs might possibly fail in bacterial cultures after few hours unless the created topography is somehow designed to possess certain roughness characteristics. Particularly, peaks with heights much taller than the average height of the surface (Ra) facilitate the air pockets failure of the superhydrophobic surface.

7.5 Protein Adsorption on Superhydrophobic Surfaces

In order to verify the results obtained from bacteria adhesion on various superhydrophobic PTFE substrates, the extent of protein adsorption on to the same superhydrophobic samples were also tested. Femtosecond uniaxially scanned and biaxially scanned PTFE surfaces were incubated in two different protein solutions and fresh blood plasma for 4 hrs at 37° and 80-100 rpm. These tests are described in detail in this section.

First in order to test protein adsorption on the surface of the samples, commercially available bovine serum albumin (BSA), and Immunoglobulin G (IgG2a-FITC) from mouse plasma were chosen as model proteins. Both proteins were conjugated to fluorescent tags (commercial fluorescently labeled). Serum albumin is the most abundant blood plasma protein. Because of its high concentration and moderate diffusion coefficient, albumin dominates initial interactions with the surface. Immunoglobulin G (IgG) is another plasma protein which with its lower concentration and larger size (smaller diffusion coefficient), has a slower rate of reaching at the surface. The adherent protein was semi-quantified based on the surface fluorescent light intensity of images using ImageJ software in a similar manner as described for the bacteria results. Results were normalized to the flat surface of PTFE (control substrates) for comparison and plotted in Figure 7-15.

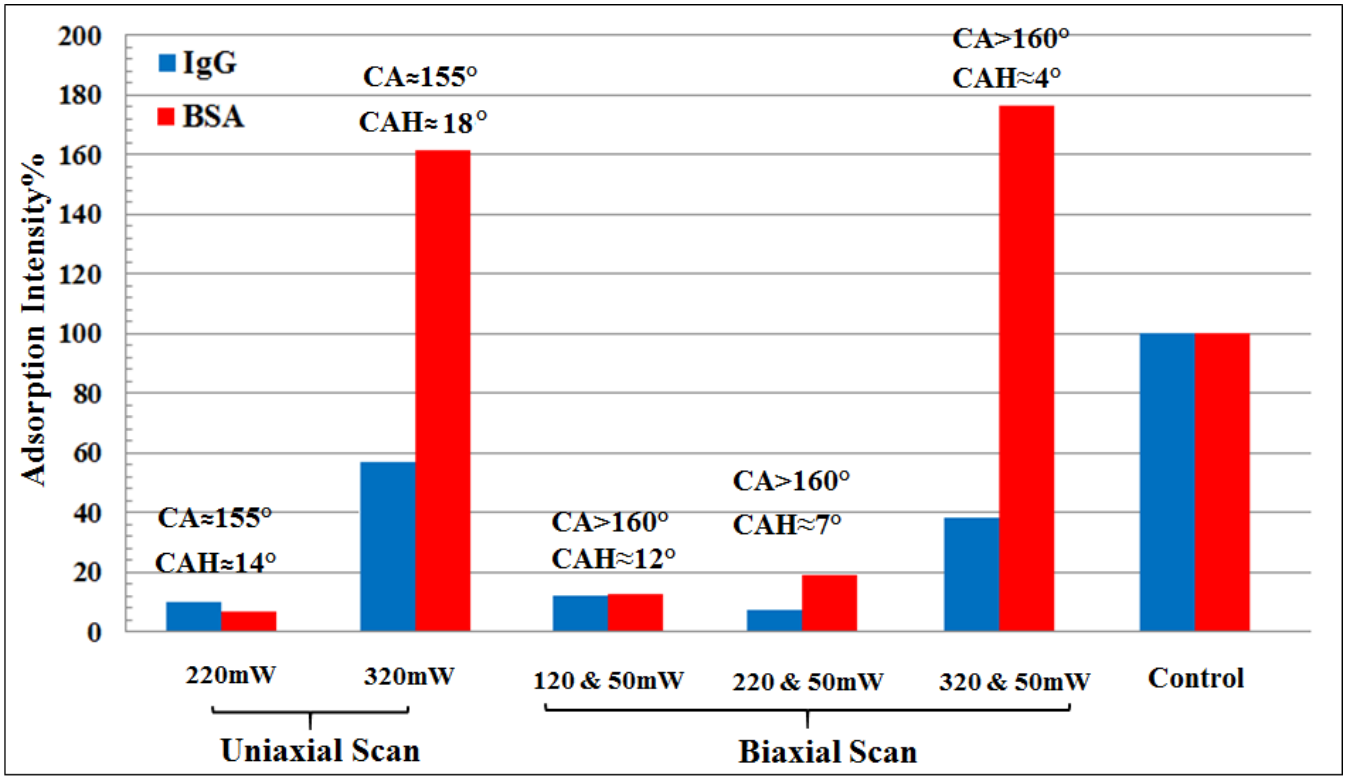

Figure 7.16. Relative BSA and IgG adsorption intensity on flat and laser ablated surfaces of PTFE

The results obtained from BSA and IgG adsorption on the surface of superhydrophobic PTEF are in full agreement with the results reported earlier on the bacteria adhesion. Results from the protein adsorption test show that not all superhydrophobic surfaces behaved similar; the superhydrophobic surfaces fabricated with very higher laser fluence (320 mW) in both uniaxial and biaxial scan, failed dramatically in contact with protein solutions. The same superhydrophobic samples which were stable in bacteria adhesion test for 4 hrs, were also stable at Cassie-Baxter state for 4 hrs in the protein adsorption test. $R_{a1}=R_{a2}$

As the last test, samples were incubated in human fresh plasma for 4 hrs at 37° and 80 rpm. Blood plasma is a complex matrix of approximately three hundred distinct proteins with different size, hydrophobicity, charge, and characteristics. However, all these proteins are made up of the same building units called amino acids. The amino acids are linked to form a protein by linking the amino group on one amino acid with the carboxylic acid group on another amino acid to form an amide bond. Amide I and amide II bands are two major bands of the protein infrared spectrum and they arise from the amide bonds that link the amino acids. Amide I band is found

between 1600 and 1700 cm^{-1}, near 1650 cm-1. Amide II band is found in the 1510 cm^{-1} and 1580 cm^{-1} region, near 1540 cm^{-1}. The presence of amide I and amide II bands is an indication that protein was present on the sample's surface after the adsorption experiment

A flat surface of PTFE along with two biaxial scanned samples (scanned with 220&50mW, and 320&50mW) were incubated in human fresh blood plasma. Infrared spectra of the three samples are presented in Figure 7-17.

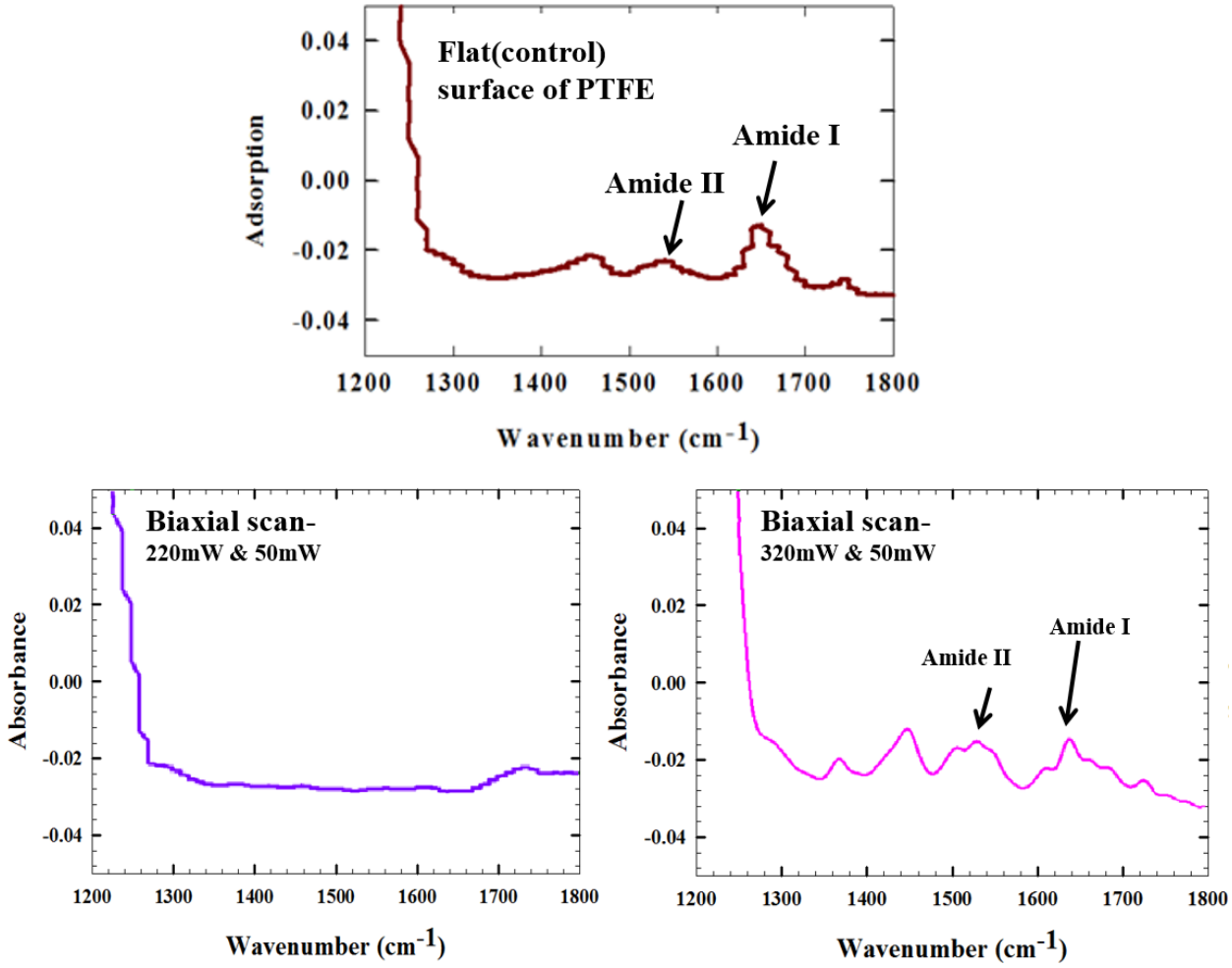

Figure 7.17. Infrared spectra of a flat and biaxially scanned PTFE substrates; presence of amide I and amide II bands in flat surface and 320&50mW laser scanned PTFE surface is an indication that protein(s) exists on the sample's surface after the adsorption experiment

Results confirm the presence of protein on the flat surface of PTFE after 4 hrs of incubation (top graph in Figure 7.17). The superhydrophobic samples displayed the opposite behaviour (lower graphs in Figure 7.17). The Infrared Spectra of the sample scanned with 220&50 mW (the

substrate found stable at Cassie-Baxter state in bacteria runs), didn't show any amide I and/or Amide II bands. While, the Infrared Spectra of the superhydrophobic sample scanned with 320&50 mW (the substrate failed to Wenzel state in bacteria runs), showed bands for amide I and amide II.

The results obtained from protein solution test and plasma protein adsorption tests are very similar with the results obtained earlier on the bacteria adhesion experiments. The superhydrophobic surfaces failed in bacteria adhesion tests also failed in contact with proteins (both protein solutions and blood plasma). These failed substrates were fabricated with very higher laser fluence (320 mW) in both uniaxial and biaxial scan. The same superhydrophobic samples which were stable in bacteria adhesion test for 4 hrs, were also stable at Cassie-Baxter state for 4 hrs in the blood plasma and protein solutions.

7.6 Summary

Conflicting results have been reported in the literature when describing the influence of surface superhydrophobicity on the extent of protein/bacteria adhesion [121]. These conflicts have arisen as the interactions between the protein/bacteria and substrate are largely influenced by the presence of different types of surface nano/micro structures. Along with high contact angle, and low contact angel hysteresis (which are the main characteristics of superhydrophobic surfaces), the size, morphology, and topography of the patterns also significantly impact the efficiency of superhydrophobic surfaces in repelling biological species.

In this chapter superhydrophobic PTFE samples fabricated in chapter 5 were characterized for protein adsorption and bacteria adhesion. It was found that channeled morphology possesses a high risk of failure due to their high contact angle hysteresis and the influence of the capillary effect.

In order to eliminate the capillary effect of the channels and minimize the CAH of PTFE samples, substrates were laser scanned biaxially. By this method, pillared dual structured substrates with large CA (>150º) and small CAH (<10º) are obtained. The influence of roughness factors on bacteria and protein adsorption were studied since all the sample examined are truly superhydrophobic and therefore merely CA and CAH cannot explain the experimental observations.

It was found that SH surfaces with high R_z/R_a values are not stable to be used in applications where protein adsorption or bacteria adhesion is the main concern. Bacteria adhesion and protein adsorption considerably increases for the samples that their R_z to R_a ratio is significantly large. It is noted that high R_z/R_a values imply non-uniform substrates containing bumps with depths or heights exceeding the average R_a. These bumps leads to fast failure of the air pockets and allowing the transition from Cassie-Baxter to impregnated state and eventually to Wetzel state.

Chapter 8: Conclusion

8.1. Conclusions

This PhD thesis investigated the processing and properties of superhydrophobic polymeric surfaces (with focus on PTFE) created through two different micr/nano fabrication methods; femtosecond laser ablation and thermal imprinting through hot embossing. The wetting properties and antibacterial activities (as potential application to medical sciences) of these surfaces were studied in detail. The main results from the experimental work can be summarized as follows:

1- Two distinctly different methods were used to ablate the PTFE surface; uniaxial and biaxial scanning. In each method, the effect of femtosecond laser irradiation parameters (fluence, scanning speed and beam overlap) on the morphology, topography, and wettability of the resulted micro/nano-patterns was studied in details. Scanning electron microscopy images have shown that the uniaxial laser ablation of the surface creates micro-channels partially covered with sub micron- and nano- scale features. The effects of increasing the laser fluence and decreasing the scan speed are similar as both increase the laser energy received per spot and result into the formation of more well-defined channels with bigger height. Uniaxial laser scanning of PTFE surface, could increase the CA of PTFE surface up to 160° and decrease the CAH as low as 12°.

2- A novel method of laser scanning of polymers (biaxial scanning) has been proposed which could create uniform morphology on the surface. Biaxial scanning creates pillared morphology which offers non-anisotropic wetting behaviour. Biaxial scanning of PTFE surface with non-identical laser fluences (laser fluence of first scan and second scan are not equal) increases the superhydrophobicity of PTFE surfaces into extremely high levels. This method decreases the CAH of the PTFE surface to below 3°, while the CA can be as high as 170º. For these laser ablated PTFE samples, the high density of nano features is responsible for the air-trapping and long term.

3- Femtosecond laser ablated SS templates with three different patterns were used to imprint dual scale roughness onto the surface of three different thermoplastics (PLA, HDPE, and medical-PVC) through hot embossing technique. The very high water repellency of imprinted PLA substrates is due to the more accurate micron/submicron replication of SS template's patterns on its surface. The much lower viscosity of PLA compared to the viscosity of HDPE (at the embossing temperature) is responsible for the higher CA and lower CAH of imprinted PLA compared to imprinted HDPE. PLA and HDPE imprinted substrates both became superhydrophobic with water CA well above 160° and CAH below 5°.

4- A re-entrant fibrous structure was created on the surface of HDPE when the metallic templates were removed from the replicated polymeric surface at higher temperatures where the polymer partially adheres on the metal. In addition, applying directional peeling force created angled micro-fibers (hook-like structure) which promote the anisotropic morphology. Fibrils were formed as a result of the micro-adhesion between the HDPE chains and the SS template. This bioinspired morphology is highly liquid (water and other organic liquids of low surface tension) repellant, and thus possesses superomniphobic properties.

5- The effect of micron, submicron, and nano scale surface textures on the initial attachment of bacteria and proteins on superhydrophobic PTFE surface was studied; for this matter in 5 individual runs, superhydrophobic PTFE samples were incubated in two different types of bacteria (one Gram positive and one Gram negative), two different types of protein solution (BSA and IgG), and fresh blood plasma for 4 hrs. This study shows that in addition to water contact angle and water contact angle hysteresis of the samples (which are the main characteristics of superhydrophobic surfaces), size and topography of the patterns also significantly impact the efficiency of superhydrophobic surfaces in repelling biological species. It was found that the relative adhesion of bacteria cells onto the superhydrophobic PTFE surface (the probability of Cassie-Baxter failure) correlates

well with critical roughness parameter of Rz to Ra ratio. Profilometery results depicted that Rt and Rz of the samples laser scanned with 320mW (both uniaxial and biaxial) are significantly larger compared to other superhydrophobic samples used in this study. The large difference between Rz and Ra leads to fast failure of the air pockets surrounded the tips of these sub-micron peaks/grains (due to lack of sufficient support); As a result, the wetting state of the superhydrophobic surface shifts from Cassie-Baxter to Wenzel state. However, we identified that SH surfaces with high Rz/Ra values are not suitable to be used in applications where protein adsorption or bacteria adhesion is the main concern.

8.2 Contributions to Knowledge

8.2.1 Biaxial Scanning to Fabricate a Variety of Superhydrophobic Patterns

In the present PhD work, we report a novel method of laser scanning (biaxial scanning) to produce various pillared type surface morphologies on PTFE. Biaxial scans generate pillared superhydrophobic surfaces which along with the high contact angle (as high as 170°), display extremely low contact angle hysteresis in all directions (as low as 3°). This is due to the large number of nano-features which maximize the air trapping capacity of the PTFE surface. As a result, PTFE surfaces with outstanding water repellant properties are obtained. Incubation of these pillared PTFE substrates in bacteria culture, protein solution, and blood plasma confirms that these PTFE surfaces are highly capable of preventing the initial attachment of biological species through promoting superhydrophobicity and reducing the contact area.

8.2.2 Nano-imprinting of Fibrous Morphology

An innovative strategy was developed to utilize thermal imprinting process to fabricate re-entrant superomniphobic micro-structures on polymeric surfaces and in particular on HDPE. The created re-entrant patterns on HDPE closely resemble the patterns found on the surface of filefish skin that is densely angled microfiber arrays. This bioinspired surface is highly capable of repelling both polar (water) and non-polar liquids of low surface tension and meets the superhydrophobicity and superominophobicity criteria. HDPE super-repellent surfaces hold great promise to be developed in large scales via simple templation methods and may subsequently find more practical applications in the near future.

8.2.3 Roughness parameters influencing the bacteria adhesion and protein adsorption onto superhydrophobic surfaces

All truly superhydrophobic surfaces of PTFE exhibit less bacteria adhersion and protein adsorption compared to the flat surface of PTFE. Some are stable at Cassie-Baxter state for a long time, while some compeletly fail and shift into Wenzel state after couple of hrs of incubation. In this study, we found that by investigating the CA, CAH, and R_a of the superhydrophobic samples, it is not possible to attain enough information regarding the durability of the samples which have a great influence on protein/bacteria adhesion of the surface. Thus, a new roughness parameter is defined which affect the probability of Cassie-Baxter failure during the incubation. The probability of superhydrophobicity failure during the incubation correlates well with the R_z to R_a ratio. It was found that the relative adhesion of bacteria cells and plasma proteins onto the superhydrophobic PTFE surface considerably increases for the samples that their R_z to R_a ratio is significantly large.

8.3 Recommendations for Future work

In order to complement the above studies on the effect of surface topography on durability of superhydrophobic surface, the following suggestions can be considered for future work:

1- The density and frequency of the micro grains appeared on top and sides of the micro channels/pillars at high laser powers (e.g. 320mW and 320&50mW) have a significant effect on the durability of the superhydrophobic surface. The effect of laser parameters on the density and frequency of these grains have to be closely studied.

2- It would be a good idea to incubate the superhydrophobic surfaces in bacteria culture in the presence of plasma proteins as well. In this case a more realistic biological system will be tested.

3- HDPE films are largely being used in catheter industry. Superomniphobic HDPE film fabricated in chapter 6, might be a very effective anti-biofouling substrate which could find its way in anti-biofouling catheters fabrication. In this regard, Gram positive and

Gram negative bacteria have to be tested on the surface of this superomniphobic polymer in the absence and presence on plasma proteins.

4- In this work, PTFE was used as a main polymeric model. However, it would be great to create superhydrophobic patterns on more biocompatible polymers such as Polyurethane, and repeat the bacteria and protein tests.

5- The majority of micro/nano fabrication methods are usually expensive and time consuming. Finding affordable faster methods (laser splitting and parallel ablation) that can be applied to larger scales are always desired.

Bibliography:

[1] L. E. Nicolle, “Catheter associated urinary tract infections,” Antimicrobial Resistance and Infection Ctrl. vol. 3, pp. 1–8, 2014.

[2] B. W. Trautner; R. O. Darouiche, “Catheter associated infections,” Arch Intern Med., vol. 164, pp. 842–850, 2004.

[3] J. Hasan, R. J. Crawford, and E. P. Ivanova, “Antibacterial surfaces : the quest for a new generation of biomaterials,” Trends Biotechnol., vol. 31, pp. 295–304, 2013.

[4] E. P. Ivanova, V. K. Truong, H. K. Webb, V. A. Baulin, J. Y. Wang, N. Mohammodi, F. Wang, C. Fluke, and R. J. Crawford, “Differential attraction and repulsion of Staphylococcus aureus and Pseudomonas aeruginosa on molecularly smooth titanium films.,” Sci. Rep., vol. 1, p. 165, 2011.

[5] B. Mrabet, M. N. Nguyen, A. Majbri, S. Mahouche, M. Turmine, A. Bakhrouf, and M. M. Chehimi, “Anti-fouling poly(2-hydoxyethyl methacrylate) surface coatings with specific bacteria recognition capabilities,” Surf. Sci., vol. 603, pp. 2422–2429, 2009.

[6] M. B. Gorbet and M. V Sefton, “Biomaterial-associated thrombosis: roles of coagulation factors, complement, platelets and leukocytes.,” Biomaterials, vol. 25, pp. 5681–703, 2004.

[7] M. S. Kim, G. Khang, and H. B. Lee, “Gradient polymer surfaces for biomedical applications,” Prog. Polym. Sci., vol. 33, pp. 138–164, 2008.

[8] D. Li and H. Chen, “Regulation of Protein / Surface Interactions by Surface Chemical Modification and Topographic Design,” Proteins at Interfaces III State of the Art, pp. 301–319, 2012.

[9] H. J. Ensikat, P. Ditsche-Kuru, C. Neinhuis, and W. Barthlott, “Superhydrophobicity in perfection: The outstanding properties of the lotus leaf,” Beilstein J. Nanotechnol., vol. 2, pp. 152–161, 2011.

[10] X. Zhang, F. Shi, J. Niu, Y. Jiang, and Z. Wang, “Superhydrophobic surfaces : from structural control to functional application,” J. Mater. Chem., vol. 18, pp. 621–633, 2008.

[11] K. Bhushan, J.C. Jung, K. Koch, “Micro- , nano- and hierarchical structures for superhydrophobicity , self-cleaning and low adhesion,” Phil. Trans. R. Soc. A, vol. 367, pp. 1631–1672, 2009.

[12] S. F. Toosi, S. Moradi, M. Ebrahimi, and S. G. Hatzikiriakos, “Microfabrication of polymeric surfaces with extreme wettability using hot embossing,” Appl. Surf. Sci., vol. 378, pp. 426–434, 2016.

[13] R. N. Wenzel, “Resistance of solid surfaces to wetting by water.,” J. Ind. Eng. Chem. (Washington, D. C.), vol. 28, pp. 988–994, 1936.

[14] B. D. Cassie and S. Baxter, “Wettability of porous surfaces,” Trans. Faraday Soc., no. 5, pp. 546–551, 1944.

[15] K. Bazaka, R. J. Crawford, and E. P. Ivanova, “Do bacteria differentiate between degrees of nanoscale surface roughness ?,” Biotechnol. J., vol. 6, pp. 1103–1114, 2011.

[16] P. Moazzam, A. Razmjou, M. Golabi, D. Shokri, and A. Landarani-isfahani, “Investigating the BSA protein adsorption and bacterial adhesion of Al-alloy surfaces after creating a hierarchical (micro / nano) superhydrophobic structure,” J. Biomed. Mater. Res. A, vol. 104A, pp. 2220–2233, 2016.

[17] S. Moradi, N. Hadjesfandiari, S. F. Toosi, J. N. Kizhakkedathu, and S. G. Hatzikiriakos, “E ff ect of Extreme Wettability on Platelet Adhesion on Metallic Implants : From Superhydrophilicity to Superhydrophobicity,” ACS Appl. Mater. Interfaces, vol. 8, pp. 17631–17641, 2016.

[18] Y. Koc, A. J. De Mello, G. Mchale, M. I. Newton, P. Roach, and J. Neil, “Nano-scale Superhydrophobicity : Suppression of Protein Adsorption and Promotion of Flow-Induced Detachment,” Lab Chip, vol. 8, pp. 582–586, 2008.

[19] X. Zhang, L. Wang, and E. Levänen, “Superhydrophobic surfaces for reduction of bacterial adhesion,” RCS Adv., pp. 1–53, 2013.

[20] A. Marmur, “Soft contact: measurement and interpretation of contact angles,” Soft Matter, vol. 2, no. 1, p. 12, 2006.

[21] S. S. Latthe, “Recent Progress in Preparation of Superhydrophobic Surfaces: A Review,”

J. Surf. Eng. Mater. Adv. Technol., vol. 2, , pp. 76–94, 2012.

[22] D. Qu, "Wetting and Roughness," Annu. Rev. Mater. Res., vol. 38, pp. 99, 2008.

[23] A. Marmur, "Contact Angle Hysteresis on heterogeneous smooth surfaces," J. Colloid Interface Sci., vol. 168, pp. 40–46, 1994.

[24] A. Marmur, "Line Tension and the Intrinsic Contact Angle in Solid-Liquid-Fluid Systems," J. Colloid Interface Sci., vol. 186, pp. 462–6, 1997.

[25] G. Wolansky and A. Marmur, "Apparent contact angles on rough surfaces: the Wenzel equation revisited," Colloids Surfaces A Physicochem. Eng. Asp., vol. 156, pp. 381–388, 1999.

[26] B. He, N. A. Patankar, and J. Lee, "Multiple Equilibrium Droplet Shapes and Design Criterion for Rough Hydrophobic Surfaces," Langmuir, vol. 19, pp. 4999–5003, 2003.

[27] S. Mettu and M. K. Chaudhury, "Motion of liquid drops on surfaces induced by asymmetric vibration: role of contact angle hysteresis.," Langmuir, vol. 27, pp. 10327–33, 2011.

[28] J. Bico, U. Thiele, and D. Quéré, "Wetting of textured surfaces," Colloids Surfaces A Physicochem. Eng. Asp., vol. 206, pp. 41–46, 2002.

[29] a J. B. Milne and a Amirfazli, "The Cassie equation: how it is meant to be used.," Adv. Colloid Interface Sci., vol. 170, no. 1–2, pp. 48–55, Jan. 2012.

[30] L. Cao, H.-H. Hu, and D. Gao, "Design and fabrication of micro-textures for inducing a superhydrophobic behavior on hydrophilic materials.," Langmuir, vol. 23, pp. 4310–4, 2007.

[31] D. Quéré, "Non-sticking drops," Reports Prog. Phys., vol. 68, pp. 2495–2532, 2005.

[32] M. Strobel and C. S. Lyons, "An Essay on Contact Angle Measurements," Plasma Process. Polym., vol. 8, pp. 8–13, 2011.

[33] J.-H. Kim, H. P. Kavehpour, and J. P. Rothstein, "Dynamic contact angle measurements on superhydrophobic surfaces," Phys. Fluids, vol. 27, pp. 32107, 2015.

[34] G. McHale, N. J. Shirtcliffe, and M. I. Newton, "Contact-Angle Hysteresis on Super-Hydrophobic Surfaces," Langmuir, vol. 20, pp. 10146–10149, 2004.

[35] M. Nosonovsky and B. Bhushan, “Roughness-induced superhydrophobicity: a way to design non-adhesive surfaces,” J. Phys. Condens. Matter, vol. 20, pp. 225009, 2008.

[36] M. Nosonovsky and B. Bhushan, “Biomimetic superhydrophobic surfaces: Multiscale approach,” Nano Lett., vol. 7, pp. 2633–2637, 2007.

[37] S. Moradi, “Super-hydrophobic Nanopatterned Interfaces : Optimization and Manufacturing,” Thesis, open.library.ubc.ca, 2014.

[38] B. Krasovitski and A. Marmur, “Drops down the hill: theoretical study of limiting contact angles and the hysteresis range on a tilted plate.,” Langmuir, vol. 21, pp. 3881–5, 2005.

[39] E. L. Decker, B. Frank, Y. Suo, and S. Garoff, “Physics of contact angle measurement,” Colloids Surfaces A Physicochem. Eng. Asp., vol. 156, pp. 177–189, 1999.

[40] E. Bormashenko, Y. Bormashenko, G. Whyman, R. Pogreb, A. Musin, R. Jager, and Z. Barkay, “Contact angle hysteresis on polymer substrates established with various experimental techniques, its interpretation, and quantitative characterization.,” Langmuir, vol. 24, pp. 4020–5, 2008.

[41] D. Song, R. J. Daniello, and J. P. Rothstein, “Drag reduction using superhydrophobic sanded Teflon surfaces,” Exp. Fluids, vol. 55, 2014.

[42] A. Carré and K. L. Mittal, Eds., Superhydrophobic surfaces, CRC Press, 2009.

[43] A. C. Lima and J. F. Mano, “Micro-/nano-structured superhydrophobic surfaces in the biomedical field: part I: basic concepts and biomimetic approaches,” Nanomedicine, vol. 10, pp. 103–119, 2015.

[44] Y. Wang, S. Al Shakhshir, X. Li, and P. Chen, “Superhydrophobic flow channel surface and its impact on PEM fuel cell performance,” pp. 1–12, 2012.

[45] A. M. A. Mohamed, A. M. Abdullah, and N. A. Younan, “Corrosion behavior of superhydrophobic surfaces: A review,” Arab. J. Chem., vol. 8, pp. 749–765, 2015.

[46] D. Zhang, L. Wang, H. Qian, and X. Li, “Superhydrophobic surfaces for corrosion protection: a review of recent progresses and future directions,” J. Coatings Technol. Res., vol. 13, pp. 11–29, 2016.

[47] B. Bixler, Gregory D. ; Bhushan, “Bioinspired rice leaf and butterfly wing surface structures combining shark skin and lotus effects,” Soft Matter, pp. 11271–11284, 2012.

[48] N. Zhao, L. Weng, X. Zhang, Q. Xie, X. Zhang, and J. Xu, “A lotus-leaf-like superhydrophobic surface prepared by solvent-induced crystallization,” ChemPhysChem, vol. 7, pp. 824–827, 2006.

[49] Y. Zheng, X. Gao, and L. Jiang, “Directional adhesion of superhydrophobic butterfly wings,” Soft Matter, vol. 3, pp. 178–182, 2007.

[50] Y. Cai, L. Lin, Z. Xue, M. Liu, S. Wang, and L. Jiang, “Filefish-inspired surface design for anisotropic underwater oleophobicity,” Adv. Funct. Mater., vol. 24, pp. 809–816, 2014.

[51] R. G. Parkin, Ivan P. ; and Palgravea, “Self-cleaning coatings,” J. Mater. Chem., pp. 1689–1695, 2005.

[52] I. Sas, R. E. Gorga, J. A. Joines, and K. A. Thoney, “Literature Review on Superhydrophobic Self-Cleaning Surfaces Produced by Electrospinning,” polymer science part b: polymer physics, pp. 824–845, 2012.

[53] B. Bhushan and M. Nosonovsky, “The rose petal effect and the modes of superhydrophobicity,” Philos. Trans. R. Soc. A Math. Phys. Eng. Sci., vol. 368, no. 1929, pp. 4713–4728, 2010.

[54] A. Mahdavi, L. Ferreira, C. Sundback, J. W. Nichol, E. P. Chan, D. J. D. Carter, C. J. Bettinger, S. Patanavanich, L. Chignozha, E. Ben-Joseph, A. Galakatos, H. Pryor, I. Pomerantseva, P. T. Masiakos, W. Faquin, A. Zumbuehl, S. Hong, J. Borenstein, J. Vacanti, R. Langer, and J. M. Karp, “A biodegradable and biocompatible gecko-inspired tissue adhesive.,” Proc. Natl. Acad. Sci. U. S. A., vol. 105, no. 7, pp. 2307–2312, 2008.

[55] R. Blossey, “Self-cleaning surfaces - virtual realities,” Nat. Mater., vol. 2, no. 5, pp. 301–306, 2003.

[56] C. Neinhuis and W. Barthlott, “Characterization and Distribution of Water-repellent, Self-cleaning Plant Surfaces,” Ann. Bot., vol. 79, no. 6, pp. 667–677, 1997.

[57] W. Barthlott and C. Neinhuis, “Purity of the sacred lotus, or escape from contamination in biological surfaces,” Planta, vol. 202, no. 1, pp. 1–8, 1997.

[58] S. S. Latthe, C. Terashima, K. Nakata, and A. Fujishima, “Superhydrophobic surfaces developed by mimicking hierarchical surface morphology of lotus leaf,” Molecules, vol. 19, pp. 4256–4283, 2014.

[59] N. A. Patankar, “Mimicking the lotus effect: Influence of double roughness structures and slender pillars,” Langmuir, vol. 20, no. 19, pp. 8209–8213, 2004.

[60] L. Eadie and T. K. Ghosh, “Biomimicry in textiles: past, present and potential. An overview,” J. R. Soc. Interface, vol. 8, no. 59, pp. 761–775, 2011.

[61] B. L. Feng, S. H. Li, Y. S. Li, H. J. Li, L. J. Zhang, J. Zhai, Y. L. Song, B. Q. Liu, L. Jiang, L. Feng, S. H. Li, Y. S. Li, H. J. Li, L. J. Zhang, J. Zhai, Y. L. Song, B. Q. Liu, L. Jiang, and D. B. Zhu, “Super-hydrophobic surfaces: From natural to artificial,” Adv. Mater., vol. 14, no. 24, pp. 1857–1860, 2002.

[62] J. A. N. Genzer and K. Efimenko, “Recent developments in superhydrophobic surfaces and their relevance to marine fouling : a review,” Biofouling, vol. 22, no. 5, pp. 339–360, 2006.

[63] A. Nakajima, K. Hashimoto, and T. Watanabe, “Recent studies on super-hydrophobic films,” Monatshefte fur Chemie, vol. 132, no. 1, pp. 31–41, 2001.

[64] E. Celia, T. Darmanin, E. Taffin de Givenchy, S. Amigoni, and F. Guittard, “Recent advances in designing superhydrophobic surfaces,” J. Colloid Interface Sci., vol. 402, pp. 1–18, 2013.

[65] D. Jucius, V. Grigalinas, M. Mikolajnas, a. Guobien, V. Kopustinskas, a. Gudonyt, and P. Narmontas, “Hot embossing of PTFE: Towards superhydrophobic surfaces,” Appl. Surf. Sci., vol. 257, no. 6, pp. 2353–2360, 2011.

[66] X. D. Huang, L.-R. Bao, X. Cheng, L. J. Guo, S. W. Pang, and a. F. Yee, “Reversal imprinting by transferring polymer from mold to substrate,” J. Vac. Sci. Technol. B Microelectron. Nanom. Struct., vol. 20, no. 6, p. 2872, 2002.

[67] E. Mele, S. Girardo, and D. Pisignano, “Strelitzia reginae leaf as a natural template for

anisotropic wetting and superhydrophobicity," Langmuir, vol. 28, no. 11, pp. 5312–5317, 2012.

[68] J. Feng, M. T. Tuominen, and J. P. Rothstein, "Hierarchical superhydrophobic surfaces fabricated by dual-scale electron-beam-lithography with well-ordered secondary nanostructures," Adv. Funct. Mater., vol. 21, no. 19, pp. 3715–3722, 2011.

[69] S. Zanini, R. Barni, R. Della Pergola, and C. Riccardi, "Modification of the PTFE wettability by oxygen plasma treatments: influence of the operating parameters and investigation of the ageing behaviour," J. Phys. D. Appl. Phys., vol. 47, p. 325202, 2014.

[70] P. Slepička, S. Trostová, N. Slepičková Kasálková, Z. Kolská, P. Sajdl, and V. Švorčík, "Surface modification of biopolymers by argon plasma and thermal treatment," Plasma Process. Polym., vol. 9, no. 2, pp. 197–206, 2012.

[71] C. Yang, X. M. Li, J. Gilron, D. feng Kong, Y. Yin, Y. Oren, C. Linder, and T. He, "CF4 plasma-modified superhydrophobic PVDF membranes for direct contact membrane distillation," J. Memb. Sci., vol. 456, pp. 155–161, 2014.

[72] W. Xi, Z. Qiao, C. Zhu, A. Jia, and M. Li, "The preparation of lotus-like super-hydrophobic copper surfaces by electroplating," Appl. Surf. Sci., vol. 255, no. 9, pp. 4836–4839, 2009.

[73] G. Y. Li, X. P. Li, H. Wang, Z. Q. Yang, J. Y. Yao, and G. F. Ding, "Fabrication and characterization of superhydrophobic surface by electroplating regular rough micro-structures of metal nickel," Microelectron. Eng., vol. 95, pp. 130–134, 2012.

[74] Z. K. Wang, H. Y. Zheng, and H. M. Xia, "Femtosecond laser-induced modification of surface wettability of PMMA for fluid separation in microchannels," Microfluid. Nanofluidics, vol. 10, no. 1, pp. 225–229, 2011.

[75] I. Jun, Y. Chung, Y. Heo, H. Han, J. Park, H. Jeong, and H. Jeon, "Creating Hierarchical Topographies on Fibrous Platforms Using Femtosecond Laser Ablation for Directing Myoblasts Behavior," ACS Appl. Mater. Interfaces, 2016.

[76] C. De Marco, S. M. Eaton, R. Suriano, S. Turri, M. Levi, R. Ramponi, G. Cerullo, and R. Osellame, "Surface Properties of Femtosecond Laser Ablated PMMA," ACS Appl. Mater. Interfaces, vol. 2, no. 8, pp. 2377–2384, 2010.

[77] K. M. Tanvir Ahmmed, C. Grambow, and A. M. Kietzig, “Fabrication of micro/nano structures on metals by femtosecond laser micromachining,” Micromachines, vol. 5, no. 4, pp. 1219–1253, 2014.

[78] F. Liang, J. Lehr, L. Danielczak, R. Leask, and A. Kietzig, “Robust Non-Wetting PTFE Surfaces by Femtosecond Laser Machining,” Int. J. Mol. Sci., pp. 13681–13696, 2014.

[79] S. Moradi, S. Kamal, P. Englezos, and S. G. Hatzikiriakos, “Femtosecond laser irradiation of metallic surfaces: effects of laser parameters on superhydrophobicity.,” Nanotechnology, vol. 24, pp. 415302, 2013.

[80] N. J. Shirtcliffe, G. McHale, and M. I. Newton, “The superhydrophobicity of polymer surfaces: Recent developments,” J. Polym. Sci. Part B Polym. Phys., vol. 49, pp. 1203–1217, 2011.

[81] M. Wolfs, T. Darmanin, and F. Guittard, “Superhydrophobic Fibrous Polymers,” Polym. Rev., vol. 53, pp. 460–505, 2013.

[82] D. Kim, W. Hwang, H. C. Park, and K.-H. Lee, “Superhydrophobic nano-wire entanglement structures,” J. Micromechanics Microengineering, vol. 16, pp. 2593–2597, 2006.

[83] D. Han and A. J. Steckl, “Superhydrophobic and Oleophobic Fibers by Coaxial Electrospinning,”, Langmuir, vol. 25, no. 17, pp. 9454–9462, 2009.

[84] H. Pazokian, a Selimis, J. Barzin, S. Jelvani, M. Mollabashi, C. Fotakis, and E. Stratakis, “Tailoring the wetting properties of polymers from highly hydrophilic to superhydrophobic using UV laser pulses,” J. Micromechanics Microengineering, vol. 22, p. 35001, 2012.

[85] J. Lawrence, D. Waugh, and H. Liang, Laser Surface Modification and Adhesion. CRC Press, 2015.

[86] J. Y. Benjamin Li-Ping Leea, Hojeong Jeonc, Aijun Wangb, Zhiqiang Yanb and and S. L. Costas Grigoropoulosc, “Femtosecond Laser Ablation Enhances Cell Infiltration into Three-Dimensional Electrospun Scaffolds,” vol. 8, no. 7, pp. 2648–2658, 2012.

[87] M. D. Shirk and P. a. Molian, “A review of ultrashort pulsed laser ablation of materials,” J. Laser Appl., vol. 10, no. 1, p. 18, 1998.

[88] J. Yong, Y. Fang, F. Chen, J. Huo, Q. Yang, H. Bian, G. Du, and X. Hou, “Femtosecond laser ablated durable superhydrophobic PTFE films with micro-through-holes for oil/water separation: Separating oil from water and corrosive solutions,” Appl. Surf. Sci., vol. 389, pp. 1148–1155, 2016.

[89] W. Li, Q. Yang, F. Chen, J. Yong, Y. Fang, and J. Huo, “Femtosecond laser ablated durable superhydrophobic PTFE sheet for oil/water separation,” vol. 10256, pp. 102563, 2017.

[90] M. Womack, M. Vendan, and P. Molian, “Femtosecond pulsed laser ablation and deposition of thin films of polytetrafluoroethylene,” Appl. Surf. Sci., vol. 221, pp. 99–109, 2004.

[91] S. Küper and M. Stuke, “Ablation of polytetrafluoroethylene (Teflon) with femtosecond UV excimer laser pulses,” Appl. Phys. Lett., vol. 54, no. 1989, pp. 4–6, 1989.

[92] H. Kumagai, K. Midorikawa, K. Toyoda, S. Nakamura, T. Okamoto, and M. Obara, “Ablation of polymer films by a femtosecond high-peak-power Ti:sapphire laser at 798 nm,” Appl. Phys. Lett., vol. 65, no. 14, pp. 1850–1852, 1994.

[93] H. Niino and A. Yabe, “Laser Ablation of Transparent Materials by UV fs-Laser Irradiation.,” J. Photopolym. Sci. Technol., vol. 14, no. 2, pp. 197–202, 2001.

[94] Z. B. Wang, M. H. Hong, Y. F. Lu, D. J. Wu, B. Lan, and T. C. Chong, “Femtosecond laser ablation of polytetrafluoroethylene (Teflon) in ambient air,” J. Appl. Phys., vol. 93, no. 2003, pp. 6375–6380, 2003.

[95] M. Hashida, H. Mishima, S. Tokita, and S. Sakabe, “Non-thermal ablation of expanded polytetrafluoroethylene with an intense femtosecond-pulse laser.,” Opt. Express, vol. 17, no. 15, pp. 13116–13121, 2009.

[96] M. Huber, G. Reinisch, G. Trettenhahn, K. Zweymüller, and F. Lintner, “Presence of corrosion products and hypersensitivity-associated reactions in periprosthetic tissue after aseptic loosening of total hip replacements with metal bearing surfaces,” Acta Biomater., vol. 5, no. 1, pp. 172–180, 2009.

[97] N. William Hudson Hofmeister, T. (US); A. Yuryevich, T. (US); J. Terekhov, Murfreesboro, T. Lino Vasconcelos da Costa, T. (US); K. S. Lansford, and T. (US); D. R. Manchester, "Nanostructures from Laser-Ablated Nanohole Templates," 2013.

[98] M. Psarski, J. Marczak, J. Grobelny, and G. Celichowski, "Superhydrophobic surface by replication of laser micromachined pattern in epoxy/alumina nanoparticle composite," J. Nanomater., 2014.

[99] X. C. Wang, L. Y. L. Wu, Q. Shao, and H. Y. Zheng, "Laser micro structuring on a Si substrate for improving surface hydrophobicity," vol. 85025, 2009.

[100] L. Y. L. Wu, Q. Shao, X. C. Wang, H. Y. Zheng, and C. C. Wong, "Hierarchical structured sol–gel coating by laser textured template imprinting for surface superhydrophobicity," Soft Matter, vol. 8, no. 23, p. 6232, 2012.

[101] "Fabrication of anti-reflective structures using hot embossing with a stainless.pdf." .

[102] H. Tanaka and R. J. Wood, "Fabrication of corrugated artificial insect wings using laser micromachined molds," J. Micromechanics Microengineering, vol. 20, no. 7, p. 75008, 2010.

[103] H. W. Choi, S. Bong, D. F. Farson, C. Lu, and L. J. Lee, "Femtosecond laser micromachining and application of hot embossing molds for microfluid device fabrication," J. Laser Appl., vol. 21, no. 4, p. 196, 2009.

[104] H. Urayama, T. Kanamori, and Y. Kimura, "Properties and biodegradability of polymer blends of poly(L-lactide)s with different optical purity of the lactate units," Macromol. Mater. Eng., vol. 287, no. 2, pp. 116–121, 2002.

[105] C. Hu, S. Liu, B. Li, H. Yang, C. Fan, and W. Cui, "Micro-/nanometer rough structure of a superhydrophobic biodegradable coating by electrospraying for initial anti-bioadhesion," Adv. Healthc. Mater., vol. 2, no. 10, pp. 1314–1321, 2013.

[106] C. Sousa, D. Rodrigues, R. Oliveira, W. Song, J. F. Mano, and J. Azeredo, "Superhydrophobic poly (L-lactic acid) surface as potential bacterial colonization substrate," AMB Express, vol. 1, no. 1, p. 34, 2011.

[107] B. N. Lourenço, G. Marchioli, W. Song, R. L. Reis, C. a. van Blitterswijk, M. Karperien, A. van Apeldoorn, and J. F. Mano, "Wettability influences cell behavior on superhydrophobic surfaces with different topographies," Biointerphases, vol. 7, pp. 1–11, 2012.

[108] C.-F. Huang, H.-C. Cheng, Y. Lin, C.-W. Wu, and Y.-K. Shen, "Study on cellar behaviors on different nanostructures by nanoporous alumina template," Int. J. Precis. Eng. Manuf., vol. 15, no. 4, pp. 689–693, 2014.

[109] I.-C. Chung, C.-W. Li, and G.-J. Wang, "The influence of different nanostructured scaffolds on fibroblast growth," Sci. Technol. Adv. Mater., vol. 14, no. 4, p. 44401, 2013.

[110] R. Truckenmüller, S. Giselbrecht, M. Escalante-Marun, M. Groenendijk, B. Papenburg, N. Rivron, H. Unadkat, V. Saile, V. Subramaniam, A. Van Den Berg, C. Van Blitterswijk, M. Wessling, J. De Boer, and D. Stamatialis, "Fabrication of cell container arrays with overlaid surface topographies," Biomed. Microdevices, vol. 14, no. 1, pp. 95–107, 2012.

[111] C. a. M. Portugal, R. Truckenmüller, D. Stamatialis, and J. G. Crespo, "Effect of tissue scaffold topography on protein structure monitored by fluorescence spectroscopy," J. Biotechnol., vol. 189, pp. 166–174, 2014.

[112] J. Lee, Y. Lin, and W. Chen, "The Nano-topology Influence of Osteoblast-like Cell on the Bio-nanostructure Thin Film by Nanoimprint,", International Conference on Nanotechnology and Biosensors, IPCBEE, vol. 2, pp. 67–71, 2011.

[113] N. M. Alves, J. Shi, E. Oramas, J. L. Santos, H. Tomás, and J. F. Mano, "Bioinspired superhydrophobic poly(L-lactic acid) surfaces control bone marrow derived cells adhesion and proliferation," J. Biomed. Mater. Res. - Part A, vol. 91, no. 2, pp. 480–488, 2009.

[114] J. Shi, N. M. Alves, and J. F. Mano, "Towards bioinspired superhydrophobic poly(L-lactic acid) surfaces using phase inversion-based methods.," Bioinspir. Biomim., vol. 3, no. 3, p. 34003, 2008.

[115] Z. Xue, Z. Sun, Y. Cao, Y. Chen, L. Tao, K. Li, L. Feng, Q. Fu, and Y. Wei, "Superoleophilic and superhydrophobic biodegradable material with porous structures for oil absorption and oil–water separation," RSC Adv., vol. 3, no. 45, p. 23432, 2013.

[116] H. Iwase, "Biological Effects of the Plasticizer Tris (2-Ethylhexyl) Trimellitate," Clin.

Pharmacol. Biopharm., vol. S2, no. e001, 2014.

[117] D. C. Leslie, A. Waterhouse, J. B. Berthet, T. M. Valentin, A. L. Watters, A. Jain, P. Kim, B. D. Hatton, A. Nedder, K. Mullen, E. H. Super, C. Howell, C. P. Johnson, T. L. Vu, S. Rifai, A. Hansen, M. Aizenberg, M. Super, J. Aizenberg, and D. E. Ingber, "A bioinspired surface coating for medical devices that prevents thrombosis and biofouling," Nat. Biotechnol., vol. submitted, no. 11, pp. 1134–1140, 2014.

[118] H. Lin, L. Ding, W. Deng, X. Wang, J. Long, and Q. Lin, "Coating of Medical-Grade PVC Material with ZnO for Antibacterial Application," vol. 2013, no. October, pp. 236–241, 2013.

[119] K. K. Chung, J. F. Schumacher, E. M. Sampson, R. A. Burne, and P. J. Antonelli, "Impact of engineered surface microtopography on biofilm formation of Staphylococcus aureus," Biointerphases, vol. 2, no. 2, pp. 89–94, 2007.

[120] K. Bazaka, M. V Jacob, R. J. Crawford, and E. P. Ivanova, "Efficient surface modification of biomaterial to prevent biofilm formation and the attachment of microorganisms," Appl Microbiol Biotechnol, vol. 95, pp. 299–311, 2012.

[121] R. J. Crawford, H. K. Webb, V. K. Truong, J. Hasan, and E. P. Ivanova, "Surface topographical factors in fl uencing bacterial attachment," Adv. Colloid Interface Sci., vol. 179–182, pp. 142–149, 2012.

[122] H. J. Busscher, W. Norde, P. K. Sharma, and H. C. van der Mei, "Interfacial re-arrangement in initial microbial adhesion to surfaces," Curr. Opin. Colloid Interface Sci., vol. 15, no. 6, pp. 510–517, 2010.

[123] P. Thevenot, W. Hu, and L. Tang, "Surface chemistry influences implant biocompatibility.," Curr. Top. Med. Chem., vol. 8, no. 4, pp. 270–280, 2008.

[124] A. Nouri, C. Wen, Introduction to surface coating and modification for metallic biomaterials, 2015.

[125] H. Dadafarin, E. Konkov, and S. Omanovic, "Electrochemical functionalization of a 316L stainless steel surface with a 11-mercaptoundecanoic acid monolayer: Stability studies," Int. J. Electrochem. Sci., vol. 8, no. 1, pp. 369–389, 2013.

[126] P. Chu, “Plasma-surface modification of biomaterials,” Mater. Sci. Eng. R Reports, vol. 36, no. 5–6, pp. 143–206, 2002.

[127] D. T. K. Kwok, H. Wang, Y. Zhang, K. W. K. Yeung, and P. K. Chu, “Effects of long pulse width and high pulsing frequency on surface superhydrophobicity of polytetrafluoroethylene in quasi-direct-current plasma immersion ion implantation,” J. Appl. Phys., vol. 105, 2009.

[128] “High density plasma enhanced chemical vapor deposition of optical thin films,” Eur. Phys. J. Appl. Phys., vol. 26, pp. 3–9, 2004.

[129] D. R. Schmidt and H. Waldeck, “Protein Adsorption to Biomaterials Biological Interactions on Materials Surfaces,” in Biological Interactions on Materials Surfaces, vol. 4, p. 98161.

[130] Y. Su, B. Ji, K. Zhang, H. Gao, Y. Huang, and K. Hwang, “Nano to micro structural hierarchy is crucial for stable superhydrophobic and water-repellent surfaces,” Langmuir, vol. 26, no. 7, pp. 4984–4989, 2010.

[131] Y. T. Cheng, D. E. Rodak, C. A. Wong, and C. A. Hayden, “Effects of micro- and nano-structures on the self-cleaning behaviour of lotus leaves,” Nanotechnology, vol. 17, pp. 1359–1362, 2006.

[132] C. Zhao, P. Cao, W. Ji, P. Han, J. Zhang, F. Zhang, Y. Jiang, and X. Zhang, “Hierarchical titanium surface textures affect osteoblastic functions,” J. Biomed. Mater. Res. - Part A, vol. 99 A, no. 4, pp. 666–675, 2011.

[133] Y. Lee, S. H. Park, K. B. Kim, and J. K. Lee, “Fabrication of hierarchical structures on a polymer surface to mimic natural superhydrophobic surfaces,” Adv. Mater., vol. 19, no. 17, pp. 2330–2335, 2007.

[134] T. Nuutinen, M. Silvennoinen, K. Päiväsaari, and P. Vahimaa, “Control of cultured human cells with femtosecond laser ablated patterns on steel and plastic surfaces,” Biomed. Microdevices, vol. 15, no. 2, pp. 279–288, 2013.

[135] Xuefeng Gao, Lei Jiang, “Biophysics: water-repellent legs of water striders,” Nature, vol. 432, pp.36 , 2004.

[136] L. R. Freschauf, J. McLane, H. Sharma, and M. Khine, “Shrink-induced superhydrophobic and antibacterial surfaces in consumer plastics,” PLoS One, vol. 7, no. 8, pp. 1–7, 2012.

[137] C. R. Crick, S. Ismail, J. Pratten, and I. P. Parkin, “An investigation into bacterial attachment to an elastomeric superhydrophobic surface prepared via aerosol assisted deposition,” Thin Solid Films, vol. 519, no. 11, pp. 3722–3727, 2011.

[138] J. Ma, Y. Sun, K. Gleichauf, J. Lou, and Q. Li, “Nanostructure on Taro Leaves Resists Fouling by Colloids and Bacteria under Submerged Conditions,” Langmuir, vol. 27, pp. 10035–10040, 2011.

[139] E. Fadeeva, V. K. Truong, M. Stiesch, B. N. Chichkov, R. J. Crawford, J. Wang, and E. P. Ivanova, “Bacterial Retention on Superhydrophobic Titanium Surfaces Fabricated by Femtosecond Laser Ablation,” Langmuir, pp. 3012–3019, 2011.

[140] P. Tang, W. Zhang, Y. Wang, B. Zhang, H. Wang, C. Lin, and L. Zhang, “Effect of Superhydrophobic Surface of Titanium on Staphylococcus aureus Adhesion,” Nanomaterials, pp. 1–8, 2011.

[141] B. J. Privett, J. Youn, S. A. Hong, J. Lee, J. Han, J. H. Shin, and M. H. Schoen, “Antibacterial Fluorinated Silica Colloid Superhydrophobic Surfaces,” Langmuir, vol. 27, pp. 9597–9601, 2011.

[142] R. Franke and F. Jung, “Interaction of Blood Components and Blood Cells with Body Foreign Surfaces,” Ser. Biomech., vol. 27, no. 1, pp. 51–58, 2012.

[143] R. P. Garrod, L. G. Harris, W. C. E. Schofield, J. Mcgettrick, L. J. Ward, D. O. H. Teare, and J. P. S. Badyal, “Mimicking a Stenocara Beetle ’ s Back for Microcondensation Using Plasmachemical Patterned Superhydrophobic - Superhydrophilic Surfaces,” Langmuir, no. 18, pp. 689–693, 2007.

[144] H. Nygren, “Initial reactions of whole blood with hydrophilic and hydrophobic titanium surfaces,” Colloids Surfaces B Biointerfaces, vol. 6, pp. 329–333, 1996.

[145] J. J. Gray, “The interaction of proteins with solid surfaces,” Curr. Opin. Struct. Biol., vol. 14, pp. 110–115, 2004.

[146] J. Hlady, Vladimir ; Buijs, “Protein adsorption on solid surfaces,” Curr Opin Biotechnol,

vol. 7, no. 1, pp. 72–77, 1996.

[147] E. A. Noh, Hyeran ; Vogler, “Volumetric Interpretation of Protein Adsorption: Competition from Mixtures and the Vroman Effect,” Biomaterials., vol. 28, no. 3, pp. 405–422, 2007.

[148] R. Dee, Kay C; Puleo, David A. ; Bizios, “An Introduction To Tissue-Biomaterial Interactions,” Cell Mol. Biol., pp. 1–15, 2003.

[149] S. Falah Toosi, S. Moradi, S. Kamal, and S. G. Hatzikiriakos, “Superhydrophobic laser ablated PTFE substrates,” Appl. Surf. Sci., vol. 349, no. MAY, pp. 715–723, 2015.

[150] S. Moradi, S. G. Hatzikiriakos, and S. Kamal, “Superhydrophobic Laser Ablated Stainless Steel Substrates and their Wettability,” Surf. Innov., pp. 1–27, 2015.

[151] S. Moradi, P. Englezos, and S. G. Hatzikiriakos, “Contact angle hysteresis of non-flattened-top micro/nanostructures,” Langmuir, vol. 30, no. 3, pp. 3274–3284, 2014.

[152] P. T. Mannion, J. Magee, E. Coyne, G. M. O’Connor, and T. J. Glynn, “The effect of damage accumulation behaviour on ablation thresholds and damage morphology in ultrafast laser micro-machining of common metals in air,” Appl. Surf. Sci., vol. 233, pp. 275–287, 2004.

[153] H. L. Jiang, L., Tsai, “Femtosecond Lasers Ablation : Challenges and Opportunities,” in In: NSF Workshop on Research Needs in Thermal, Aspects of Material Removal., pp. 166–173, 2003.

[154] S. F. Toosi, S. Moradi, S. Kamal, and S. G. Hatzikiriakos, “Superhydrophobic Laser Ablated PTFE Substrates,” Appl. Surf. Sci., vol. 349, pp. 715–723, 2015.

[155] R. J. Crawford and E. P. Ivanova, Superhydrophobic Surfaces, 2015.

[156] L. Wang, J. Wei, and Z. Su, “Fabrication of surfaces with extremely high contact angle hysteresis from polyelectrolyte multilayer,” Langmuir, vol. 27, no. 24, pp. 15299–15304, 2011.

[157] K. Grundke, Handbook of Applied Surface and Colloid Chemistry, K. Holmberg, Ed. p. 49083, 2002.

[158] B. M. L. Koch, A. Amirfazli, and J. A. W. Elliott, “Wetting of rough surfaces by a low surface tension liquid,” J. Phys. Chem. C, vol. 118, no. 41, pp. 23777–23782, 2014.

[159] S. Enders, H. Kahl, and J. Winkelmann, “Surface tension of the ternary system water + acetone + toluene,” J. Chem. Eng. Data, vol. 52, no. 3, pp. 1072–1079, 2007.

[160] G. Vazquez, E. Alvarez, and J. M. Navaza, “Surface Tension of Alcohol + Water from 20 to 50 C,” J. Chem. Eng. Data, vol. 40, no. 3, pp. 611–614, 1995.

[161] B. N. Lourenço, G. Marchioli, W. Song, R. L. Reis, C. a. van Blitterswijk, M. Karperien, A. van Apeldoorn, and J. F. Mano, “Wettability influences cell behavior on superhydrophobic surfaces with different topographies,” Biointerphases, vol. 7, no. 1–4, pp. 1–11, 2012.

[162] W. Song and J. F. Mano, “Interactions between cells or proteins and surfaces exhibiting extreme wettabilities,” Soft Matter, vol. 9, no. 11, p. 2985, 2013.

[163] C. Y. Loo, P. M. Young, W. H. Lee, R. Cavaliere, C. B. Whitchurch, and R. Rohanizadeh, “Superhydrophobic, nanotextured polyvinyl chloride films for delaying Pseudomonas aeruginosa attachment to intubation tubes and medical plastics,” Acta Biomater., vol. 8, no. 5, pp. 1881–1890, 2012.

[164] X. Hou, X. Wang, Q. Zhu, J. Bao, C. Mao, L. Jiang, and J. Shen, “Preparation of polypropylene superhydrophobic surface and its blood compatibility,” Colloids Surfaces B Biointerfaces, vol. 80, no. 2, pp. 247–250, 2010.

[165] Y. Koc, A. J. De Mello, G. Mchale, M. I. Newton, P. Roach, and N. J. Shirtcliffe, “Nano-scale superhydrophobicity : suppression of protein adsorption and promotion of flow-induced detachment,” LabChip, pp. 582–586, 2008.

[166] E. Luong-Van, I. Rodriguez, H. Y. Low, N. Elmouelhi, B. Lowenhaupt, S. Natarajan, C. T. Lim, R. Prajapati, M. Vyakarnam, and K. Cooper, “Review: Micro- and nanostructured surface engineering for biomedical applications,” J. Mater. Res., vol. 28, no. 2, pp. 165–174, 2012.

[167] L. C. Hsu, J. Fang, D. A. Borca-tasciuc, R. W. Worobo, and I. Moraru, “Effect of Micro- and Nanoscale Topography on the Adhesion of Bacterial Cells to Solid Surfaces,” Appl. Environ. Microbiol., vol. 79, no. 8, pp. 2703–2712, 2013.

[168] O. Habimana, A. Joana, C. Semiao, and E. Casey, “The role of cell-surface interactions in bacterial initial adhesion and consequent biofilm formation of nanofilteration/reverse osmosis membrane,” J. Memb. Sci., vol. 454, pp. 82–96, 2014.

[169] W. R. Jong, T. H. Kuo, S. W. Ho, H. H. Chiu, and S. H. Peng, “Flows in rectangular microchannels driven by capillary force and gravity,” Int. Commun. Heat Mass Transf., vol. 34, no. 2, pp. 186–196, 2007.